NAVAL POSTGRADUATE SCHOOL

MONTEREY, CALIFORNIA

THESIS

MODELING A LINEAR GENERATOR FOR ENERGY HARVESTING APPLICATIONS

by

Dominic J. Simone

December 2014

Thesis Advisor: Alexander L. Julian
Second Reader: Roberto Cristi

Approved for public release; distribution is unlimited

THIS PAGE INTENTIONALLY LEFT BLANK

REPORT DOCUMENTATION PAGE

Form Approved OMB No. 0704–0188

1. AGENCY USE ONLY *(Leave blank)*	**2. REPORT DATE** December 2014	**3. REPORT TYPE AND DATES COVERED** Master's Thesis

4. TITLE AND SUBTITLE
MODELING A LINEAR GENERATOR FOR ENERGY HARVESTING APPLICATIONS

5. FUNDING NUMBERS

6. AUTHOR(S) Dominic J. Simone

7. PERFORMING ORGANIZATION NAME(S) AND ADDRESS(ES)
Naval Postgraduate School
Monterey, CA 93943-5000

8. PERFORMING ORGANIZATION REPORT NUMBER

9. SPONSORING /MONITORING AGENCY NAME(S) AND ADDRESS(ES)
N/A

10. SPONSORING/MONITORING AGENCY REPORT NUMBER

11. SUPPLEMENTARY NOTES The views expressed in this thesis are those of the author and do not reflect the official policy or position of the Department of Defense or the U.S. Government. IRB protocol number ____N/A____.

12a. DISTRIBUTION / AVAILABILITY STATEMENT
Approved for public release; distribution is unlimited

12b. DISTRIBUTION CODE
A

13. ABSTRACT (maximum 200 words)

The intent of this research is to draw attention to linear generators and their potential uses. A flexible model of a linear generator created in MATLAB Simulink is presented. The model is a three-phase, 12-pole, non-salient, synchronous permanent magnet linear generator with a non-sinusoidal back electromotive force (EMF) but could easily be adapted to fit any number of poles or any back EMF waveform.

The emerging technologies related to linear generators such as wave energy converters and free-piston engines are explained. A selection of these technologies is generically modeled and their results are discussed and contrasted against one another.

The model clearly demonstrates the challenges of using linear generators in different scenarios. It also proves itself a useful tool in analyzing and improving the performance of linear generators under a variety of circumstances.

14. SUBJECT TERMS linear generator, permanent magnet, synchronous machine, non-sinusoidal, Simulink model, rotor reference frame, wave energy converter, free-piston engine	**15. NUMBER OF PAGES** 179
	16. PRICE CODE

17. SECURITY CLASSIFICATION OF REPORT	**18. SECURITY CLASSIFICATION OF THIS PAGE**	**19. SECURITY CLASSIFICATION OF ABSTRACT**	**20. LIMITATION OF ABSTRACT**
Unclassified	Unclassified	Unclassified	UU

NSN 7540–01-280-5500

Standard Form 298 (Rev. 2–89)
Prescribed by ANSI Std. 239–18

THIS PAGE INTENTIONALLY LEFT BLANK

Approved for public release; distribution is unlimited

MODELING A LINEAR GENERATOR FOR ENERGY HARVESTING APPLICATIONS

Dominic J. Simone
Lieutenant, United States Navy
B.S., United States Naval Academy, 2006

Submitted in partial fulfillment of the
requirements for the degree of

MASTER OF SCIENCE IN ELECTRICAL ENGINEERING

from the

NAVAL POSTGRADUATE SCHOOL
December 2014

Author: Dominic J. Simone

Approved by: Alexander L. Julian
Thesis Advisor

Roberto Cristi
Second Reader

R. Clark Robertson
Chair, Department of Electrical and Computer Engineering

THIS PAGE INTENTIONALLY LEFT BLANK

ABSTRACT

The intent of this research is to draw attention to linear generators and their potential uses. A flexible model of a linear generator created in MATLAB Simulink is presented. The model is a three-phase, 12-pole, non-salient, synchronous permanent magnet linear generator with a non-sinusoidal back electromotive force (EMF) but could easily be adapted to fit any number of poles or any back EMF waveform.

The emerging technologies related to linear generators such as wave energy converters and free-piston engines are explained. A selection of these technologies is generically modeled and their results are discussed and contrasted against one another.

The model clearly demonstrates the challenges of using linear generators in different scenarios. It also proves itself a useful tool in analyzing and improving the performance of linear generators under a variety of circumstances.

THIS PAGE INTENTIONALLY LEFT BLANK

TABLE OF CONTENTS

THIS PAGE INTENTIONALLY LEFT BLANK

LIST OF FIGURES

THIS PAGE INTENTIONALLY LEFT BLANK

LIST OF TABLES

THIS PAGE INTENTIONALLY LEFT BLANK

LIST OF ACRONYMS AND ABBREVIATIONS

ac	alternating current
AUV	autonomous underwater vehicle
BMS	battery management system
BH_{max}	maximum energy product (magnet performance)
B_m	mechanical damping due to friction
B_r	remanence
dc	direct current
DARPA	Defense Advanced Research Projects Agency
DOD	Department of Defense
qd0	direct-quadrature-zero
EMALS	electromagnetic aircraft launch system
EMF	electromotive force
F	force
H	magnetic field strength
I,i	current
i_{as}, i_{bs}, i_{cs}	stator current for the a, b and c phases, respectively
$\mathbf{i}_{abcs}$	stator current matrix
IEEE	Institute of Electrical and Electronics Engineers
J	rotational inertia
$\mathbf{K}_s^r$	*qd0* transformation matrix
l_{lm}	linear machine length
L	inductance
$\mathbf{L}_s$	stator self-inductance matrix
LC	inductance-capacitance
MBARI	Monterey Bay Aquarium Research Institute
p	number of poles
P	power
P_m	mechanical power
PM	permanent magnet

r	resistance
$\mathbf{r}_s$	stator resistance matrix
rms	root mean square
R	radius
RC	resistance–capacitance
RPM	rotation per minute
RTG	radioisotope thermoelectric generator
SRG	Stirling radioisotope generator
T	tesla (SI unit of magnetic flux density)
THD	total harmonic distortion
v	voltage
v_{as}, v_{bs}, v_{cs}	stator voltage for the *a*, *b* and *c* phases variables, respectively
$\mathbf{v}_{abcs}$	stator voltage matrix
v_{pk}	peak voltage
v'_{qs}, v'_{ds}, v'_{0s}	stator voltage in the rotor reference frame for the *q, d and 0* variables, respectively
$\mathbf{v}'_{qd0s}$	stator voltage matrix in the rotor reference frame for the *q, d and 0* variables
V	velocity
Wb	weber – unit of magnetic flux
WEC	wave energy converter
ε	electromotive force
θ_{re}	electrical rotor angle
θ_{rm}	mechanical rotor angle
λ	flux linkage
λ_{as}, λ_{bs}, λ_{cs}	flux linkage for the *a*, *b* and *c* phases variables, respectively
$\boldsymbol{\lambda}_{abcs}$	stator flux linkage matrix
λ'_m	peak magnetizing flux linkage due to the permanent magnet
λ'_{qs}, λ'_{ds}, λ'_{0s}	stator flux linkage in the rotor reference frame for the *q, d and 0* variables, respectively
$\boldsymbol{\lambda}'_{qd0}$	stator flux linkage matrix in the rotor reference frame for the *d*, *q* and *0* variables

τ	torque
τ_e	electrical torque
τ_i	mechanical torque
τ_{RC}	*RC* time constant
Φ	magnetic flux

THIS PAGE INTENTIONALLY LEFT BLANK

EXECUTIVE SUMMARY

MAGLEV trains, electromagnetic railguns and electric rollercoasters are all examples of linear motors, a technology that, through years of development, is finally coming of age. A cousin of the linear motor, the linear generator has historically not received the same level of focus and development. The linear generator's level of attention is growing, however, and new and emerging technologies that incorporate linear generators are becoming less niche and more mainstream.

Wave energy converters, including wave surge converters, surface and subsurface point absorbers, and surface attenuators, all stand to benefit from the inclusion of linear generators in their existing designs. Some companies have begun to develop and test wave energy converters that include linear generators, but the vast majority of wave energy production is still done through hydraulic turbine technology. The Department of Defense and the United States Navy stand to benefit from the development of this technology for use in small-scale wave energy production to power remote sensors and recharge unmanned vehicles without the need of a support vessel.

Free-piston devices are another example of a burgeoning use of linear generators. These devices can be either Stirling engines or more conventional internal combustion engines. In both cases the reciprocating piston is driving a linear generator, resulting in direct electrical power production and eliminating several energy conversion processes along the way. Free-piston engine designs also naturally lend themselves to the use of different fuels from gases like hydrogen and natural gas to combustible fluids like kerosene and gasoline. These devices are ideal as electric vehicle range extenders, and they are already in development by major brands like Toyota. This flexible, modular design also lends itself to distributed backup electrical generation on the Navy's electric ships of tomorrow.

Solid state power electronics is an enabling technology for linear generator development. Linear generators by their nature come to a stop twice per cycle, when the translator reaches either end of its travel. At this point, the generator is producing no

power. This start/stop action causes a less-than-ideal power quality on the output bus. This can be seen in the simulation results as well. It is thanks to advances in power electronics that the output of linear generators can be transformed into usable power.

Mathematically, a linear generator is very closely related to a standard rotary generator. For this reason the generator model is based on a rotary machine described by Chapman et al. in [1]. This machine is a three-phase, non-salient, non-sinusoidal permanent magnet synchronous motor. The variables in the model used for this thesis still reference the angle and angular velocity of the rotor despite the linear generator having a translator that is described in terms of speed, position and force. External to the model, the torque of the rotor is converted to the force of the translator; similarly the angular velocity is converted to speed and the rotor angle to translator position. The model also employs a rotor reference frame using a *qd0* transformation, a method closely related to a Park's transformation.

The advantages of using a *qd0* transform do not apply to this machine because it has a non-sinusoidal back electromotive force (EMF), as seen in Figure 1. The transformation is included, however, for added utility in future work. If the values of the harmonics in the flux distribution are set to zero then the model becomes sinusoidal and the advantages offered by the *qd0* transform of simplified control and constant state variables in steady state conditions can be utilized.

For the simulation, each phase of the generator model feeds a full bridge diode rectifier. The outputs of the three diode rectifiers feed a common dc bus and a 150Ω load resistor. Only the bus voltage is shown because the load is purely resistive.

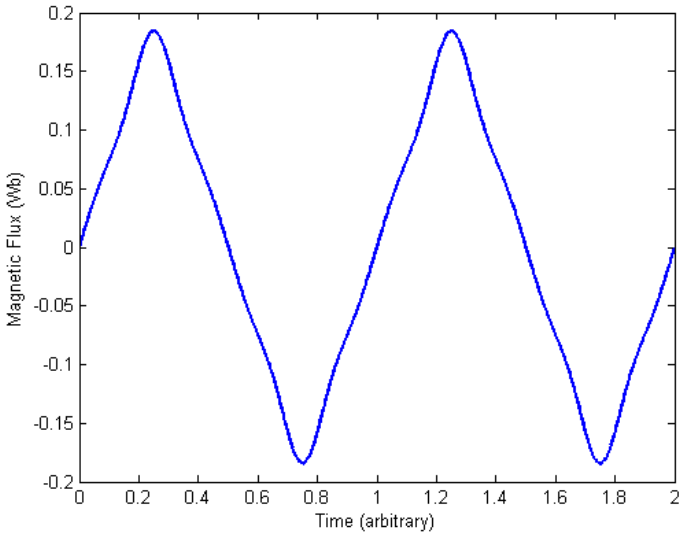

Figure 1. Non-sinusoidal back EMF.

Several different mechanical torques are used as inputs to the simulation. In the case where a wave energy converter is being emulated, the simulation uses a 1Hz low-amplitude sine-wave mechanical torque as the input function. This input torque is presented as the equivalent mechanical force on the translator, as seen in Figure 2. The linear generator does produce a useful amount of output power in this scenario, but the power is of poor quality, as seen in Figure 3. The output voltage has a ripple that is greater than half of the bus voltage, which can be seen by comparing Figures 2 and 3 as a function of the absolute value of the input force.

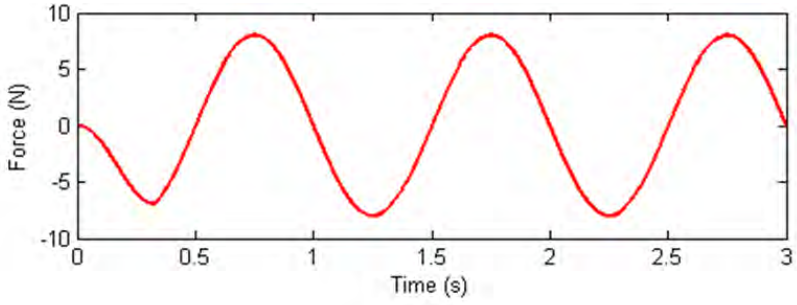

Figure 2. Mechanical input force applied to the translator.

To use this type of power as an ac source or a regulated dc source more work must be done, either with filter components or with active power electronics. If the power

into the machine (torque times angular velocity) is calculated and compared to the power out of the machine (voltage times current) this scenario sees the model generator operating at 54.1% efficiency.

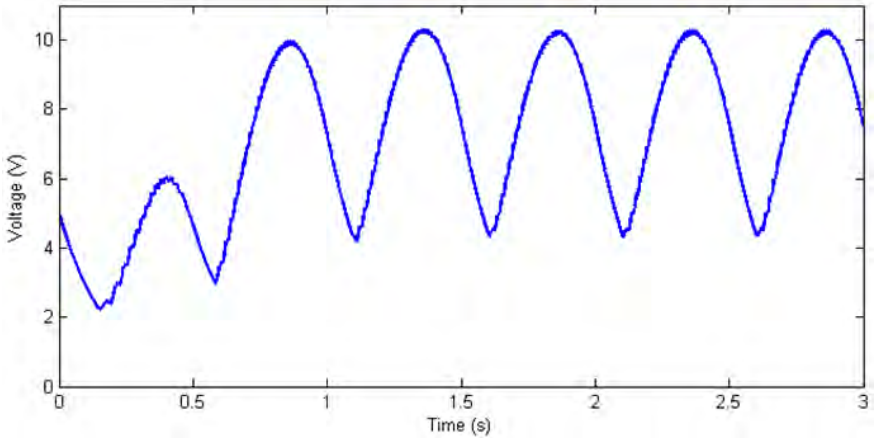

Figure 3. Output voltage on the dc bus for a 1Hz sinusoidal input torque.

In a different setup, the simulation uses an impulse that fires additively in the direction of travel of the translator each time the translator passes the midpoint of the generator. The simulated response of the model generator can be seen in Figure 4, where the parameters are scaled in order to best be displayed together in an intuitive manner.

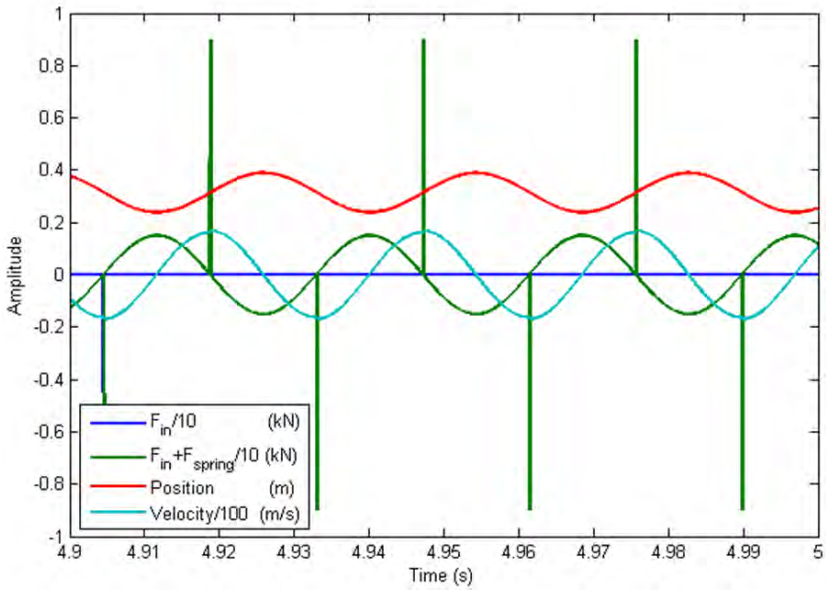

Figure 4. Input and spring forces acting on the translator and its resultant motion.

The F_{spring} in Figure 4 represents the force of a centering spring that is attached to the translator to aid in the stability of the system and in this case, as a return force for the translator. This setup draws parallels to the free-piston engine arrangement already discussed; most free-piston devices employ an air cushion spring to act as a return force.

The frequency of the input force in this scenario is controlled by behavior of the machine. In this simulation the machine stabilized at a frequency of 70.4Hz or about 4225RPMs if equated to the terms of an internal combustion engine (although there is no rotation here). This higher frequency results in a marked improvement in power quality on the dc bus. This can be seen in Figure 5, where the voltage ripple is reduced to 2.7% of the total dc bus voltage. The machine also exhibits an improved efficiency of 71.2%. This improved efficiency is somewhat expected since it is in keeping with the trends laid out by Eric Laithwaite's goodness factor formula, which states that machine efficiency is proportional to its speed among other factors.

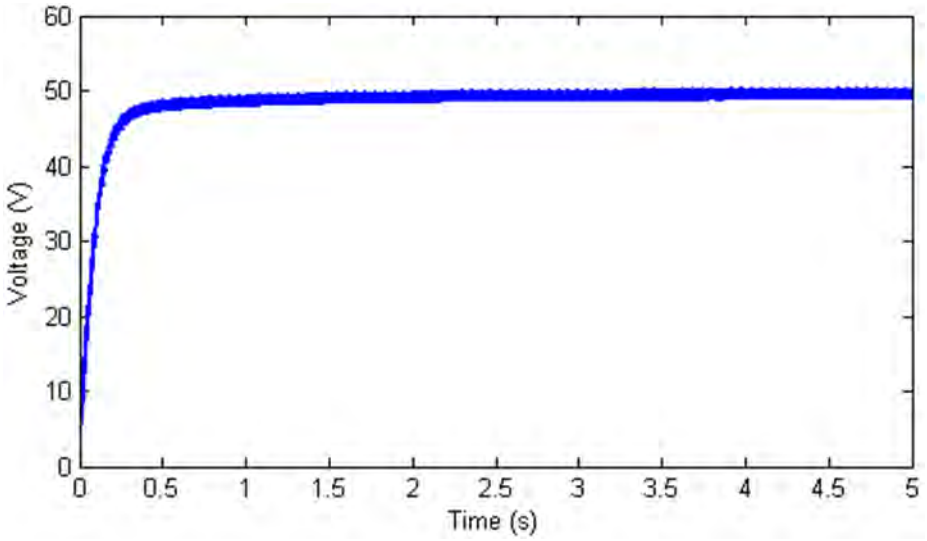

Figure 5. Output voltage on the dc bus from a floating frequency impulse input torque.

Through various simulations the Simulink model proved to be a useful and flexible tool in analyzing the performance and operating characteristics of a linear generator.

There is more work needed, to include some of the non-ideal characteristics of a generator such as demagnetization and core saturation. The model could also benefit from the inclusion of cogging torque, especially in the low speed situations where its effects would be the most observable.

LIST OF REFERENCES

[1] P. L. Chapman, S. D. Sudhoff and C. A. Whitcomb, "Multiple reference frame analysis of non-sinusoidal brushless dc drives," *IEEE Transactions on Energy Conversion,* vol. 14, no. 3, pp. 440–446, 1999.

ACKNOWLEDGMENTS

I would like to thank my wife, who has suffered my thesis-induced grumpiness these past months.

THIS PAGE INTENTIONALLY LEFT BLANK

I. INTRODUCTION: A BRIEF OVERVIEW OF ELECTRICAL MACHINES, THEIR ORIGINS AND USES

A. BACKGROUND

In 1820, Hans Christian Ørsted discovered he could make a compass needle deflect when he passed current through a nearby wire, thus uncovering a relationship between electricity and magnetism. Just eight years later, in 1828, Ányos Jedlik had already created the first commutated rotating electromechanical machine. In 1831, Michael Faraday discovered that a current could be generated by varying a magnetic field, discovering induction and paving the road for Hippolyte Pixii's invention of the electric generator a year later. Shortly thereafter, in 1837, the first United States patent was awarded for an electric motor to Thomas Davenport, it was U.S. Patent Number 132 [1], [2], [3].

The first U.S. patent for a linear machine would not occur for another 68 years; it would be awarded to Alfred Zehden under the description of "Electric Traction Apparatus" in 1905 [4]. Zehden's invention was the forerunner to the modern day maglev system. One of several configurations described by Zehden, in his patent, is shown in Figure 1.

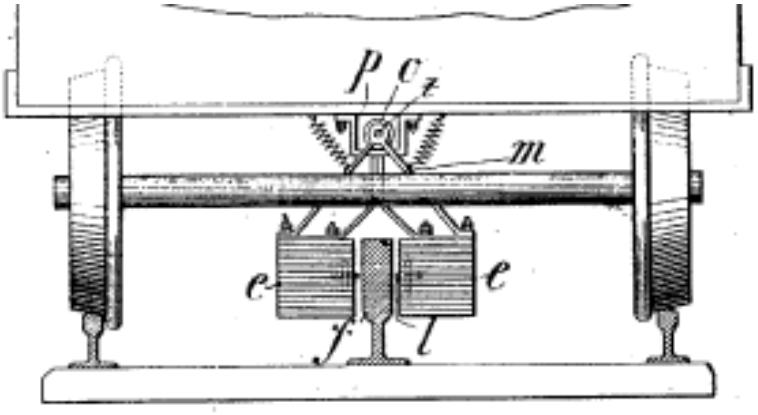

Figure 1. Linear motor propulsion system as shown in U.S. Patent No. 132, from [4].

Progress in linear *motors* has been greatly fueled by interest in maglev technology for transportation and by military interest in devices such as the electromagnetic railgun and the electromagnetic aircraft launch system. Recently, there has been a growing and significant application of linear motors in industry for use in robotics. Linear *generators*, on the other hand, have had their progress chiefly fueled by interest in new forms of energy production which will be discussed in detail in Chapter II.

An enabling technology for linear generators is the advancement of permanent magnets. While some of the earliest electric machines employed the use of permanent magnets, those machines' capacity and usefulness were severely stunted by the lack of strength that early magnets suffered from. Developed in 1982, the neodymium magnet can achieve a remanence (B_r) of more than 1.6 teslas (T), with 1.3T being representative of their standard strength [5]. It is true that neodymium magnets are stronger than other forms of permanent magnets, but also that they are more expensive by weight than most forms of permanent magnet. To understand why neodymium magnets are utilized to such a large extent one must compare cost per maximum energy product (BH_{max}), in units of megagauss-oersteds. BH_{max} is also referred to as magnet performance and is often used as a rating system for magnets. A comparison of different magnet materials and their relative costs, by magnet manufacturer Integrated Magnets, can be seen in Table 1 where NdFeB is the neodymium material.

Table 1. Relative costs of different permanent magnet materials, after [5].

Material	BH_{max} (MGOe)	Relative Cost ($ / lb)	Relative Cost ($ / BH_{max})
NdFeB	40	35	1.7
SmCo	26	60	4.9
Alnico	5	25	9.5
Ceramic	3	2	0.9
Flexible	1	1	1

Another important factor to consider, when discussing the economics of neodymium magnets, is the added benefit of miniaturization of the devices the magnets are used in. Using neodymium magnets allows electric machines to have higher force

densities, allowing for smaller and cheaper machines or more powerful machines for a given size depending on the constraints. The effect that magnet strength has on the performance of an electric machine will be discussed in detail in Chapter III, but it is evident that the development of neodymium magnets has had a profound effect on the performance of permanent magnet electrical machines and has enabled new and compelling applications for them.

B. POTENTIAL INTEREST TO THE DEPARTMENT OF DEFENSE AND U.S. GOVERNMENT

The Department of Defense (DOD) has been spending a lot of money developing linear *motors* in recent years, agreeing to pay $676.2 million for the development of the electromagnetic aircraft launch system (EMALS) for use on Ford class aircraft carriers and another $240 million on phase one of the U.S. Navy electromagnetic railgun system [6], [7]. Linear *generators* do not share this level of funding or attention but, with growing interest in the government in green energy sources and distributed electricity generation, some might argue they should.

1. The Electric Ship and the Future of Electricity Generation

Emerging technology, such as the pairing of a free-piston crankless internal combustion engine with a linear generator, allows for a more direct production of electricity than traditional means. In this configuration the piston becomes the translator of a linear generator with the cylinder acting as the stator. One advantage of this setup is that it reduces mechanical losses caused by gearing. It also has the potential to eliminate drivetrain parts such as transmissions, reduction gears and separate electric generators. Eliminating portions of the drivetrain will reduce weight and cost and will improve reliability.

This setup is also very suitable to a modular design, allowing for flexible electricity generation capacity to meet the demands of separate mission packages. The nature of a standalone modular design would also allow for distributed generation across a ship leading to better survivability. While traditional engines used in direct drives, such as marine diesel or gas turbine, are less efficient at lower power settings where they

operate for the majority of the time, the modular free-piston engine can always runs at peak efficiency by changing the number of pistons operating instead of the load of each piston in order to meet demand.

The simplicity of this system has led to NASA investigating a related free-piston Stirling engine coupled to a linear generator for use in space. This is discussed more in Chapter II but is mentioned here to emphasize the simplicity and reliability that such a system promises.

2. Unmanned Sensor Energy Needs

Whether they are stationary sensor arrays or autonomous underwater vehicles (AUVs), the U.S. Navy has an interest in sensing more areas of the ocean utilizing less manpower and resources. The current fleet of AUVs operated by the Navy is primarily powered by batteries which require the vehicles to be recovered every few days or even every few hours so they can be recharged [8]. There has been research on AUVs using inductive charging to recharge their batteries underwater utilizing shore or surface based power transmitted via undersea cables. Undersea power sources are non-existent in remote areas of the ocean, however, so in order to reduce the resource requirements and increase the capabilities of the AUVs an independent power source must be developed.

The focus of the Navy is increasingly toward the littorals where shallow water depth presents an obstacle to a fleet that is designed to be effective in deep water. AUVs are a big portion of the emerging solution to this dilemma since they operate effectively in very shallow water depths, but their support vessels cannot always do the same. This same shallow water is ideal for many designs of wave energy converters. While the majority of the development in wave energy converters is on a commercial scale, it is feasible to scale them down to cheaper, simpler versions of existing designs. For example, DARPA worked with the Monterey Bay Aquarium Research Institute (MBARI) to develop a power generation buoy in the Monterey Bay that developed more than 400 watts in normal conditions [9]. This buoy utilized hydraulic pressure to generate power, but it is a perfect example of where a linear generator could have been substituted to simplify the design.

The Remus 600 Survey line of AUVs that the Navy uses extensively have an 11.8kWh battery pack which allows for mission times of at least 33 hours [8]. At that power rate, the MBARI buoy could provide the power needs of one of these AUVs indefinitely in normal operating conditions, and if a similar setup were employed by the Navy it has the potential to eliminate the AUVs dependence on a support ship. The drawback is that a bright yellow buoy is not practical in every situation where the Navy may want to deploy one of their AUVs. Other designs of wave energy converters lend themselves better to being deployed in a non-obvious fashion if that is important; see Chapter II for more details on wave energy converter designs.

A persistent presence of these types of devices without a need for constant support vessel use is a game changing idea. Whether providing surveillance for the defense of U.S. ports and bodies of water or gathering intelligence in areas of interest, the benefits gained through the use of minimally supported AUVs would be significant.

C. THESIS OBJECTIVES, CONTRIBUTIONS AND ORGANIZATION

The expressed interest of this research is to aid in the understanding of linear generators for use by the DOD. In particular, what are the benefits and limitations of linear generators and where is it appropriate to commit further research for their use. In order to accomplish this goal a Simulink model is developed that allows for a flexible study of linear generator behavior in different configurations. The model is used to explore the feasibility of differing input functions as well as the effects of changing certain parameters of a model generator.

This work is separated into five chapters. Chapter I discusses background information that is germane to the research in order to aid the reader in understanding the motivations and implications of the work. Chapter II is a dialog on technologies that are related to the real world application of linear generators. Chapter III speaks to the methods and specific scenarios used in developing various linear generator models. In Chapter IV, the results from the simulations are discussed and the meanings behind said results are teased out. Chapter VI draws conclusions on the work and discusses the need for future work. All MATLAB and Simulink code is included in its entirety in the Appendix.

THIS PAGE INTENTIONALLY LEFT BLANK

II. RELATED TECHNOLOGY: POWER ELECTRONICS AND ENERGY HARVESTERS

This chapter will discuss technologies that are related to power generation utilizing linear generators. This includes a look at power electronics such as solid state power converters and battery management systems. There will also be a discussion of emerging methods of power generation that are applicable to linear generators such as energy harvesting of mechanical vibrations and various wave energy converters.

A. SOLID STATE POWER CONVERTERS

The recent progress in brushless dc machines would not be possible without the use of advanced solid state power converters. In order to allow for a dc machine to operate without brushes, the mechanical commutation that was being performed by the brushes must be replaced with electronics that perform the same function. When this is done the machine is said to be electrically commutated.

Solid state power converters exist in a large variety of topologies. Generically, they fall into four groups: ac-ac converters, dc-dc converters, ac-dc converters and dc-ac converters. It is also possible for a single converter to be designed to operate in both directions. Within each of these groups the power supplies can be again split into two additional types: linear and switching power supplies.

Linear power supplies operate the transistors in linear mode in order to provide the desired output power level and quality. The advantage of linear power supplies is their performance. The disadvantage of linear power supplies is their generation of excess heat and inherent need to dissipate it, this heat is also a form of wasted power and thus, linear power supplies have lower peak efficiencies than switching power supplies [10].

Switching power supplies operate by turning a solid state switch, which connects the source power to the output power, on and off at a high frequency. By using an inductance (L) or inductance-capacitance (*LC*) circuit design the output voltage can made lower or higher than the source voltage. The disadvantages of switching power supplies

are added complexity, which can lead to higher cost and lower reliability. The advantages to switching power supplies are their efficiency, weight and size.

By regulating their duty cycle, switching power supplies can continuously correct to provide a regulated output voltage from a non-regulated source. In this way, one could charge a battery at a precise voltage or a precise current, even using a power source which fluctuates. The reverse is also true; switching power supplies can provide a variable output utilizing a constant power source.

A power supply that takes a variable input voltage (usually, but not necessarily periodic) and creates a dc output is called a rectifier. Most of the power supplies that are associated with small portable electronics are this type. The output of a rectifier can be regulated or unregulated, depending on the quality of the source and the quality desired in the output. For sensitive equipment, such as computers, the output will be regulated. In less sensitive applications, like simple battery chargers, the output may be less regulated to reduce complexity and cost.

The Institute of Electrical and Electronics Engineers (IEEE) defines a power supply that takes a dc input and creates an ac output as an inverter [11]. Inverters range from simple oscillators to sophisticated solid state electronic circuits. An inverter does not have to create a sine wave output, it could create a triangle wave, square wave or any other periodic output as this would still meet the definition of an ac output. As with the other power supplies, the degree of complexity depends on the application. A common means of quantifying the quality of an inverter that produces a sine wave output is to measure its total harmonic distortion (THD), where THD is a ratio of the root mean square (rms) of the amplitude of all of the distortion harmonics over the rms of the amplitude of the fundamental [10]. Companies often specify requirements for, or the quality of, their products in this manner.

B. BATTERY CHARGERS AND MANAGEMENT SYSTEMS

The variety of batteries available on the market is seemingly endless, and while not all batteries need a charger designed specific to their specifications, quite a large number of them do. There are then, appropriately, a large number of battery chargers

available as well. Despite these large numbers, these chargers can be reduced to two categories: simple (dumb) chargers and smart chargers.

Simple chargers supply a constant output voltage without regard to the state of the battery. This output can be a constant dc or a pulsed output that remains at a set value. Because simple chargers lack any ability to sense the condition of the battery, they typically charge at a slower rate (utilizing a lower voltage) to prevent severe overcharging which can permanently damage a battery. Simple chargers are generally cheaper which makes them an attractive option under certain circumstances [12].

Smart chargers vary their output based on the conditions of the battery. Some smart chargers are designed to be used with smart batteries which have onboard sensors which communicate to the charger, while other smart chargers operate without the luxury of on-battery sensors. For those operating without the use of on-battery sensors, they monitor their own output voltage and current to determine the state of the battery, and in many cases this method is sufficient and safe. In the case of lithium batteries; however, it is insufficient, which is why lithium ion batteries always contain onboard sensors in order to communicate their state to their charger [12].

When a smart charger acts to maintain a battery, whether it is a single cell or a pack, within a set of parameters it is performing the duties of a battery management system (BMS). This is necessary because many modern battery types become unstable and seriously dangerous outside of a small window of conditions. According to [12] a BMS may perform any of the following functions:

- Monitor the battery;
- Protect the battery;
- Estimate the battery's state;
- Maximize the battery's performance;
- Report status and/or history of the battery to users or devices.

Some devices have only single cell batteries (like cell phones), while other devices utilize a battery pack which contains multiple cells arranged in series or parallel or a combination of the two. Where the technology of BMSs is concerned, there is a sizeable leap in complexity associated with charging a battery pack vice a single cell.

This is because individual cells still need individual attention in order to charge quickly and safely and maintain their health. As a result, these BMSs may have entire arrays of sensors and may require multiple outputs to be tailored to different groups or individual cells.

Regulated power supplies enable complex management systems created for the purpose of safely and efficiently charging batteries. It is this pair of technologies that could enable an inexpensive linear generator with low power quality output to be used to supply power to a bus or a battery bank.

C. APPLICATIONS OF LINEAR GENERATORS

Linear generators, also called linear alternators, have a growing list of modern applications. Linear generators are particularly well suited to cases which involve reciprocating motion. Some of the most prominent or promising applications are in free-piston Stirling engines, crankless internal combustion engines and energy harvesting, including wave energy converters and vibration harvesting attenuators.

1. Free-piston Stirling Engine

Free-piston Stirling engines have become an emerging technology use of the linear generator. Stirling engines require only a difference in temperature to operate, which allows them to be useful in a vast number of situations. They can operate with a traditional fuel source (i.e., burning of fossil fuels) or more extraordinary heat sources like radioisotope decay or concentrated sunlight; they are also useful for utilizing waste heat from various processes [13].

Two uses stand out in the realm of free-piston Stirling engines. The first is a space application, the Stirling radioisotope generator (SRG), shown in Figure 2. The SRG is a new and more efficient take on the radioisotope thermoelectric generator (RTG) that NASA has been using for years. While the RTG achieves an efficiency of around six percent, the new SRG will be four times as efficient and therefore use only a fourth of the plutonium required of the older units [14].

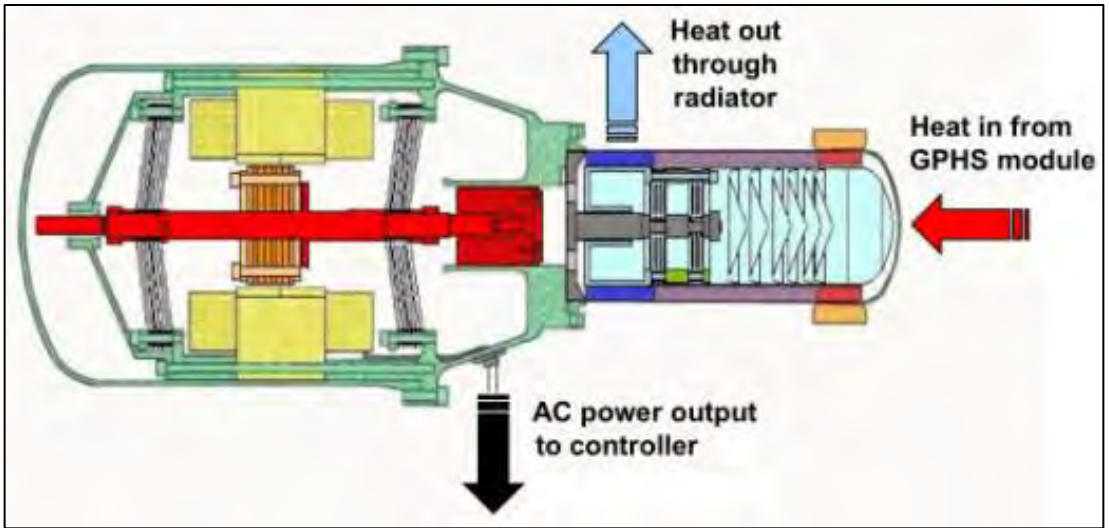

Figure 2. Free-piston Stirling engine and linear generator portions of an SRG, from [14].

The second application of the free-piston Stirling engine is its employment in solar concentrators. When utilized with solar concentrators, the power of the sun is reflected by a parabolic dish or trough and focused on a free-piston Stirling engine, which operates a linear generator to produce electricity from solar energy without the need of expensive photovoltaic cells; a depiction of this setup can be seen in Figure 3. In this configuration, solar energy can be collected at an efficiency of nearly 30 percent [15].

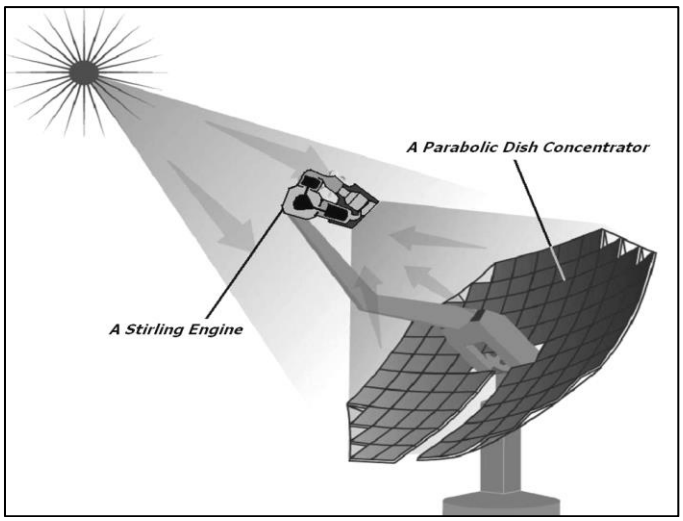

Figure 3. Depiction of a solar concentrator utilizing a reflective parabolic dish and a Stirling engine, from [15].

2. Crankless Internal Combustion Engines

In this clever application of the linear generator the standard internal combustion engine is reimagined to replace the pistons with linear generators. The resulting machine removes the need for gear boxes, drive shafts and additional generators. The benefits are three fold. The first benefit is a reduction of size and weight which adds to the overall efficiency and responsiveness of a vehicle. The second benefit is a reduction in moving parts which can lead to lower cost, greater simplicity and higher reliability in basic applications. The third benefit is an increase in efficiency by eliminating unnecessary mechanical losses caused by the outmoded mechanical systems. An example free-piston linear generator designed for a hybrid vehicle application can be seen in Figure 4, where TDC stands for top dead center and BDC for bottom dead center, representing the respective extremes of the piston stroke. The spring back volume acts as an air spring that limits the motion of the piston on one end of the cycle.

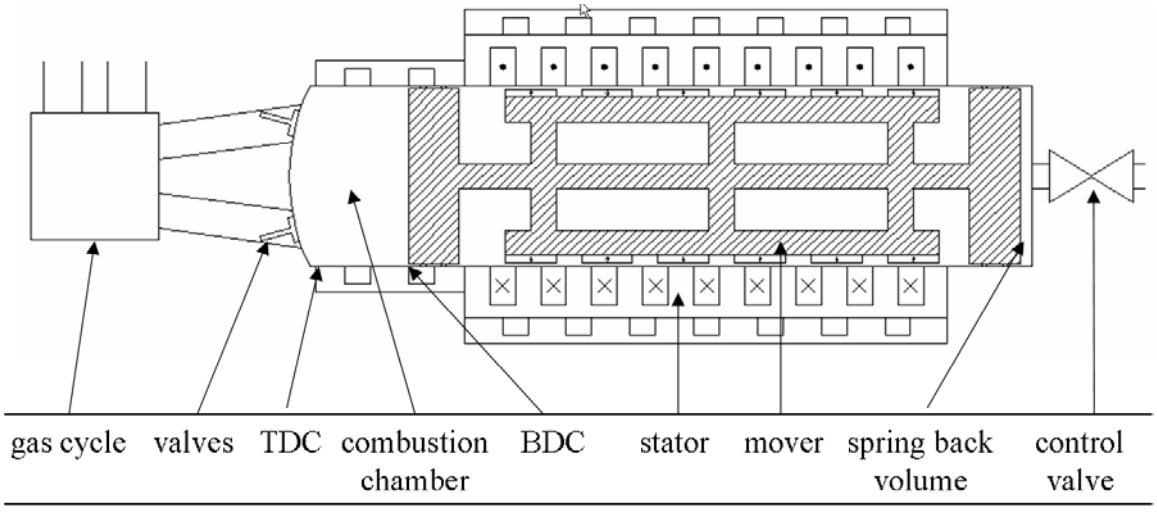

Figure 4. Example of a hybrid vehicle free-piston linear generator, from [16].

This application of the linear generator is especially relevant given the growing trend of vehicle manufactures to incorporate electric drive technologies into their vehicles. Vehicles such as the BMW i3 currently utilize range extenders with no direct connection to the drivetrain, instead these internal combustion engines solely power

generators which in turn provide power solely to charge the vehicle battery and the electric drive motors [17].

3. Vibration Harvesters

Vibration harvesters are a niche market of specialized devices which generate electric energy from wasted mechanical energy in the form of vibration. Most commonly, these devices utilize piezoelectric material to convert the mechanical vibration into electric energy utilizing the piezoelectric effect, whereby an applied mechanical stress generates an electric charge. This very low power method of energy harvesting has applications mostly in remote sensors where electrical power is not available (e.g., wireless sensors on train cars). While piezoelectric harvesters are primarily utilized in situations with high frequency vibrations, situations with relatively low frequency vibrations lend themselves better to small linear generators. Companies like LORD MicroStrain produce both types of technologies commercially for use in their accompanying sensor systems [18], [19], [20].

While vibration harvesting can be very useful for providing power to remote sensors, using a linear generator to perform this action, when appropriate, can realize several advantages. Linear alternators have the potential to provide more power than piezoelectric systems given a large enough mechanical input. More interestingly, though, linear generators can provide controlled mechanical damping in a system. Many existing damper applications could benefit from replacing existing dampers with computer controlled active dampers, such as replacing the shock absorbers in a vehicle with compact linear generators. A U.S. patent was awarded for just such an application in October of 2005 [21].

4. Wave Energy Converters

A wave energy converter (WEC) is a device which generates electrical power by capturing the power found in ocean waves. WECs are grouped into several distinct categories:

1. Surface point absorbers—are typically buoys which harness power from the up-down motion they see while riding atop waves.

2. Surface attenuators—are floating snake-like devices which harness power through flexing action as waves travel along their length.
3. Subsurface point absorbers—act like surface point absorbers except that they follow the rise and fall of the ocean surface not through buoyancy, but through the difference in pressure that is caused by the passing waves.
4. Overtopping devices—are large devices which allow incoming waves to overtop them and cause the water height in them to exceed the water height of the water's surface. This resulting potential energy is harnessed by allowing the higher level water to drain through turbines.
5. Wave surge converters—are devices which harness the side-to-side oscillations that occur in shallow water waves. These devices are often large flaps that are hinged at the sea floor.

Of all of these categories of devices, only overtopping devices do not lend themselves to the direct application of linear generators. It may be surprising then to know that the majority of existing wave energy converter projects utilize hydraulics to store power which they then use to spin turbines attached to generators. This is partially because the higher the force and the lower the speed, the more suited the application is to a hydraulic power take-off method [22]. As the technology matures, however, there is a developing affinity for direct drive linear generators as the power take-off method of choice in wave energy converters. This growing fondness for linear generators is especially true in smaller devices in the kilowatt range, and they are even being implemented in much larger devices, such as the 2MW Archimedes Wave Swing shown in Figure 5.

There are challenges still to be solved in the design and application of linear generators on the scale required for commercial energy production. But the allure of lower maintenance requirements and higher reliability on objects that reside below the ocean surface is sure to keep linear generators a topic of interest and development in the wave energy converter community.

Figure 5. Permanent magnet linear generator, with workers inside, found in the Archimedes Wave Swing, from [22].

THIS PAGE INTENTIONALLY LEFT BLANK

III. LINEAR GENERATOR SYSTEM DESIGN AND MODELING

Chapter III will explain some basic machine theory necessary for the understanding of the constructed model. Next linear synchronous machines will be covered and finally the chapter will go into detail regarding construction of the Simulink model. Some assumptions are made about the construction of the machine in order to make the model more manageable. These lead to some limitations in its use, however, and present room for further work.

Although non-sinusoidal, the model machine is assumed to be half-wave symmetric which prevents it from containing any even harmonics. It is further assumed that the model generator does not enter saturation at any point in the simulation and that it does not exhibit any demagnetization by the permanent magnets. Cogging torque has also been neglected, which may be of some significance in a linear machine that is operating at low frequencies.

Sign and naming conventions for the model, as well as the detailed governing equations, are borrowed largely from Chapmen et al [23]. Attempts are made to point out where these conventions may differ from the standard or where there may not be a standard at all.

A. SYNCHRONOUS MACHINES

A synchronous machine is one in which the physical speed of the machine is an exact multiple of the electrical frequency of the machine. In these machines the magnetic fields of the stator (the stationary part of the machine) and rotor (the rotating part of the machine) rotate at the same speed and stay aligned with each other under normal operation. While it is not fixed, and either the rotor or stator may occupy the inner portion of the machine, it is more common to see the rotor on the inside surrounded by the stator. The magnetic poles produced by the electrical windings are perpendicular to the windings. Often in figures, such as Figure 6, the machine windings are depicted as a single lump winding. In modern machines, however, this is almost never the case; instead, distributed windings are employed, with the distribution done in a manner to

produce the back electromotive force (EMF) shape desired (e.g., sinusoidal back EMF or trapezoidal back EMF).

When there is no angle between the magnetic poles in the rotor and stator there is no torque produced, but as the angle gets larger it produces greater torque until it reaches 90° where it produces the maximum torque. Adding any load beyond this maximum torque will cause the machine to produce less torque and will induce an unstable behavior where the torque angle will quickly grow. Beyond 180°, the torque flips; if this occurs in an electrical machine, the machine is said to have stalled. Conditions of maximum and minimum torque are depicted in Figure 7. Also shown in Figure 6 is the rotor angle θ_r. It should be noted that in a machine with more than two poles instability will be reached at angles less than 90°.

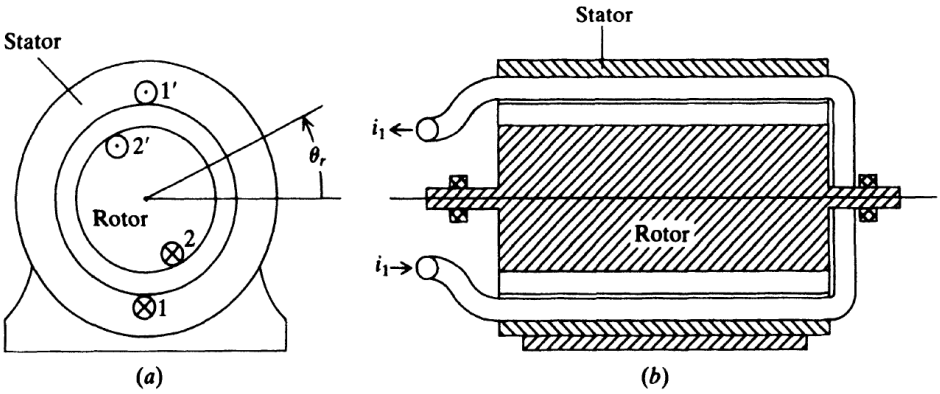

Figure 6. Simple two pole electrical machine diagram showing the rotor and stator. (a) End view; (b) cutaway cross-section view, from [24].

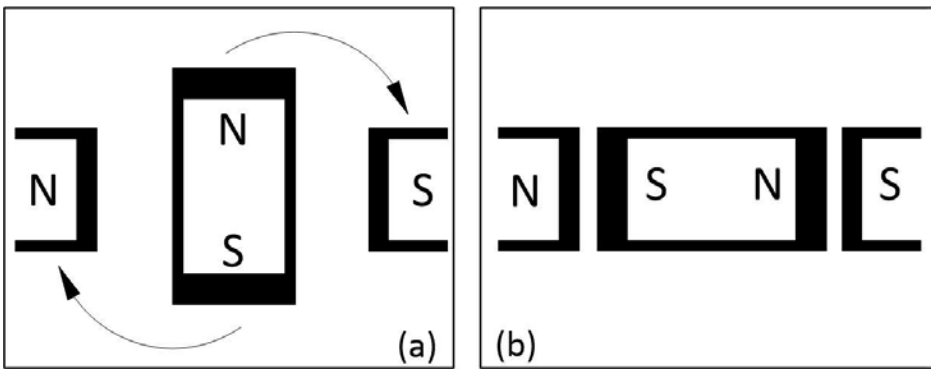

Figure 7. Magnets producing (a) maximum torque and (b) zero torque.

In terms of a synchronous motor, the rotating magnetic field of the stator is generated by a periodic current waveform supplied from a power source. The magnetic field strength H in a wire in free space is

$$H = \frac{I}{2\pi r} \tag{1}$$

where I is the current in the wire and r is the radius from the center of the wire. The flux density B is related to H by

$$B = \mu H. \tag{2}$$

Magnetic permeability μ is the measure of a material's ability to support a magnetic field. Normally, μ is expressed as the product of the permeability of free space constant μ_0 (e.g., the permeability of a vacuum) and the dimensionless relative permeability of the substance μ_r, $\mu=\mu_0\mu_r$. [24]

The magnetic field in the rotor of a synchronous machine can either be produced the same way, using an electrical current, or by placing permanent magnets on the rotor, thus eliminating the need for electrical connections to the rotating portion of the machine. In terms of a generator, it is the rotor that produces the rotating magnetic field, either through use of electrical current or permanent magnets. Each winding in the stator then sees a continuously varying magnetic field, which by the laws of magnetic induction induce a voltage on the winding. In 1833, Heinrich Lenz first stated that motors and generators were reversible; his findings were later summarized by James Clerk Maxwell in Lenz's law, which states that

$$\varepsilon = -\frac{d\lambda}{dt} \tag{3}$$

where ε is the EMF measured in volts, λ is the flux linkage, d is the derivative operator and t is time. The flux linkage of a winding is related to the vector of the magnetic field strength **B** by

$$\lambda = \int_S \mathbf{B} \bullet dS, \tag{4}$$

where • is the dot product operator and variables in bold represent vectors. The integration is taken over the area inside the winding. This can be simplified in the case of coils of wire to

$$\lambda = BA \tag{5}$$

where A is the surface area inside the coil. If there are N turns of wire in the same area with the same B field acting on them, then the total flux linkage is

$$\lambda = NBA. \tag{6}$$

To find the total voltage produced in a stator winding we need to look at both the EMF and the electrostatic voltage in the winding. The total voltage in the winding then is

$$v = ri + \frac{d\lambda}{dt}, \tag{7}$$

where r and i are the resistance and current in the stator. In a three-phase machine with stator phases a, b and c, the voltage in the stator can be described by

$$\mathbf{v}_{abcs} = r_s \mathbf{i}_{abcs} + \frac{d}{dt}\boldsymbol{\lambda}_{abcs}, \tag{8}$$

where $\mathbf{v}_{abcs}$, $\mathbf{i}_{abcs}$ and $\boldsymbol{\lambda}_{abcs}$ are generalized in the form

$$\mathbf{f}_{abcs} = \begin{bmatrix} f_{as} \\ f_{bs} \\ f_{cs} \end{bmatrix}, \tag{9}$$

and f_{as}, f_{bs} and f_{cs} are the a, b and c phases of stator voltage, current or flux linkage.

In a machine with a sinusoidal back EMF, the total flux linking the rotor and stator can be found by combining the flux from the permanent magnets on the rotor and the flux from all the windings. The flux experienced at a given winding from the permanent magnet is dependent on the rotor position at that time. More specifically, it is dependent on the rotor electrical angle θ_{re}. The electrical position of the rotor θ_{re} is related to the mechanical rotor angle θ_{rm} by the number of magnetic poles p in the motor per phase, where

$$\theta_{re} = \theta_{rm} \frac{p}{2}. \tag{10}$$

The flux linkage matrix $\boldsymbol{\lambda}_{abcs}$ then can be defined by

$$\boldsymbol{\lambda}_{abcs} = \mathbf{L}_s \mathbf{i}_{abcs} + \lambda'_m \begin{bmatrix} \sin(\theta_{re}) \\ \sin\left(\theta_{re} - 2\pi/3\right) \\ \sin\left(\theta_{re} + 2\pi/3\right) \end{bmatrix}, \tag{11}$$

where the peak flux linkage due to the permanent magnet λ'_m is a constant since it is assumed that the permanent magnets are not undergoing any demagnetization. The stator self-inductance matrix $\mathbf{L}_s$ for a non-salient machine is given by

$$\mathbf{L}_s = \begin{bmatrix} L_{ls} + L_{ms} & -1/2\, L_{ms} & -1/2\, L_{ms} \\ -1/2\, L_{ms} & L_{ls} + L_{ms} & -1/2\, L_{ms} \\ -1/2\, L_{ms} & -1/2\, L_{ms} & L_{ls} + L_{ms} \end{bmatrix}, \tag{12}$$

where L_{ls} and L_{ms} are the stator leakage and mutual inductances respectively.

Defined for generator action, the mechanical input torque τ_m and electrical counter-torque τ_e can be related to mechanical rotor speed ω_{rm} by

$$\tau_e - \tau_m = J \frac{d}{dt} \omega_{rm} + B_m \omega_{rm}, \tag{13}$$

where J is the rotational inertia of the rotor and B_m is the mechanical damping due to friction. The J term takes into account the machine's resistance to a change in speed and the B_m term accounts for losses in the machine due to friction, both in bearings and due to air resistance.

The electric torque τ_e that a machine generates is specific to the geometry of that machine. It can be complicated by a machine that has a non-sinusoidal winding distribution or by a machine that is salient (the width of the air gap between the stator and rotor varies because one or both is not round). If we assume the machine is sinusoidal in

its winding distribution and has a constant, non-salient, air gap then the electrical torque equation can be expressed by

$$\tau_e = \frac{p}{2}\left\{\frac{\sqrt{3}}{2}\left(i_{bs}^2 i_{cs}^2 - 2i_{as}i_{bs} + 2i_{as}i_{cs}\right) + \lambda_m'\left[\left(i_{as} - \frac{1}{2}i_{bs} - \frac{1}{2}i_{cs}\right)\cos\theta_{re} + \frac{\sqrt{3}}{2}\left(i_{bs} - i_{cs}\right)\sin\theta_{re}\right]\right\}. \tag{14}$$

The electrical machine that is depicted in the model will be of a non-sinusoidal nature and the equations specific to that problem will be discussed further in the modeling section.

B. LINEAR SYNCHRONOUS MACHINES

A linear machine is conceptually the same as a traditional rotating machine. It can be described as cutting and *unrolling* a rotating machine so that it is flat. A rotating machine is depicted in Figure 8, with the same machine *unrolled* in Figure 9 where

a_n, b_n, c_n stator windings depicting current flow into the page;

a_n', b_n', c_n' stator windings depicting current flow out of the page;

f_n rotor windings depicting current flow into the page;

f_n' rotor windings depicting current flow out of the page;

φ_r angular displacement along the rotor circumference;

φ_s angular displacement along the stator circumference;

ω_r rotor speed.

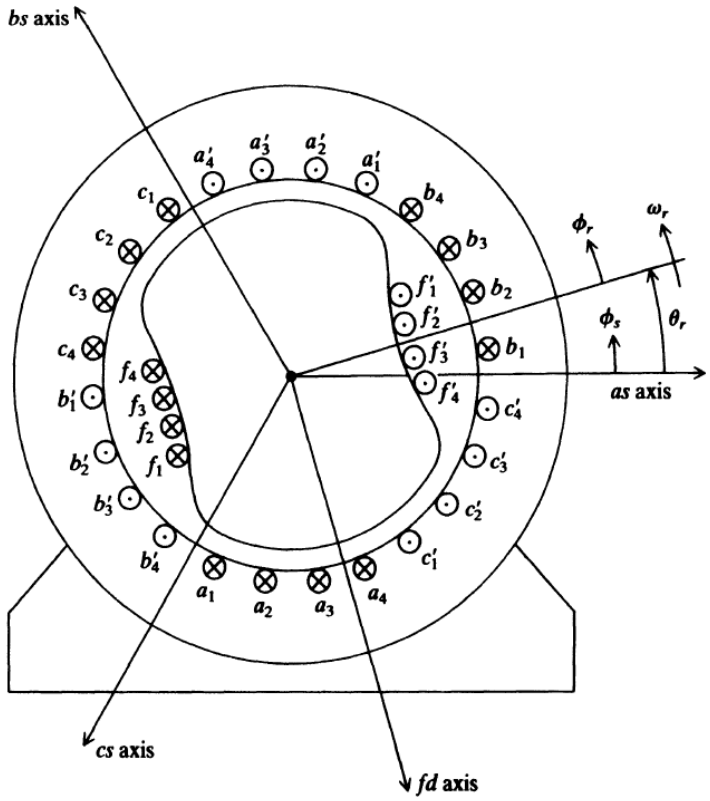

Figure 8. Example two-pole, three-phase salient-pole synchronous machine showing the general layout of windings and major axis, from [23].

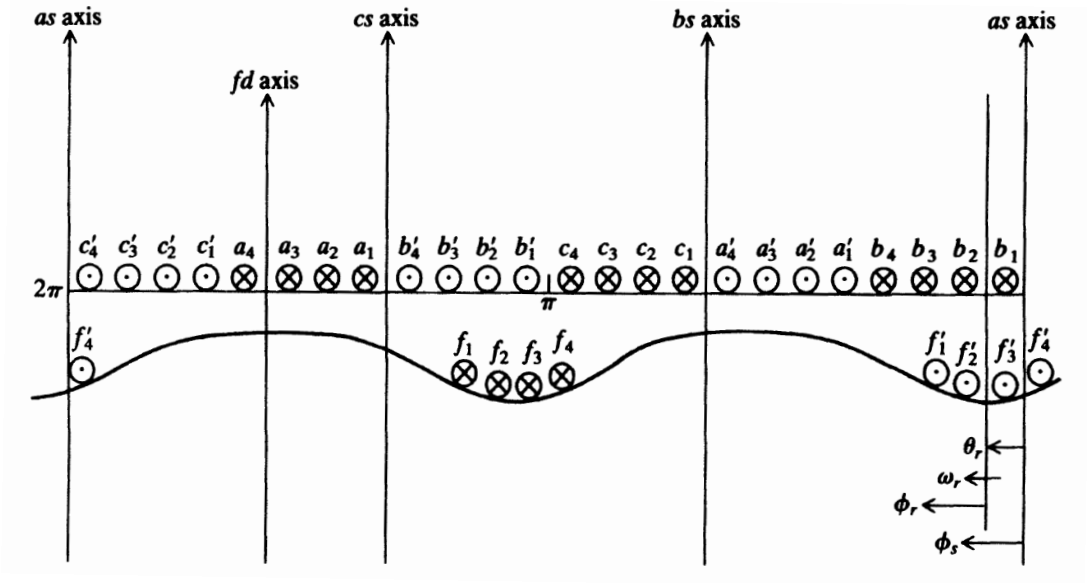

Figure 9. Rotating to linear machine *unrolling* concept visualized. The fluctuating line represents the salient air gap, from [23].

It is common to model or discuss a linear machine using the same equations and variables as a rotating machine. The results must be translated to terms and variables that can represent a linear machine. Torque can be related to force by

$$P = \tau\omega_{rm} = FV, \tag{15}$$

where P is power, F is force and V is linear velocity. Electrical power into the three phase machine P can be calculated using machine parameters by

$$P = v_{as}i_{as} + v_{bs}i_{bs} + v_{cs}i_{cs}. \tag{16}$$

The length of the linear machine l_{lm} can be approximated using the radius of the rotating machine by $l_{lm} \cong 2\pi R$. This is not exact because one has to choose a radius, as the radius of the rotor and stator will differ. In the case of small machines the difference could amount to a large percentage of the total circumference. Unlike a rotating machine where the entirety of the stator always is interacting with the rotor and likewise the entirety of the rotor is always interacting with the stator, portions of a linear machine are not interacting with each other at any given time. This is because either the stationary portion of the machine (still referred to as a stator) or the moving portion of the machine (referred to as a translator) is designed longer than the other. This extra length is the allowable travel of the linear machine without producing generally undesirable results, and is shown in Figure 10. There is no standard for whether the stator or the translator is the portion with permanent magnets, the choice is a balance of cost and performance. Permanent magnet material is more expensive than wires, but magnets do not require any electrical connections allowing for cheaper more reliable designs.

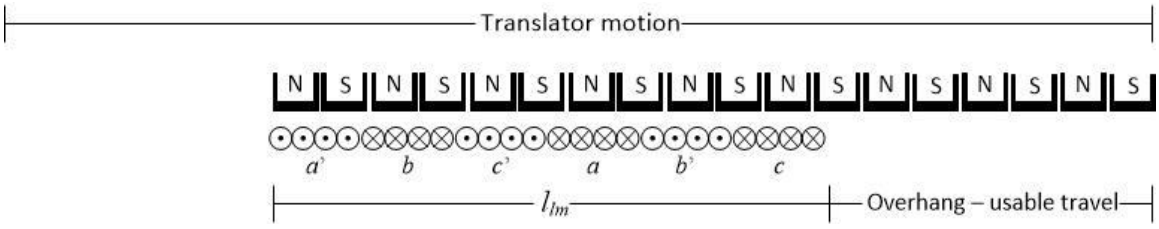

Figure 10. Example three-phase linear machine setup with permanent magnet translator.

C. MODELING

In [25], Chapman et al. discuss modeling a three-phase non-sinusoidal permanent magnet synchronous machine using a rotor reference frame method. Using the Chapman and company machine description and experimental results, the following Simulink model is developed and applied to a linear machine of notionally similar characteristics.

In the synchronous machines section, machine equations were presented for, arguably, the simplest type of rotating synchronous machine, a three phase permanent magnet machine with a constant, non-salient air gap which has a sinusoidal winding distribution resulting in a sinusoidal back EMF. The machine described and modeled here (and in [25]) however has a non-sinusoidal back EMF. A trapezoid is a common waveform for a non-sinusoidal machine to utilize. There are several reasons for choosing this including easier, cheaper construction, increased power density and smaller inverter sizes for motors [25]. The non-sinusoidal choice results in machine equations which must account for the harmonic components of the waveforms. While the equations account for an infinite number of harmonic components, in practice only a few are used in modeling. In this case it is also assumed that, although non-sinusoidal, the back EMF is half-wave symmetric which eliminates the even harmonics.

1. Machine Variable Equations for a Non-Sinusoidal Machine

In the non-sinusoidal machine equations the stator voltage equation (8) and the self-inductance matrix (12) remain the same while the flux linkage equation (11) becomes

$$\boldsymbol{\lambda}_{abcs} = \mathbf{L}_s \mathbf{i}_{abcs} + \lambda'_m \sum_{n=1}^{\infty} K_{2n-1} \begin{bmatrix} \sin\left((2n-1)\theta_{re}\right) \\ \sin\left((2n-1)\left(\theta_{re} - \frac{2\pi}{3}\right)\right) \\ \sin\left((2n-1)\left(\theta_{re} + \frac{2\pi}{3}\right)\right) \end{bmatrix}, \tag{17}$$

and the torque equation (14) becomes

$$\tau_e = \left(\frac{3}{2}\right)\left(\frac{p}{2}\right)\lambda'_m \sum_{n=1}^{\infty} K'_{2n-1} \begin{bmatrix} i_{as} & i_{bs} & i_{cs} \end{bmatrix} \begin{bmatrix} \cos\left((2n-1)\theta_{re}\right) \\ \cos\left((2n-1)\left(\theta_{re} - \frac{2\pi}{3}\right)\right) \\ \cos\left((2n-1)\left(\theta_{re} + \frac{2\pi}{3}\right)\right) \end{bmatrix}, \quad (18)$$

where the K_n coefficients from (17) represent the magnitude of the harmonic components of the flux linkage and the coefficients $K'_n = nK_n$ and represent the harmonic components of the torque in (18) [25].

2. Rotor Reference Frame Model Using *qd0* Variable

The Simulink model also utilizes the rotor reference frame through a transformation of variables. Using a transformation of variables in order to analyze three phase systems dates back to 1929 when Robert H. Park first published the Park's transformation [23]. Since then, the very similar direct-quadrature-zero (*qd0*) transformation has replaced the Park's transformation as a standard transformation for three phase systems. In the *qd0* transformation, the *a*, *b* and *c* phase variables are projected onto a new set of reference frame axes that are defined as the *q, d and 0* axes, as shown in Figure 11. Where f_{as}, f_{bs} and f_{cs} are the *a*, *b* and *c* axes and f_{ds} and f_{qs} are the d and q axis. The *0*-axis is not shown, but would originate from the intersection of the other axes and be positive out of the page.

The reason the *0*-axis is not shown is because when the *qd0* transformation is applied to a three-phase system, which has sinusoidal geometry (which is common), the *0*-axis variables go to zero and only the *q* and *d* axes variables are left. A major advantage to using the *qd0* transformation is that it allows for simplified direct torque control in electrical machines.

Despite no need for a transformation (as there is no controller and the model is non-sinusoidal), the model needs to keep this format for added utility in any follow-on work where a controller might be added.

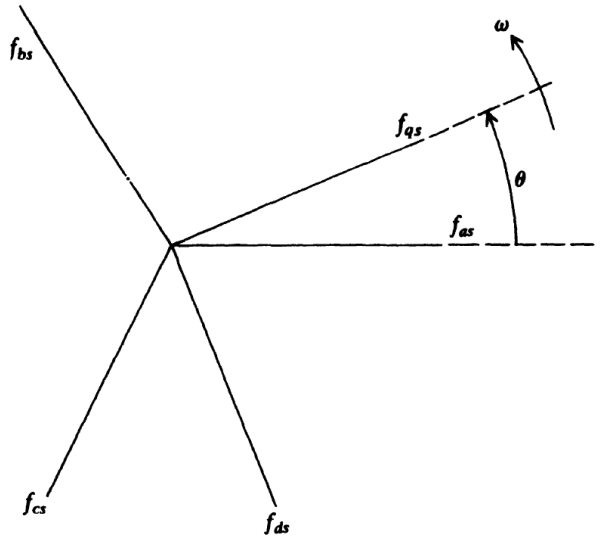

Figure 11. Axis relationships for an abc to qd0 variable transformation. The 0-axis, not depicted, originates from the intersection of the axes and is positive out of the page, from [23].

In order to perform a *qd0* transformation, multiply the machine variables by the transformation matrix **K**. Since we are interested in transforming stator variables onto the rotor reference frame, we will use an electrical rotor angle (θ_{re}) as the reference in the transformation and the resulting transformation matrix will be termed $\mathbf{K}_s^r$ where

$$\mathbf{K}_s^r = \frac{2}{3}\begin{bmatrix} \cos(\theta_{re}) & \cos\left(\theta_{re}-\frac{2\pi}{3}\right) & \cos\left(\theta_{re}+\frac{2\pi}{3}\right) \\ \sin(\theta_{re}) & \sin\left(\theta_{re}-\frac{2\pi}{3}\right) & \sin\left(\theta_{re}+\frac{2\pi}{3}\right) \\ \frac{1}{2} & \frac{1}{2} & \frac{1}{2} \end{bmatrix}, \tag{19}$$

the new stator variables in the *qd0* rotor reference frame are now generalized as $\mathbf{f}_{qd0s}^r$, where

$$\mathbf{f}_{qd0s}^r = \begin{bmatrix} f_{qs}^r \\ f_{ds}^r \\ f_{0s}^r \end{bmatrix} \tag{20}$$

and

$$\mathbf{f}_{qd0s}^{r} = \mathbf{K}_{s}^{r}\mathbf{f}_{abcs}. \tag{21}$$

The new *q* and *d* axes in the rotor reference frame are shown in Figure 12. It can be seen that the *q*-axis and the *d*-axis are in quadrature (i.e., 90° apart). Note too that the *q*-axis is the one that is referenced by θ_{rm}; this is contrary to most literature where the *d*-axis is the reference. This has the effect of reversing the sine and cosine terms in several equations which might otherwise be easily recognizable to those familiar with electrical machine analysis.

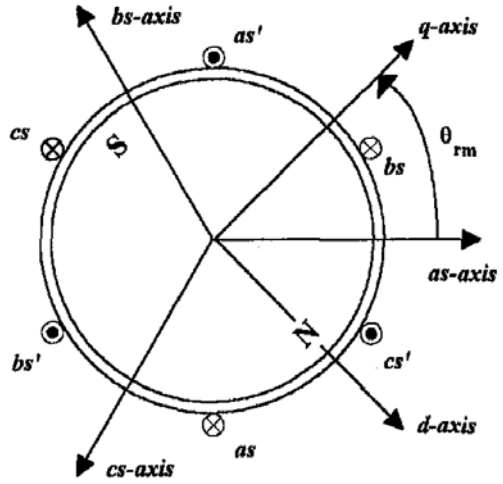

Figure 12. Cross section of a three-phase non-salient permanent magnet synchronous machine with the q-axis and d-axis shown, from [25].

To convert back from *qd0* variables to *abc* variables, the inverse transformation matrix $\left(\mathbf{K}_{s}^{r}\right)^{-1}$ is applied, where

$$\mathbf{f}_{abcs} = \left(\mathbf{K}_{s}^{r}\right)^{-1}\mathbf{f}_{qd0s}^{r}, \tag{22}$$

and

$$\left(\mathbf{K}_{s}^{r}\right)^{-1} = \begin{bmatrix} \cos(\theta_{re}) & \sin(\theta_{re}) & 1 \\ \cos\left(\theta_{re} - 2\pi/3\right) & \sin\left(\theta_{re} - 2\pi/3\right) & 1 \\ \cos\left(\theta_{re} + 2\pi/3\right) & \sin\left(\theta_{re} + 2\pi/3\right) & 1 \end{bmatrix}. \tag{23}$$

From [25], if the *qd0* transformation is applied to the machine equations for voltage, flux linkage and torque in a non-sinusoidal machine then (8) for voltage becomes

$$v_{qs}^{r} = r_s i_{qs}^{r} + \omega_{re}\lambda_{ds}^{r} + \frac{d}{dt}\lambda_{qs}^{r}; \tag{24}$$

$$v_{ds}^{r} = r_s i_{ds}^{r} - \omega_{re}\lambda_{qs}^{r} + \frac{d}{dt}\lambda_{ds}^{r}; \tag{25}$$

$$v_{0s}^{r} = r_s i_{0s}^{r} + \frac{d}{dt}\lambda_{0s}^{r}, \tag{26}$$

equation (17) for flux linkage becomes

$$\lambda_{qs}^{r} = \left(L_{ls} + \frac{3}{2}L_{ms}\right) i_{qs}^{r} + \lambda_m' \sum_{n=1}^{\infty} \left(K_{6n-1} + K_{6n+1}\right) \sin\left(6n\theta_{re}\right); \tag{27}$$

$$\lambda_{ds}^{r} = \left(L_{ls} + \frac{3}{2}L_{ms}\right) i_{ds}^{r} + \lambda_m' + \lambda_m' \sum_{n=1}^{\infty} \left(K_{6n-1} - K_{6n+1}\right) \cos\left(6n\theta_{re}\right); \tag{28}$$

$$\lambda_{0s}^{r} = \left(L_{ls} + \frac{3}{2}L_{ms}\right) i_{0s}^{r} + \lambda_m' \sum_{n=1}^{\infty} K_{6n-3} \sin\left(\left(6n-3\right)\theta_{re}\right), \tag{29}$$

and (18) for torque becomes

$$\begin{aligned} \tau_e = \left(\frac{3}{2}\right)\left(\frac{p}{2}\right)\lambda_m' \Bigg[& i_{qs}^{r} \left(1 + \sum_{n=1}^{\infty} \left(K_{6n-1}' + K_{6n+1}'\right) \cos\left(6n\theta_{re}\right)\right) \\ & + i_{ds}^{r} \sum_{n=1}^{\infty} \left(K_{6n-1}' - K_{6n+1}'\right) \sin\left(6n\theta_{re}\right) + 2 i_{0s}^{r} \sum_{n=1}^{\infty} K_{6n-3}' \cos\left(\left(6n-3\right)\theta_{re}\right) \Bigg]. \end{aligned} \tag{30}$$

In (16) it was shown that power can be calculated using *abc* machine variables; power can also be calculated using *qd0* variables where

$$P = \frac{3}{2}\left(v_{qs}^{r} i_{qs}^{r} + v_{ds}^{r} i_{ds}^{r} + 2 v_{0s}^{r} i_{0s}^{r}\right). \tag{31}$$

3. Simulink Model

The full Simulink model, along with the initial conditions file and the post script, are included in the appendix. This section will look at selected portions of the model in

some detail, including an explanation of where equations were implemented in various subsections.

In order to provide a useful reference, the top level block diagram of the model can be seen in Figure 13. Here we can see the various subsections of the model and the signals that are passed amongst them. Blocks that are labeled "To Workspace" represent variables which are passed to the MATLAB command window for use by the post-script file in creating various plots presented in Chapter IV. It is not uncommon to see the same variable represented differently on the same screen or across different screens because of restrictions on naming and repeating variables in Simulink windows.

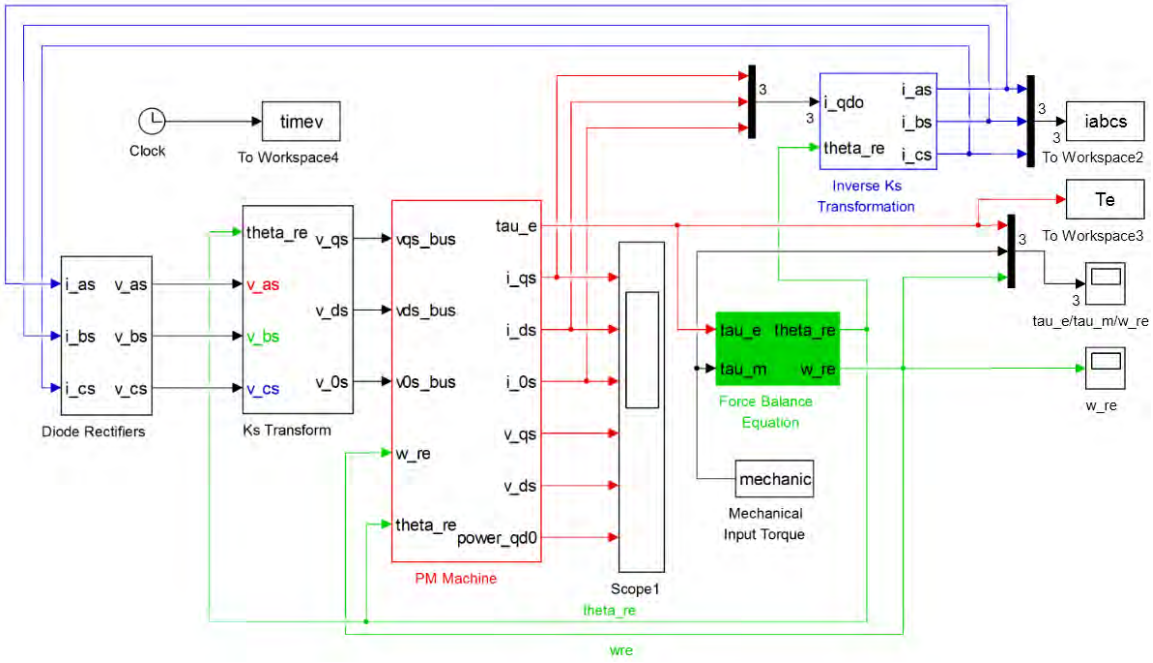

Figure 13. Simulink top level block diagram of the model.

One of several *qd0* transformations is depicted in Figure 14. This has been done through the implementation of Equations (19)–(21), and in this instance the voltage variables were transformed. Note that θ_{re} is used in this transformation. By orienting on the rotor electrical position in the transform we have implemented the rotor reference frame, which is rotating at ω_{re}. This is sometimes called the synchronous reference frame

because it is rotating at the electrical angular velocity of the air-gap rotating magnetic field. Other reference frames, such as the stationary reference frame or the mechanical rotor reference frame, are sometimes used depending on the application. Other reference frames may rotate at a speed unrelated to the machine and are termed arbitrary reference frames. Commonly, these the transformations are depicted by different superscripts above the variables. There is no established notation to reference so readers should be careful when viewing texts on the subject [23].

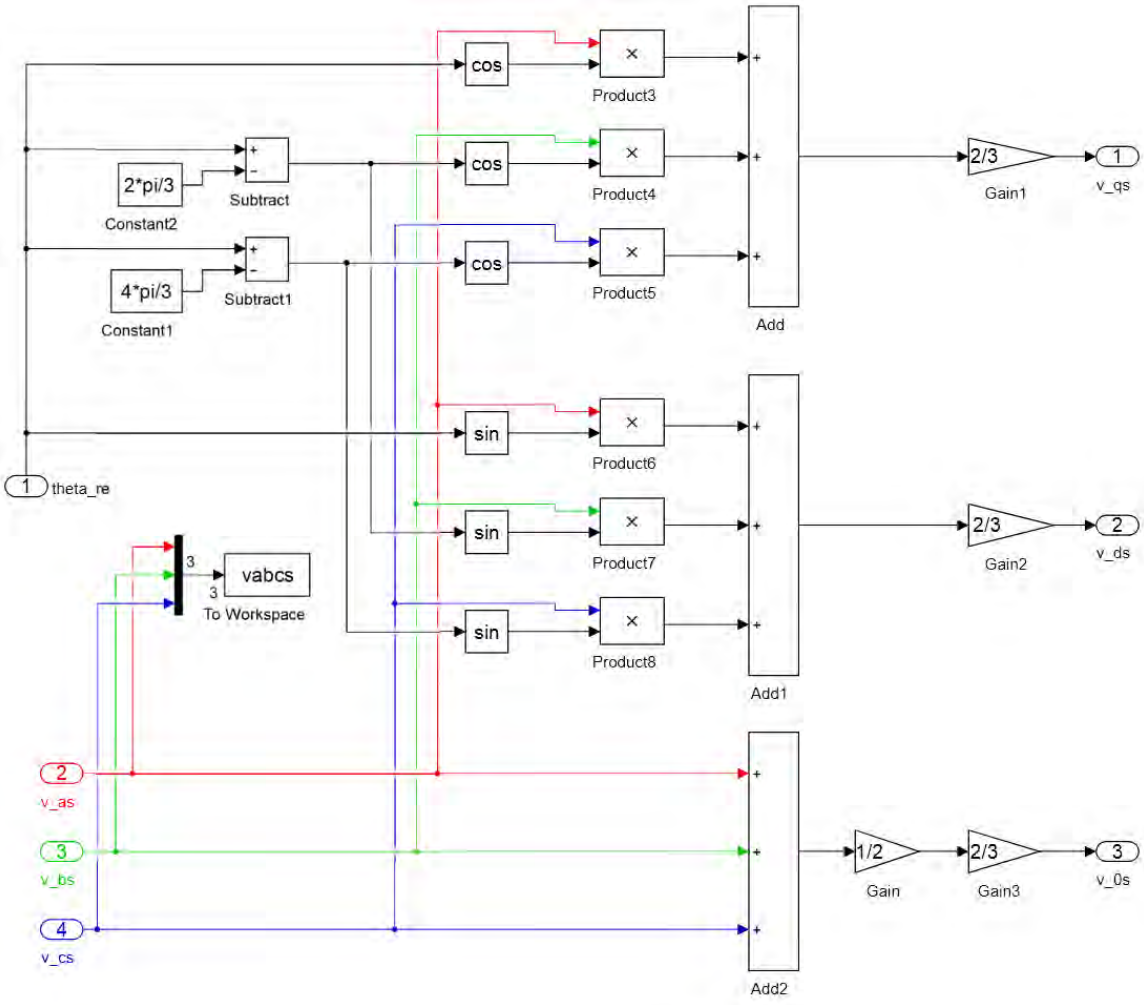

Figure 14. Simulink model subsection depicting a *qd0* transformation via the implementation of Equations (19)–(21).

The reverse transform, acting on the *qd0* current variables and reforming the *abc* current variables, is shown in Figure 15. Here we have implemented Equations (22) and (23).

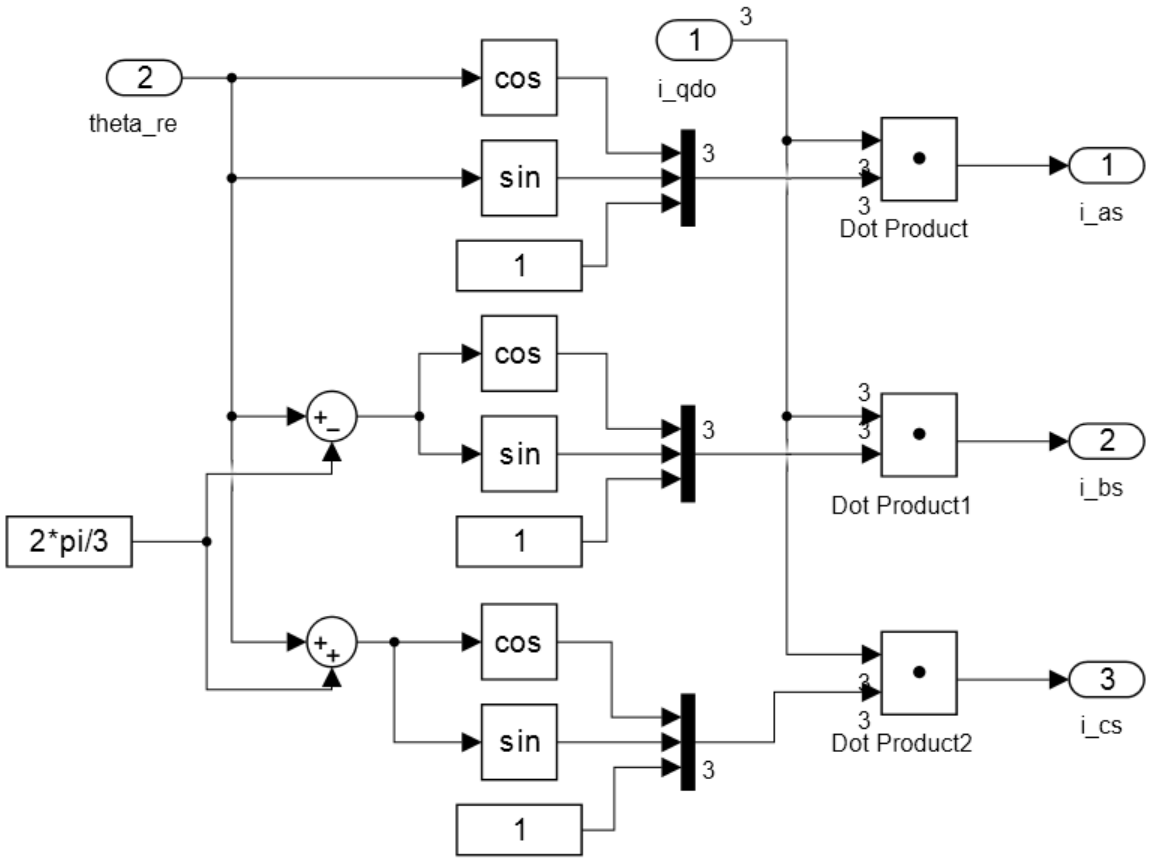

Figure 15. Simulink model subsection depicting a reverse *qd0* transformation via the implementation of Equations (22) and (23).

The bulk of the permanent magnet synchronous machine is implemented as a large subsection with several smaller subsections within it, the larger subsection can be seen in Figure 16.

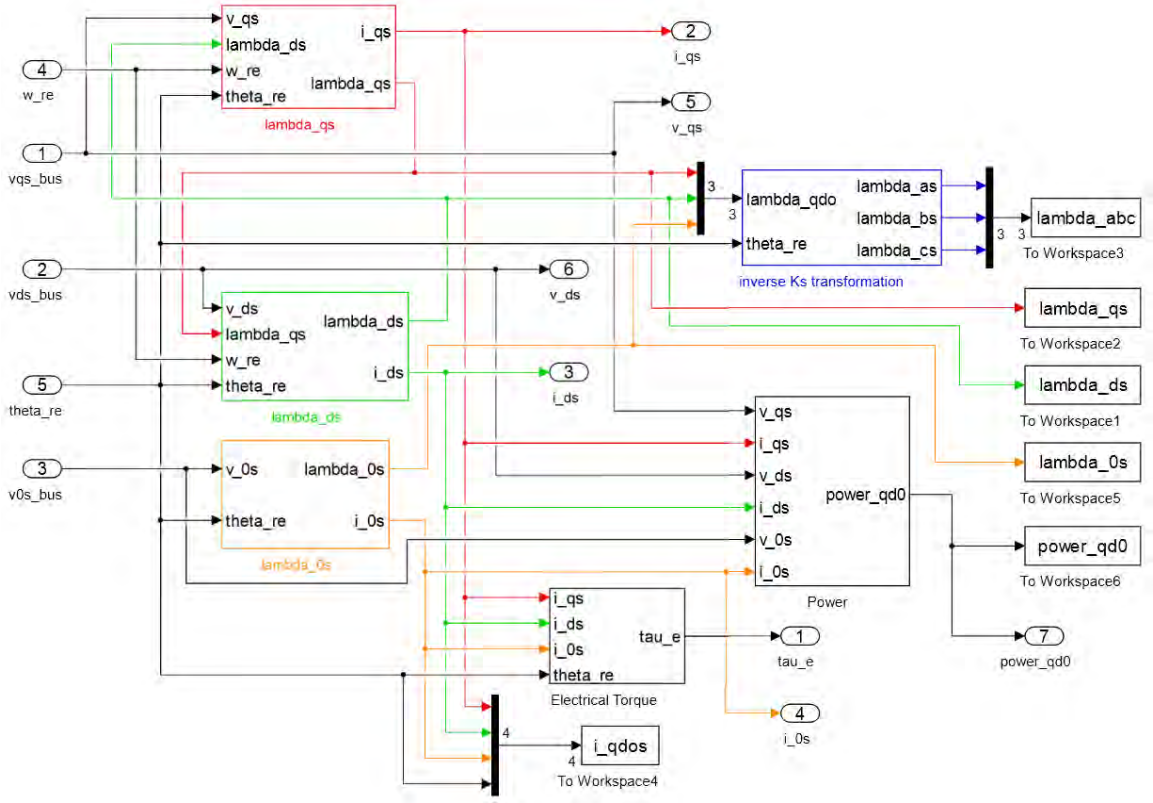

Figure 16. Simulink model subsection depicting the related smaller subsections within the permanent magnet synchronous machine block.

Progressing deeper into the permanent magnet synchronous machine, the flux linkage and current are determined separately for each of the *qd0* variables. Each variable is governed by different but related equations. For the f_{qs}^{r} variables, λ_{qs}^{r} is discovered by rearranging the v_{qs}^{r} equation (24). The *q*-axis stator current i_{qs}^{r} is found using the newly developed λ_{qs}^{r} through the rearrangement and implementation of (27), as seen in Figure 17 where "lambda_m" is the constant λ_{m}' and the gain "1/(Lss)" refers to $L_{ss} = L_{ls} + (3/2)L_{ms}$.

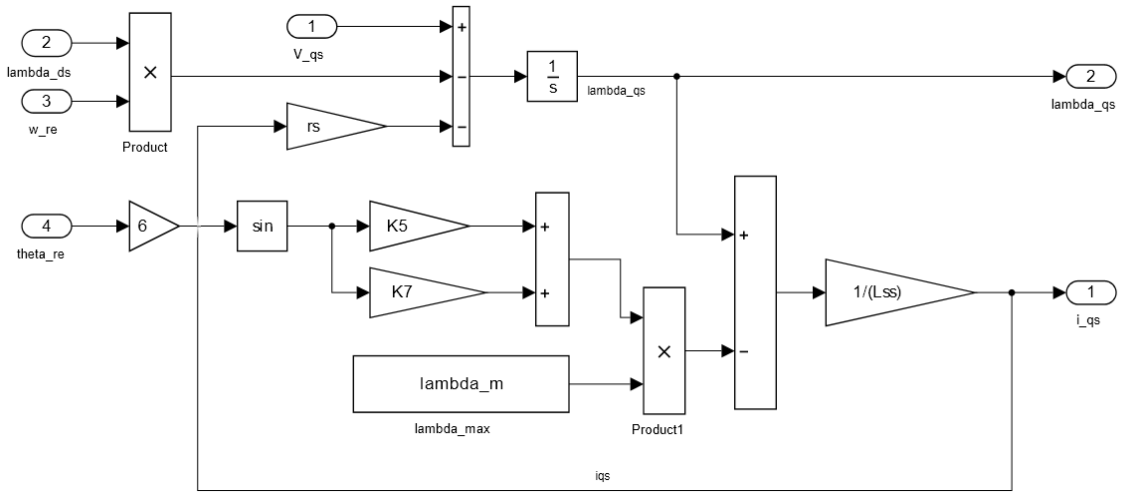

Figure 17. Simulink model subsection depicting the development of λ_{qs}^{r} and i_{qs}^{r} utilizing Equations (24) and (27) respectively.

The *d*-axis flux linkage λ_{ds}^{r} and current i_{ds}^{r} variables are found in a similar fashion using (25) and (28), and are depicted in Figure 18. While λ_{0s}^{r} and i_{0s}^{r} utilize (26) and (29) as seen in Figure 19.

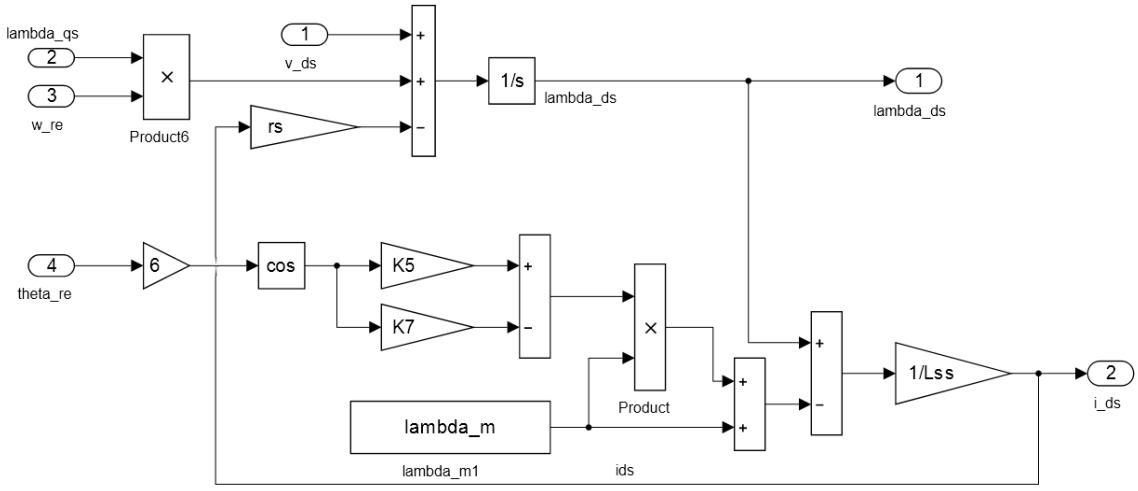

Figure 18. Simulink model subsection depicting the development of λ_{ds}^{r} and i_{ds}^{r} utilizing Equations (25) and (28) respectively.

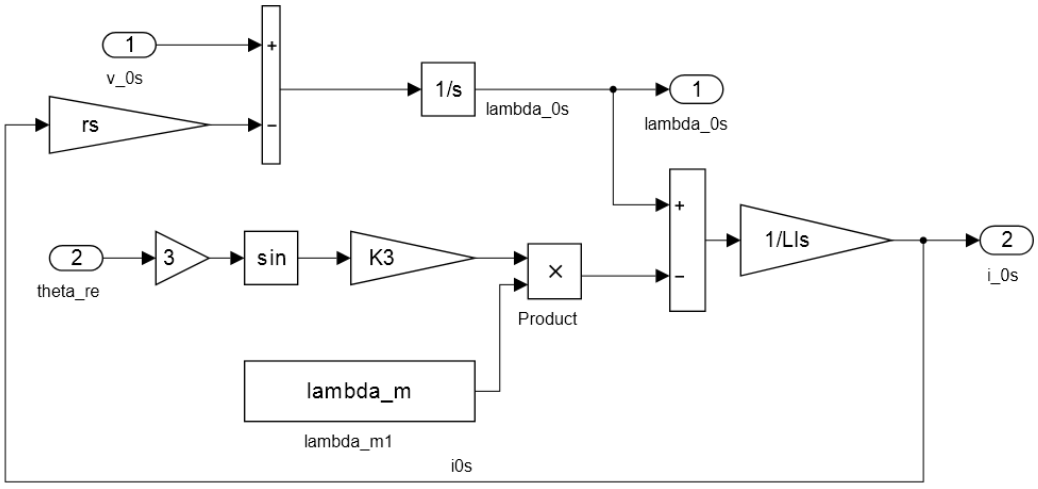

Figure 19. Simulink model subsection depicting the development of λ_{0s}^{r} and i_{0s}^{r} utilizing Equations (26) and (29) respectively.

The electrical power P that the machine generates from the input mechanical torque applied is developed from *qd0* variables by implementing (31), as seen in Figure 20.

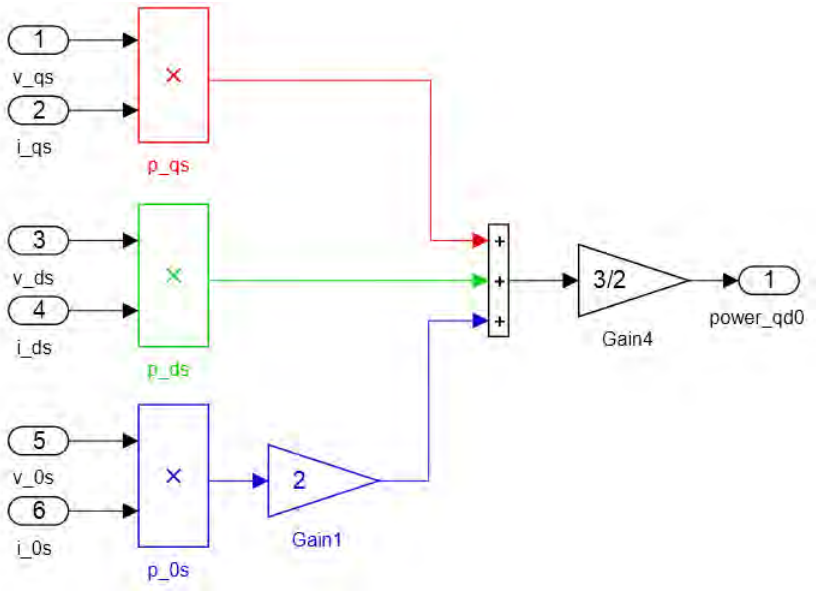

Figure 20. Simulink model subsection depicting the development of machine's output power via Equation (31).

The counter-electrical torque τ_e, that is produced by the machine in opposition to τ_m, can be calculated by (30). This has been implemented in the Simulink model of the machine in Figure 21 where gains K3, K5 and K7 are constants representing the magnitude of the third, fifth and seventh harmonic components of λ'_m in the rotor reference frame and gain "-K-" $= (3\lambda'_m / 2)(p/2)$.

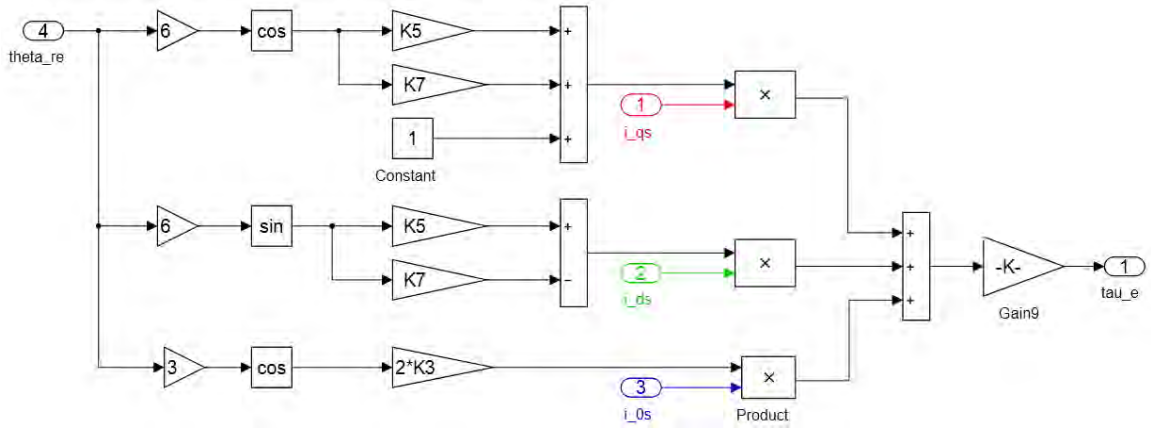

Figure 21. Simulink model subsection depicting the calculation of τ_e utilizing Equation (30).

The mechanical forces that are at work on the machine are represented by the force balance equation (13). Here the forces of friction, torque and inertia are balanced to govern the behavior of the machine. In the Simulink model, (13) is implemented in the force balance subsection as depicted in Figure 22. In addition to the friction, torque and inertia forces in (13), a lossless centering spring has been simulated out of necessity. In all linear machines the translator travel is a design constraint that must be accounted for. This can be accomplished by constraining the input forces or through the design of the machine itself. In some instances, hard stops are placed on the ends of the machine to prevent over travel. Another simple solution is to use a spring, most commonly an air spring, whereby the translator compresses a volume of air as it travels toward the extremes of its travel.

In the Simulink model, a spring is simulated which applies zero force when the translator is centered at θ_{rm} equal to π, where θ_{rm} has a total allowable travel from zero to 2π. The force applied by the spring is linear and equal to the distance from center multiplied by a spring constant. This system is lossless and has been tuned to allow for operation at the target frequency for the simulation. It is necessary to have a spring since the input force is a torque that is independent of speed, therefore as the machine speeds up more mechanical power P_m is applied since $P_m = \omega_r \tau_m$. If there is even the slightest imbalance where the machine goes faster in one direction that in the reverse direction, the machine becomes unstable and will exhibit an underdamped response, quickly exceeding the translator allowable travel in one direction. The spring force is highlighted in blue in Figure 22.

In accordance with (13), the Simulink model is defined for motor action and because of this, the summing block in Figure 22 represents τ_e as positive and τ_m and the mechanical damping $B_m \omega_{rm}$ as negative. This frame of reference is also taken into account when using the model to represent a generator and, because of this, τ_m is made negative as seen in Figure 23. Some of the results in Chapter IV have also had their signs flipped to make their values more intuitive.

The output of the generator is three separate phases that have no common node. Because of the lack of a common, the three phases are not applied to a single three phase rectifier. Instead, each phase is applied to a full bridge diode rectifier and the output of each rectifier is tied to a common dc bus. This setup is illustrated in Figure 24. The internals of the diode rectifiers are viewable in the Appendix will and not be discussed here.

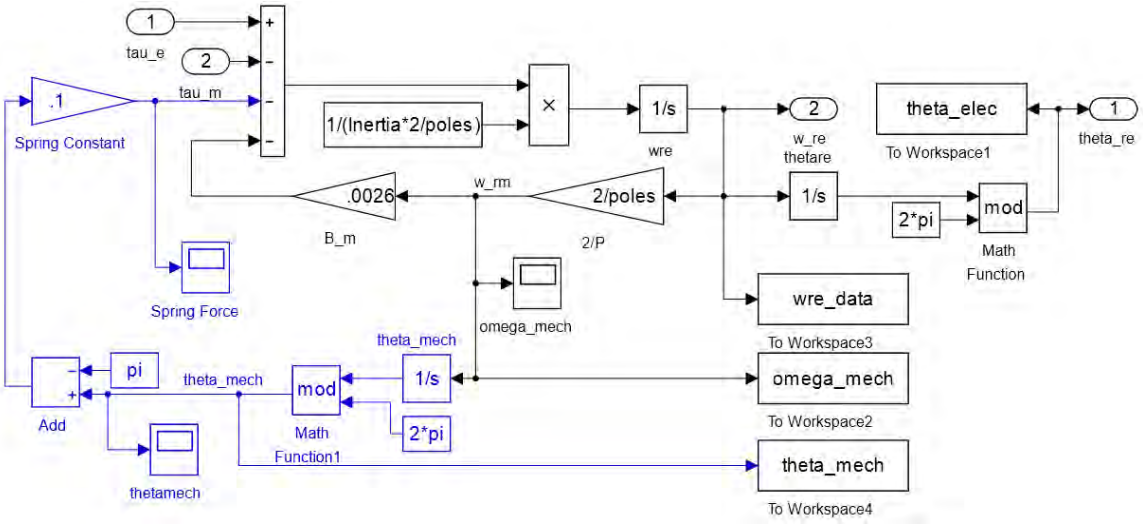

Figure 22. Simulink model subsection depicting the balance of mechanical forces on the machine employing (13). A lossless centering force is accented in blue.

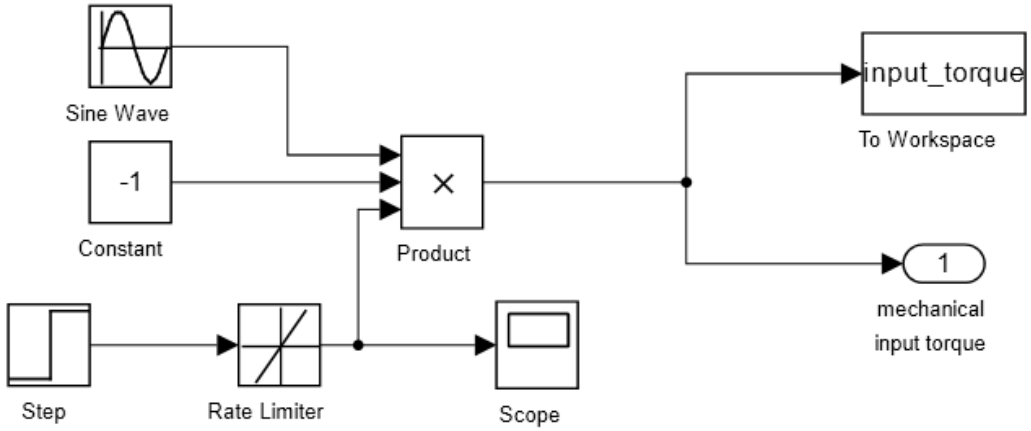

Figure 23. Simulink model subsection showing an example of the construction of τ_m for one setup of the model.

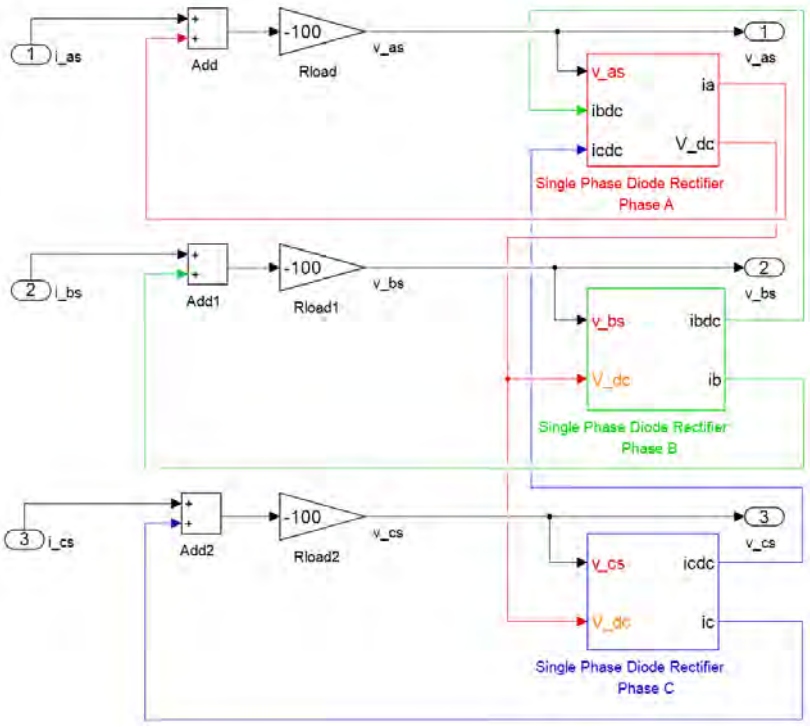

Figure 24. Simulink model subsection representing three diode rectifiers, one for each phase.

THIS PAGE INTENTIONALLY LEFT BLANK

IV. RESULTS

Chapter IV will discuss the results produced by the Simulink model of the permanent magnet synchronous linear generator, as well as look at some experimental results gathered from a physical brushless dc rotary motor acting as a generator.

A. EXPERIMENTAL RESULTS

The primary purpose of this section is to demonstrate a machine, which is designed to function as a motor, operating normally as a generator. For this experiment, a delta-connected eight-pole permanent magnet brushless dc motor rated for 24V at 4,000 RPM was used. Brushless dc motors are actually a misnomer; the motors themselves cannot operate on a dc voltage. In actuality, they are ac motors which have separate power electronics inverters on the inputs which generate ac input signals that may be from a dc input. Commonly, these motors have sensors onboard to assist the power electronics in generating the proper inputs to control the devices. In the case of the physical machine used here, it was equipped with six leads, three input-power leads, one for each of the three phases, and three sensor leads to report the status of the machine to the separate power electronics.

When operated as a generator, this physical machine becomes a permanent magnet synchronous generator, similar to the model generator. The differences are that the physical machine has sinusoidal back EMF while the model machine has non-sinusoidal back EMF and the physical machine is delta connected while the model machine has an ungrounded wye connected design.

The physical machine feeds a three-phase full bridge diode rectifier (also called a six-pulse rectifier) which is configured for a delta connected machine, with the output of the rectifier applied to a 50Ω resistor. The unrectified voltage v_a is measured across the *a*-phase (Φ_a) while the rectified load voltage v_L is measured across the load resistor. Both measurements are floating measurements using isolated voltage probes which do not share a common ground. A current measurement is taken after node *A* and measures a portion of both the *a* and *c*-phases The physical machine setup is depicted in Figure 25.

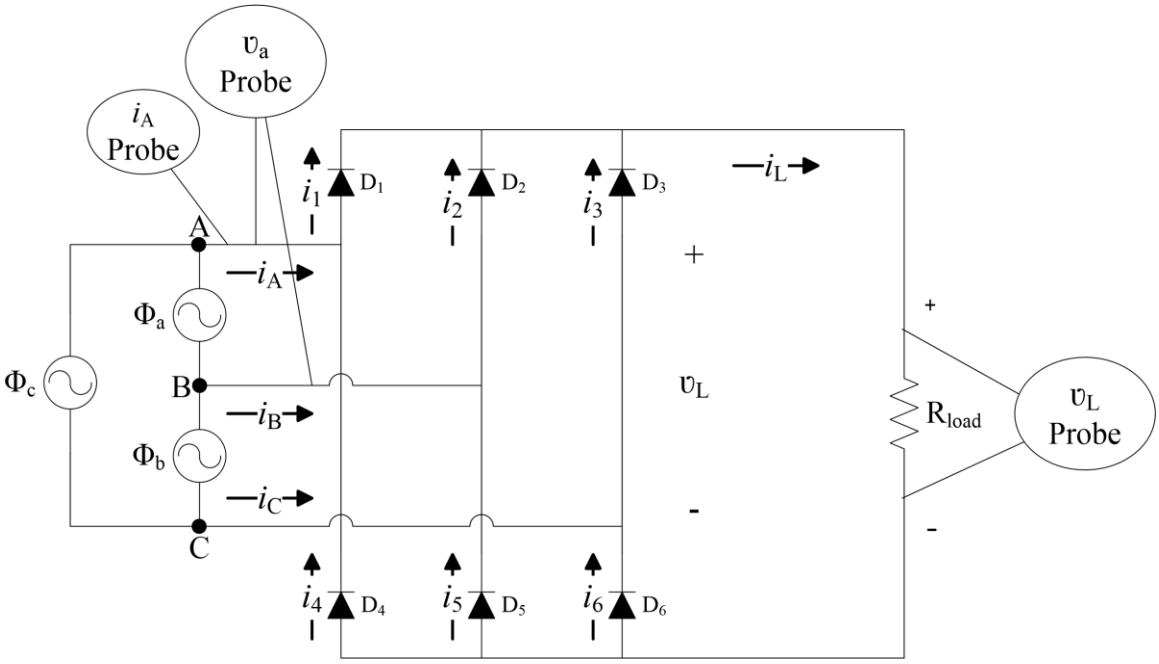

Figure 25. Three phase delta connected brushless dc motor and diode rectifier experimental setup.

The input phase voltages and resulting output voltages for a theoretical six-pulse rectifier are shown in Figure 26. Part (a) shows the theoretical three-phase sinusoidal-input line-to-line voltages at levels that approximate the experimental results in Figure 28. Similarly, part (b) shows how the theoretical input voltages are transformed through an ideal rectifier. The ideal load voltage is labeled v_L *ideal*. The non-ideal load voltage v_L *non-ideal* is 1.4V lower than the ideal due to two 0.7V losses in each line-to-line voltage incurred by the diodes.

The experimental results of the physical machine show approximately a three second oscilloscope capture depicting a torque impulse that accelerates the machine and subsequently allows it to decay to nearly zero output. These results can be seen in Figure 27 and Figure 28. In Figure 27 i_A and v_L fall to zero while v_a is still at approximately 1.2 volts peak (v_{pk}). This is expected because the full bridge rectifier suffers from voltage drop across two diodes in each phase. The diodes in this circuit were measured to have roughly 0.6–0.7V drop each in the forward direction which accounts for the missing 1.2V.

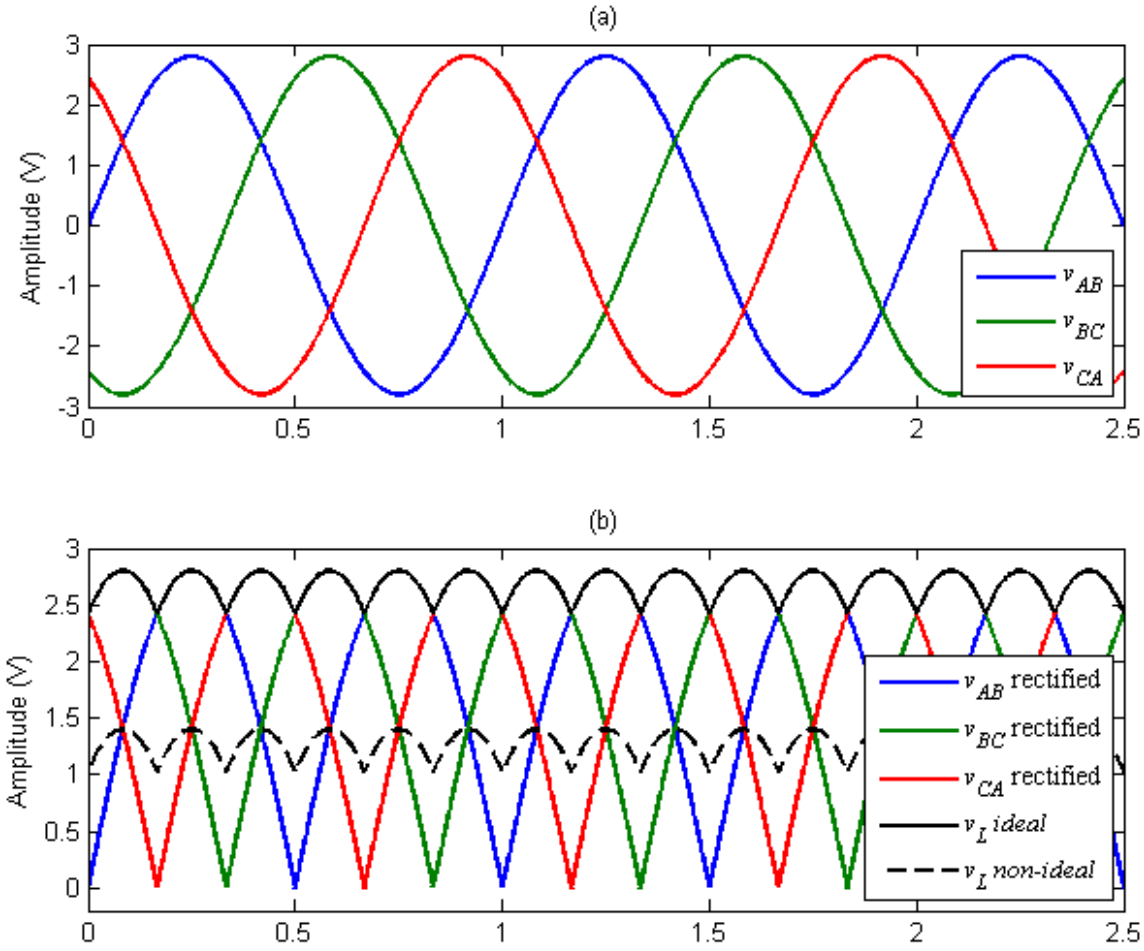

Figure 26. Theoretical three-phase diode rectifier operation over one period. (a) Sinusoidal input line to line voltages. (b) Rectified line to line voltages and load voltage with ideal and non-ideal diodes.

Although one would expect to see the rate of decay decrease after the diodes stop conducting and the machine becomes unloaded, this cannot be seen in the results. This is likely because the mechanical damping at this speed is much larger than the electrical loading and also because unloaded generators still incur some losses.

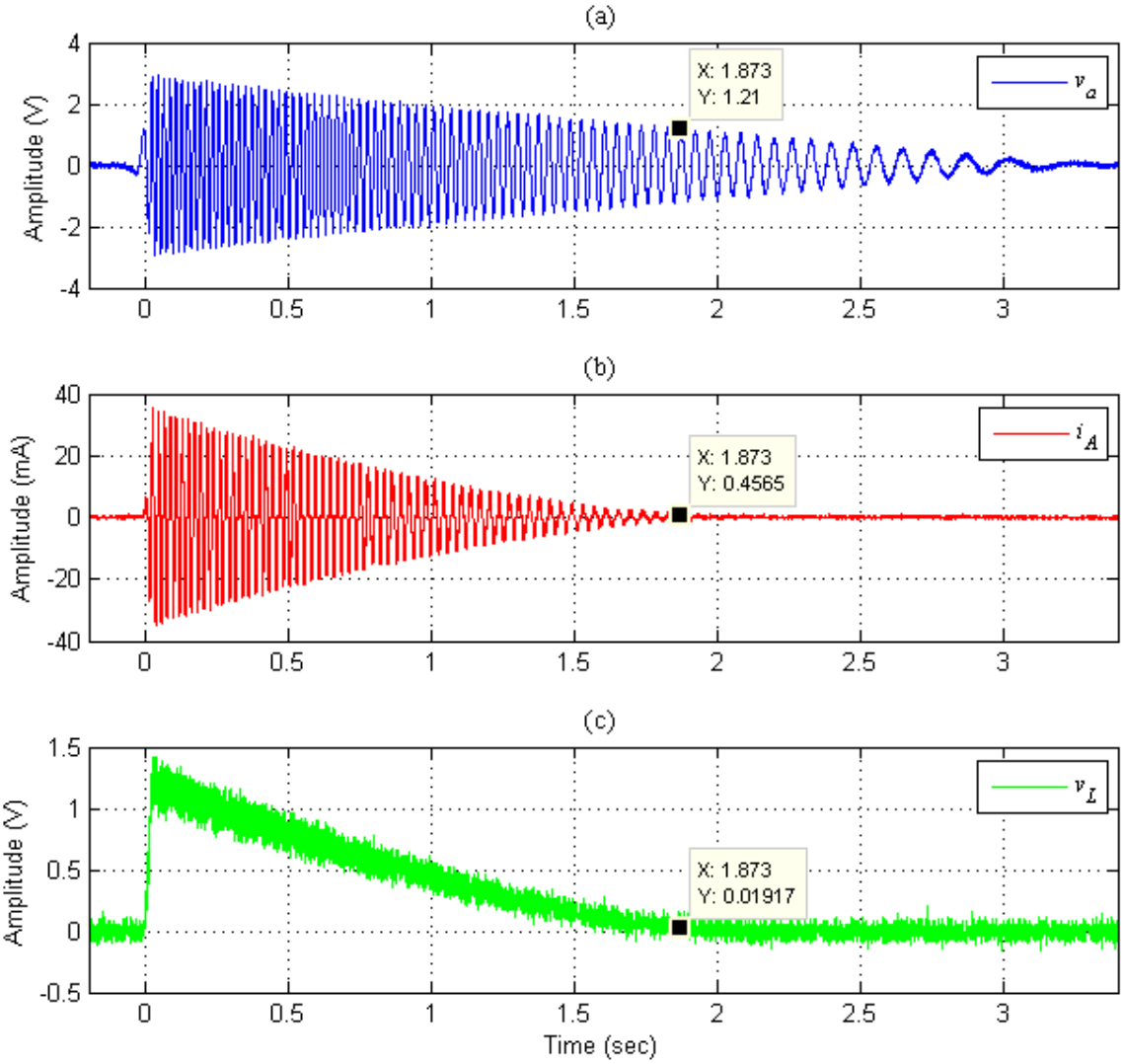

Figure 27. Results of a single input torque impulse on a brushless dc motor with data markers indicating the cutoff point of the rectifier. (a) Voltage v_{ab} between phases *a* and *c*. (b) Current i_a past node *a*. (c) Voltage v_L across the load.

The result of the current probe being used between phases on a delta connected machine can be seen in Figure 28. This placement manifests itself as the double current spikes seen in i_A. Also visible at this scale is the six-pulse ripple output of v_L caused by the full bridge rectifier, where the output voltage has two peaks per period per phase.

If the results of the theoretical six-pulse rectifier are extended and only the portions that were experimentally measured are plotted, a close relationship can be seen with the results from Figure 28. This correlation can be seen in Figure 29.

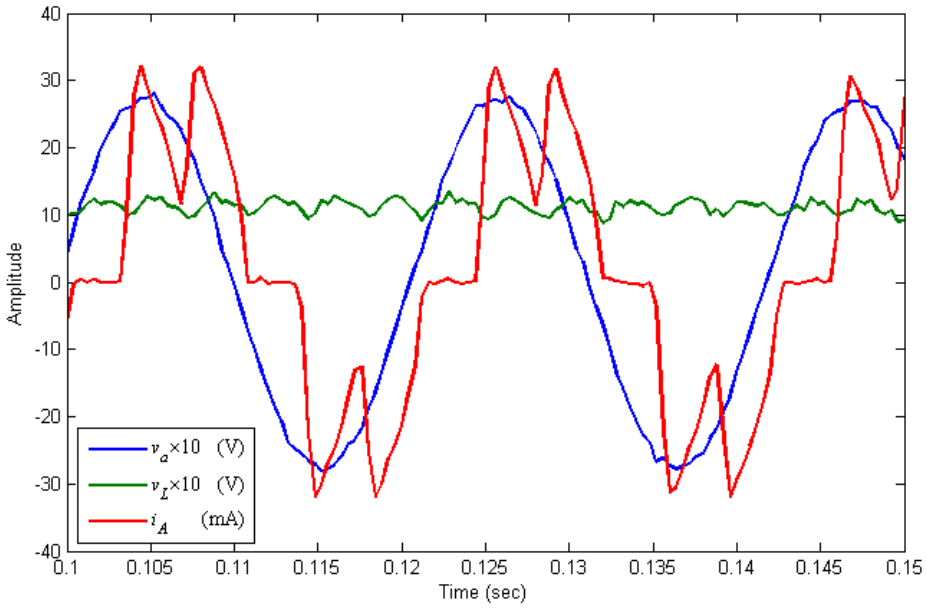

Figure 28. Enlarged selection of experimental results showing double current waveforms and six-pulse rectified voltage from Figure 27.

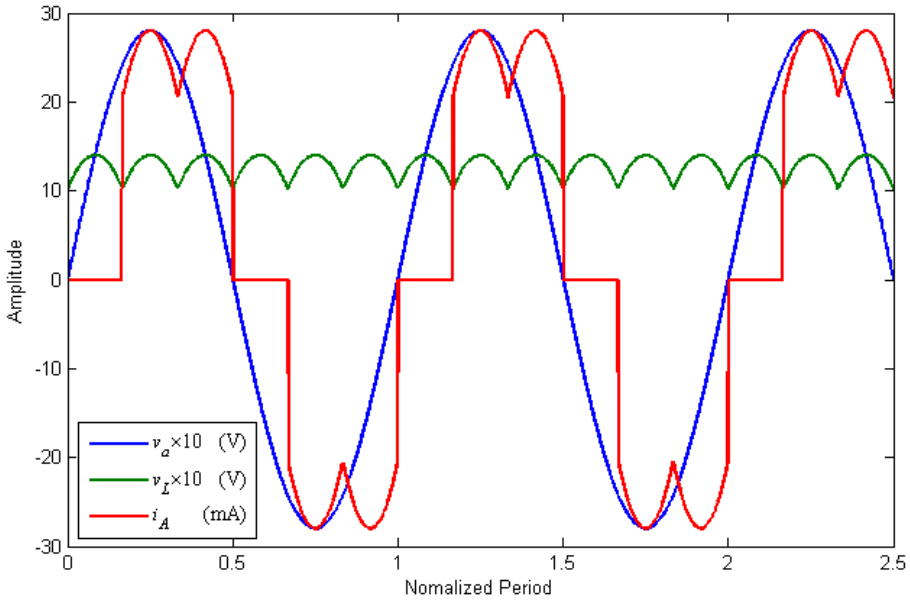

Figure 29. Theoretical six-pulse rectifier results representing the data from Figure 28.

B. LINEAR GENERATOR SIMULINK MODEL

As previously stated, the model generator is a three-phase, 12-pole, non-sinusoidal, permanent-magnet, linear synchronous machine. The model parameters are defined for motor action but have been presented in the result plots in whichever polarity is most intuitive. The workings of the model were described in detail in Chapter III and the full MATLAB and Simulink code can be found in the Appendix. Several adaptations of the model have been created, with the results presented here. The base machine parameters are presented in Table 2. These are the machine parameters used in the model in each scenario unless otherwise stated.

Plotting the portion of λ_{abcs} from (17), which is caused by the permanent magnets, allows one to see the non-sinusoidal distribution of the machine, and is shown in Figure 30.

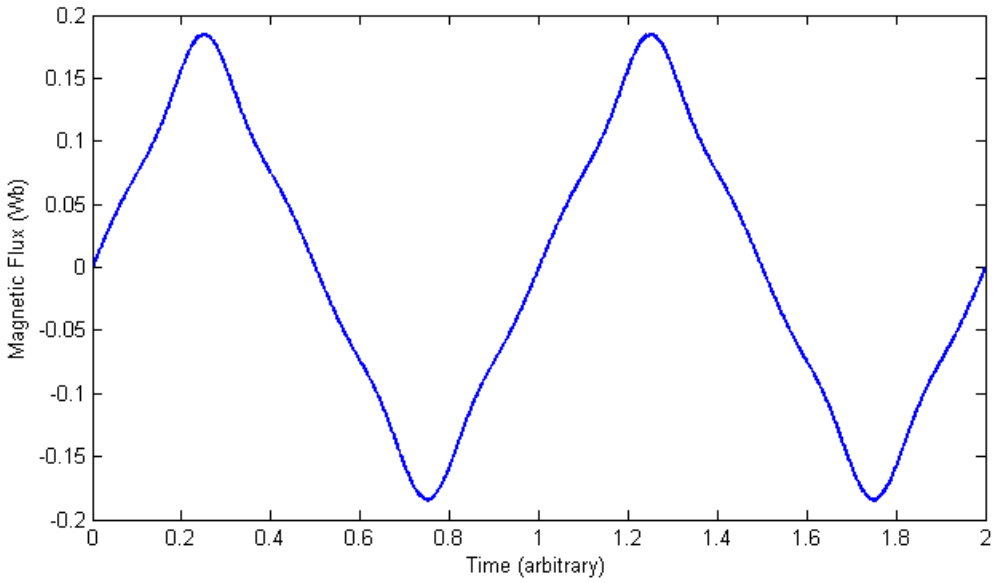

Figure 30. Magnetic flux profile caused by permanent magnets as experienced by a stator winding phase.

The exact sizes of the rotating and linear machines are unknown and therefore some assumptions are made in order to convert the model from the original design of a rotating machine into the linear machine that is being simulating. Specifically, the radius

of the rotor in the rotating machine and the length of the travel of the linear machine are needed. It is, therefore, assumed that the rotating machine has a rotor radius of 0.1 meters. Since the length of travel of a linear machine must be equal to the circumference of the rotating machine, the travel is 0.628 meters. This information is necessary in order to convert torque to force, and rotor position and angular velocity to translator distance and speed.

Table 2. Base machine parameters.

$L_{ls} = 24.5mH$	$L_{ms} = 4.12mH$	$\lambda'_m = 0.1549Wb$
$r_s = 9.1\Omega$	$B_m = 0.0026Nm \cdot s$	$J = 0.0041kg \cdot m^2$
$K'_3 = -0.121$	$K'_5 = 0.060$	$K'_7 = -0.009$

1. Low Frequency, Low Amplitude Sinusoidal Input Force Scenario

In the sinusoidal input force scenario an oscillating input is being considered, which is appropriate to linear machines associated with wave energy conversion. While a purely sinusoidal input is unrealistic in the best of ocean environments, it provides a study of the ideal wave energy converter input. As will be seen, the effects of the centering spring cause a non-sinusoidal sum of forces on the machine that will nevertheless result in significant harmonic distortion.

For the input torque to the model generator, a sine wave with an amplitude of 0.8N·m and frequency of 1Hz is used. Converting torque to force, where $F = \tau \cdot R$, gives an equivalent sinusoidal input force with an amplitude of 8N, still at the same frequency of 1Hz. This is seen in Figure 31, where the torque that is used in the model is seen in part (a) and the equivalent force is seen in part (b). Taking into account the force of the centering spring, the resulting applied mechanical force to the stator is given in Figure 32.

This input causes the translator to oscillate as depicted in Figure 33, where part (a) represents the velocity (V) of the oscillator in the plane of movement and part (b) depicts the position of the translator in time.

While the mechanical motion of the translator is discussed in terms of velocity and force, for electrical variables they are still referred to by the angle-based values of θ_{re} and ω_{re}. The response of these variables is displayed in Figure 34, where ω_{re} can be seen in part (a) in rad/s. The translator electrical angle θ_{re} covers an electrical cycle (modulated to between 0–2π) approximately six times for each time the translator mechanically travels one length of the machine. This is because there are 12 poles (six pole-pairs) in the machine.

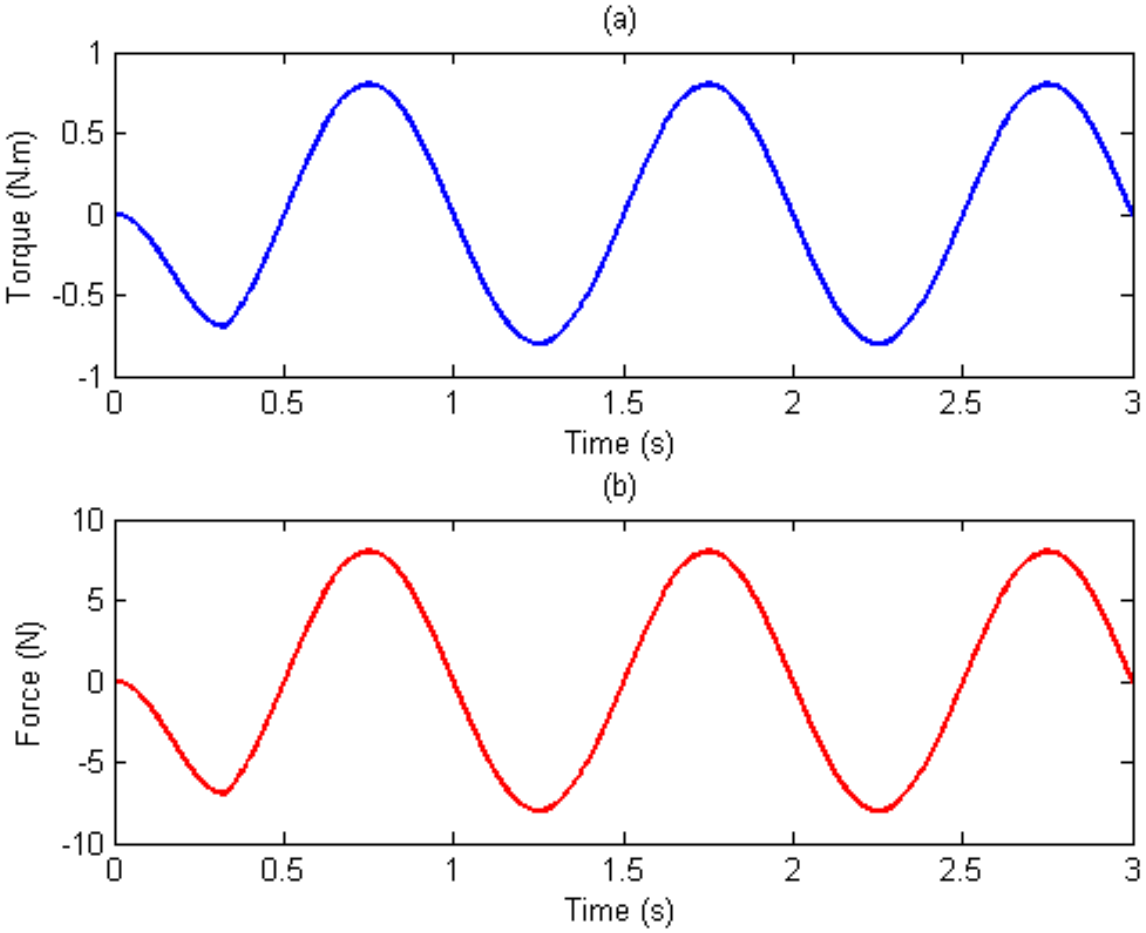

Figure 31. Sinusoidal input functions over three periods. (a) Input torque. (b) Equivalent input force.

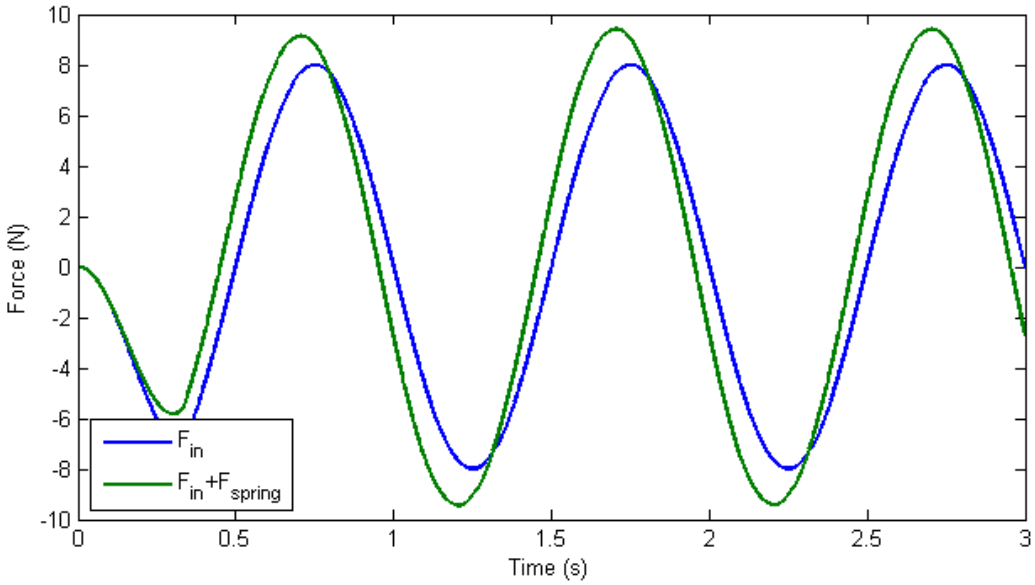

Figure 32. Sinusoidal input force and resulting applied mechanical force to the translator taking into account the force of the spring.

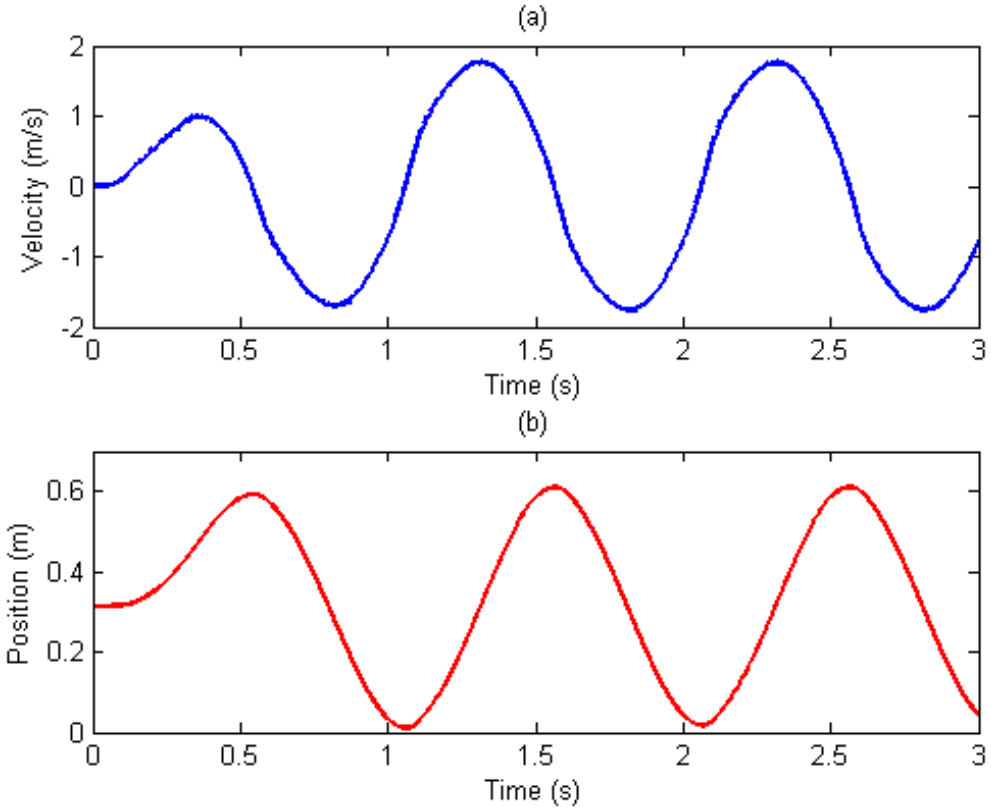

Figure 33. Translator motion over three periods. (a) Translator velocity. (b) Translator position.

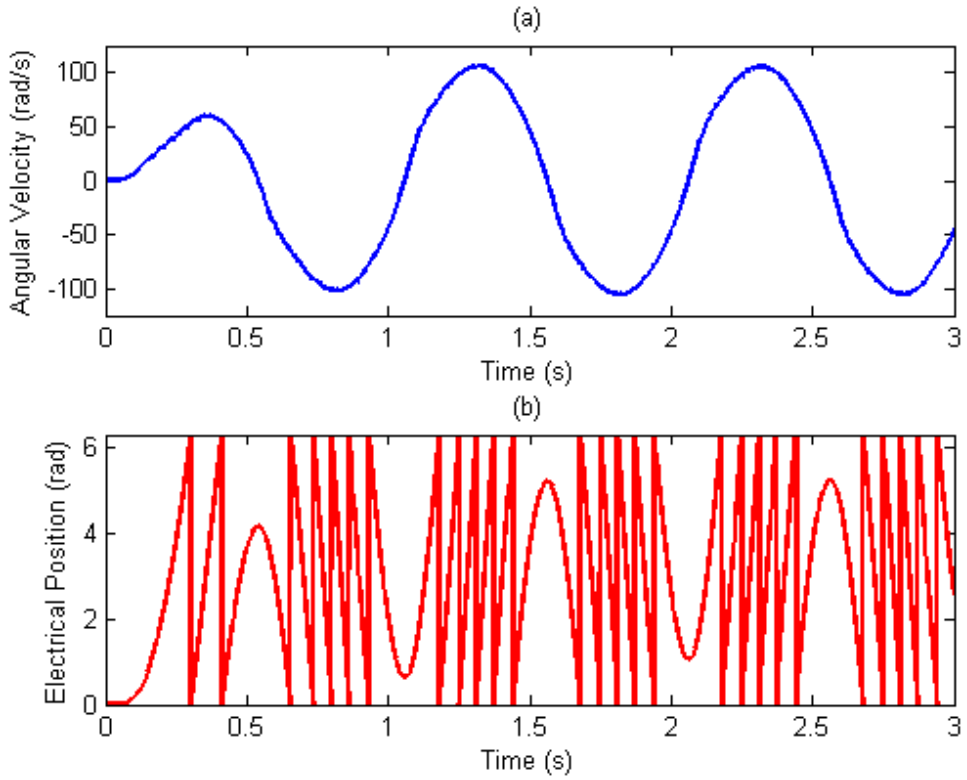

Figure 34. Electrical motion. (a) Angular velocity ω_{re}. (b) Electrical position θ_{re}.

The stator flux linkage $\boldsymbol{\lambda}_{abcs}$ from (17), is depicted in Figure 35, where the system response is seen in (a) and a more detailed view of the waveforms is seen in (b). Note that the waveforms in (b) are very similar to those in Figure 30, with the differences coming from the flux produced by currents in the stator windings.

From (7) it can be seen that the voltage developed in the stator windings is in large part representative of the rate of change of the flux linkage. Comparing the shape of the waveforms of $\boldsymbol{\lambda}_{abcs}$ and $\mathbf{v}_{abcs}$, this relationship can be seen to play out, where the roughly triangular $\boldsymbol{\lambda}_{abcs}$ waveforms produce roughly trapezoidal $\mathbf{v}_{abcs}$ waveforms. The waveforms for $\mathbf{v}_{abcs}$ can be seen in Figure 36 and Figure 37. The stator currents $\mathbf{i}_{abcs}$ are also on display in these figures. The current waveform shape is caused from a combination of factors, but they are largely controlled by the effects of the diode rectifiers which are feeding a common dc bus.

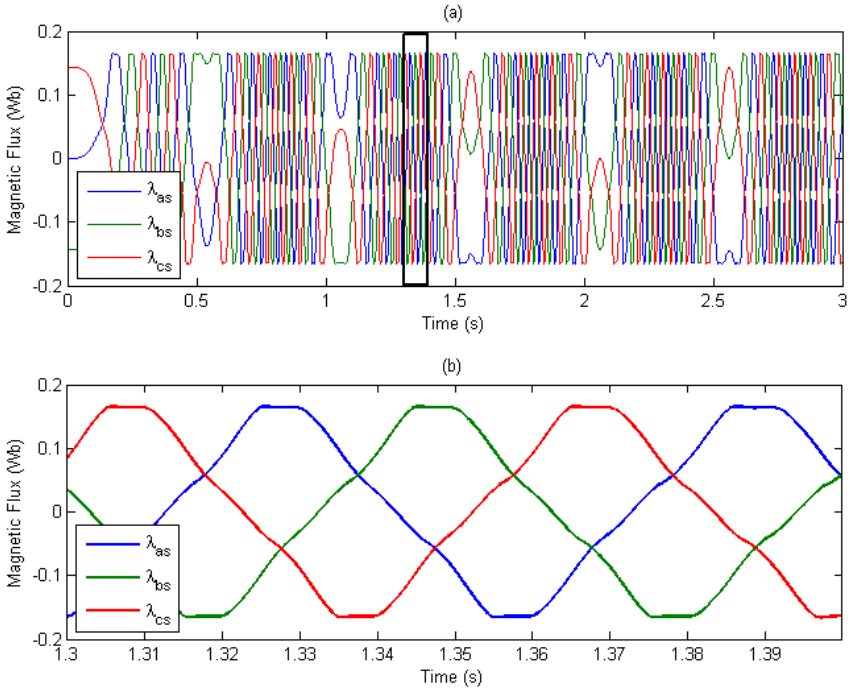

Figure 35. Stator flux linkages $\boldsymbol{\lambda}_{abcs}$ with the rectangle in (a) indicating the selection displayed in (b) in greater detail.

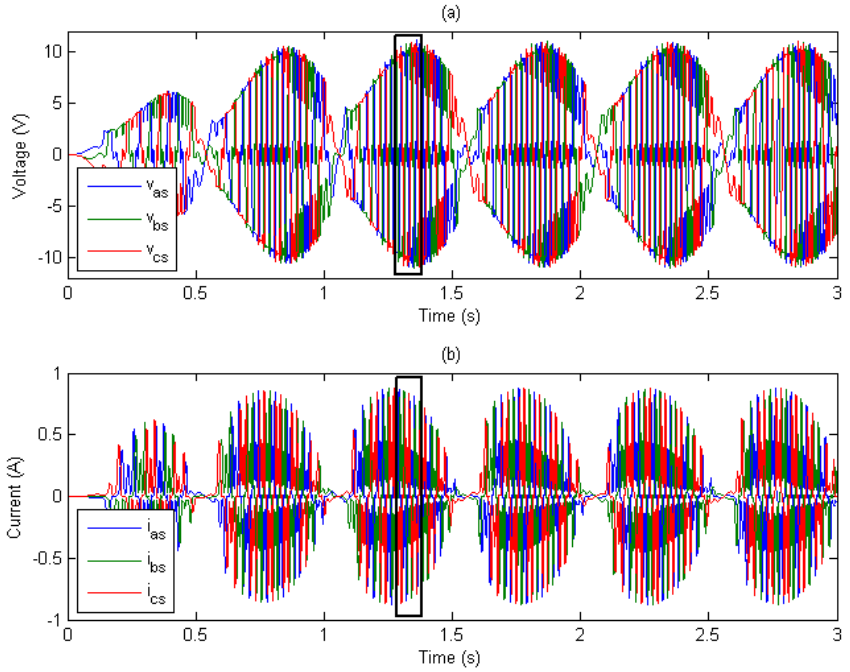

Figure 36. Stator machine variables over three periods. (a) Stator voltages $\mathbf{v}_{abcs}$. (b) Stator currents $\mathbf{i}_{abcs}$. Black boxes represent data selected for display in higher detail in Figure 37.

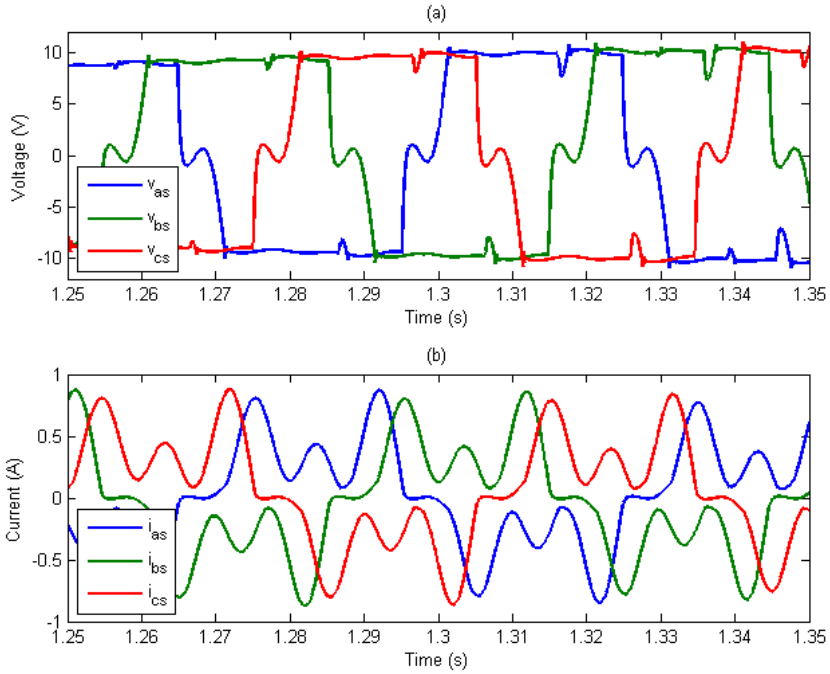

Figure 37. Stator machine variables over a fraction of a period from Figure 36. (a) Stator voltages $\mathbf{v}_{abcs}$. (b) Stator currents $\mathbf{i}_{abcs}$.

The stator voltages $\mathbf{v}_{abcs}$ are rectified and applied to a common dc bus, which can be seen in Figure 38 and Figure 39. Only the bus voltage is discussed because the load is a purely resistive 150Ω resistor. The dc bus has a single 1.1mF capacitor in parallel with the load resistor in order to help smooth the output voltage to this load. The resultant *RC* time constant (τ_{RC}), given by $\tau_{RC} = r \cdot C,$ equals 0.183s. This time constant affects the rate of change of the voltage on the dc bus by

$$v(t) = v_0 e^{-t/\tau_{RC}} \text{ when discharging,} \tag{32}$$

and

$$v(t) = v_0\left(1 - e^{-t/\tau_{RC}}\right) \text{ when charging,} \tag{33}$$

where *v(t)* is the voltage at time *t* and v_0 is some initial voltage at $t = 0$. The practical effects of this time constant can be seen by comparing parts (a) and (b) in Figure 39. In the first portion of part (a), one can see the six-pulse related ripple that is caused by the

individual phases seen in part (b). Note that even this ripple is smoother than the spiky waveforms of part (b). While this is an effect of the filter capacitor time constant, the more dramatic effect is seen by focusing on the latter portion of part (b), beginning around 1.5 seconds. At this point, the voltage ripple fades and the bus voltage is riding on the capacitor. Another effect of the filter capacitor is the apparent phase shift between part (a) and part (b) caused by the capacitor as it delays the voltage rise and fall.

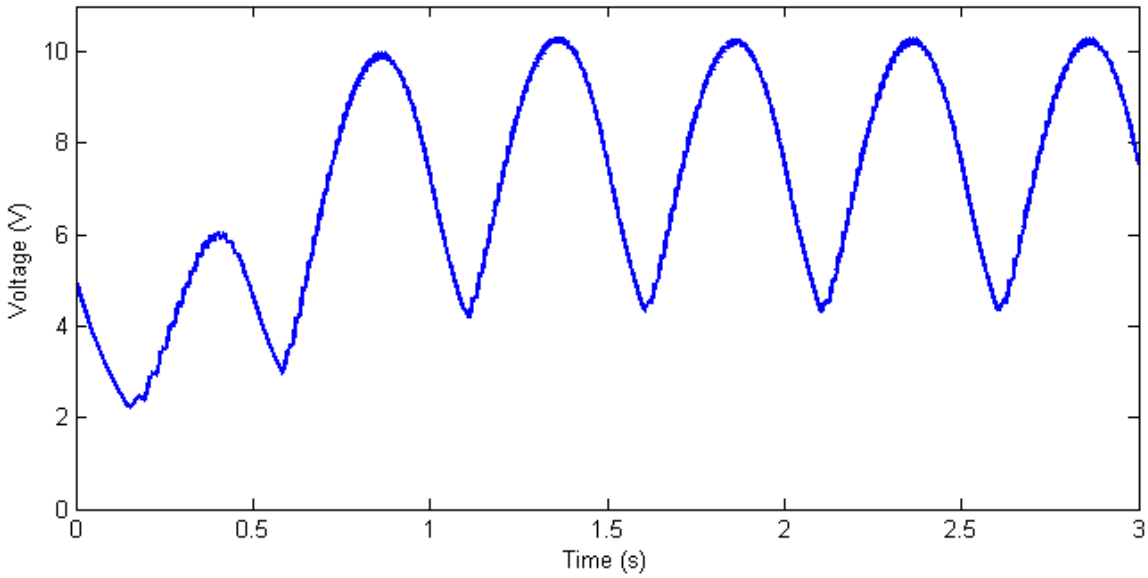

Figure 38. Voltage on the dc bus over three periods of translator motion.

Power of the machine can be quantified by the mechanical power in, where

$$P_m = \tau\omega_{rm} = FV, \tag{34}$$

or by the electrical power out, as

$$P = vi, \tag{35}$$

where each of these equations provides equivalent units. Using (34) and (35) the mechanical power put into the machine and the electrical power provided to the load can be calculated.

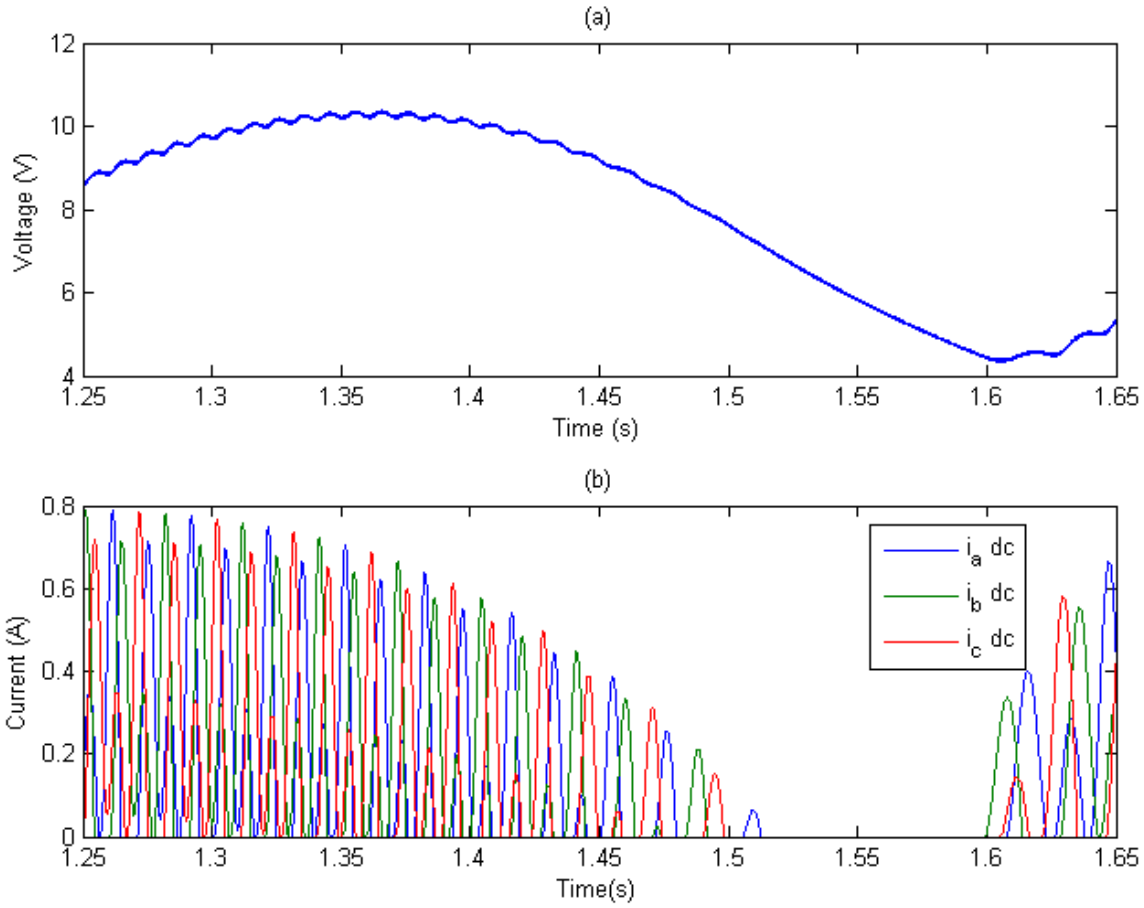

Figure 39. Demonstration of the filter capacitor's effects. (a) Voltage on the dc bus over a portion of a period. (b) Currents from individual stator phases as they pass onto the dc bus over the same elapsed time.

To find the total energy into and out of the machine, the respective power over time is integrated. By comparing these two values, the machine efficiency can be uncovered. These calculations have been performed in MATLAB and can be viewed in the Appendix. It should be noted that while negative power is defined if the machine is moving one direction while the force is applied in the other, this is still power that is being applied and so the absolute value of this power has been used to calculate the machine input power and energy.

The results for this scenario are that mechanical energy into the machine was 18.46W·s and the electrical energy delivered to the load was 9.98W·s for a total efficiency of 54.1%.

2. Low Frequency, Low Amplitude Square Input Force Scenario

In this scenario the input forcing function will be a square wave at 1Hz with an amplitude of ±0.565 N·m of torque or 5.65N of force. This value is the rms value of the amplitude of sine input force in order to make them more comparable. This is a largely academic scenario since a square input function at this frequency is not realistic to any real world energy sources for which a linear generator might be applied. It can be a crude approximation of what would occur in a free-piston Stirling engine powered generator or perhaps even less sophisticated, in a linear generator masquerading as an internal combustion engine cylinder, although both of these applications would achieve a higher frequency. These higher frequency applications will be the topic of another scenario.

The described input can be seen in Figure 40. The force resulting from this input force combined with the force of the spring can be seen in Figure 41. The combined mechanical force acting on the translator is more intuitive when viewed over the square input function, where the force of the spring adds to the input force while returning to center and subtracts as the machine approaches the extremes of its travel. The motion of the translator is depicted in Figure 42.

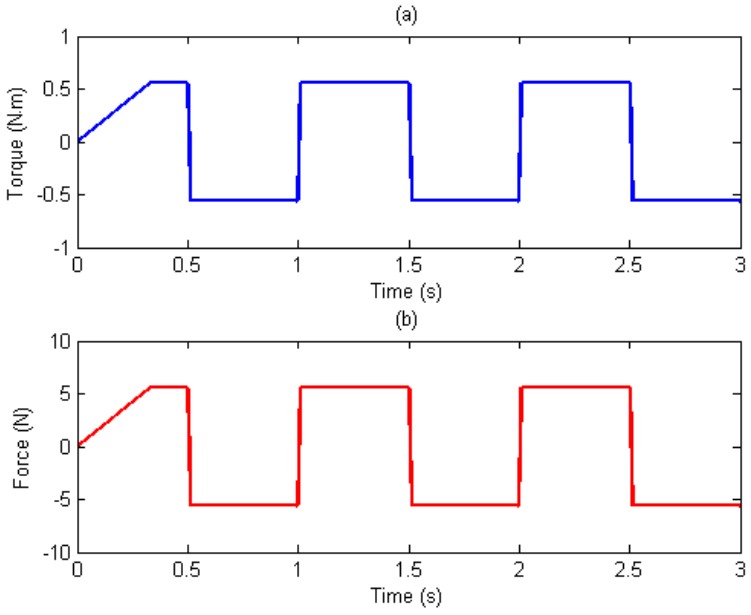

Figure 40. Square wave input functions over three periods. (a) Input torque. (b) Equivalent input force.

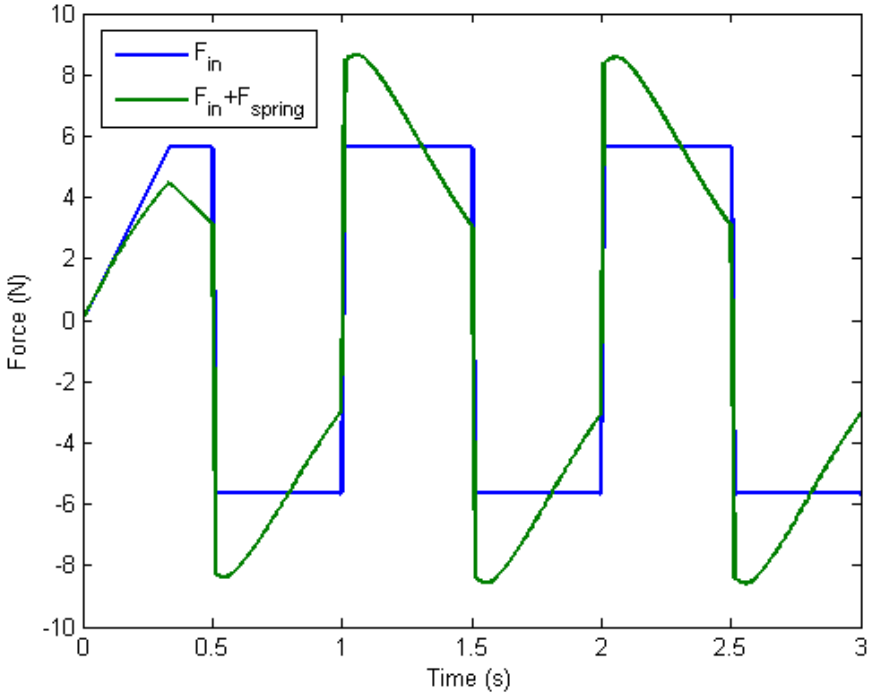

Figure 41. Square input force and resulting applied mechanical force to the translator taking into account the force of the spring.

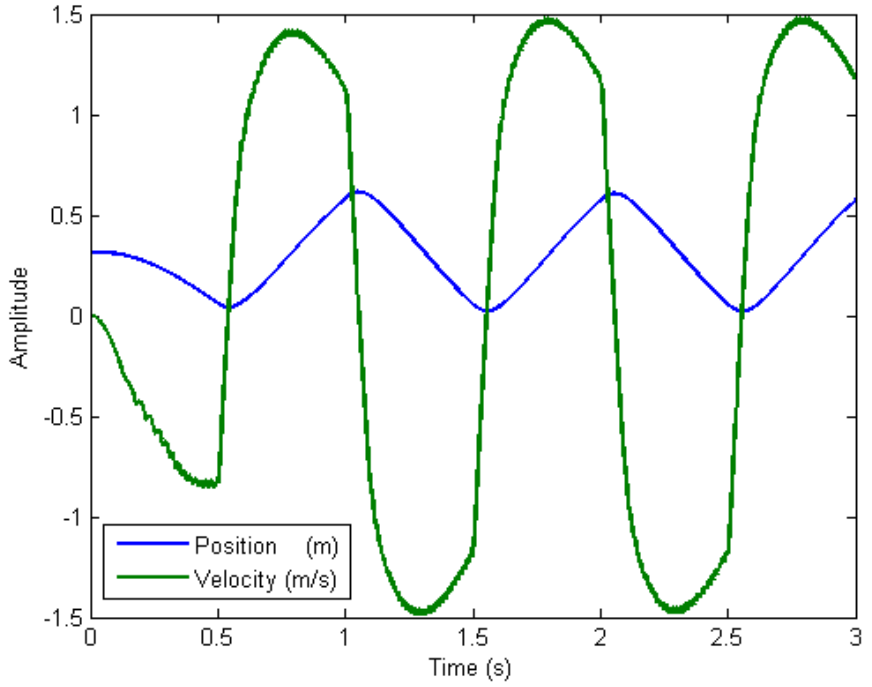

Figure 42. Mechanical motion of the translator resulting from a square input function.

The flux linkage is not differentiable from the previous scenario and does not merit repeating. The stator voltages and currents are very similar to the sine input scenario, except that the harmonics present in the flux linkage are more exaggerated. These are seen in Figure 43 and Figure 44, with Figure 44 part (a) clearly showing the harmonic presence where the voltage wave forms deviate from trapezoidal.

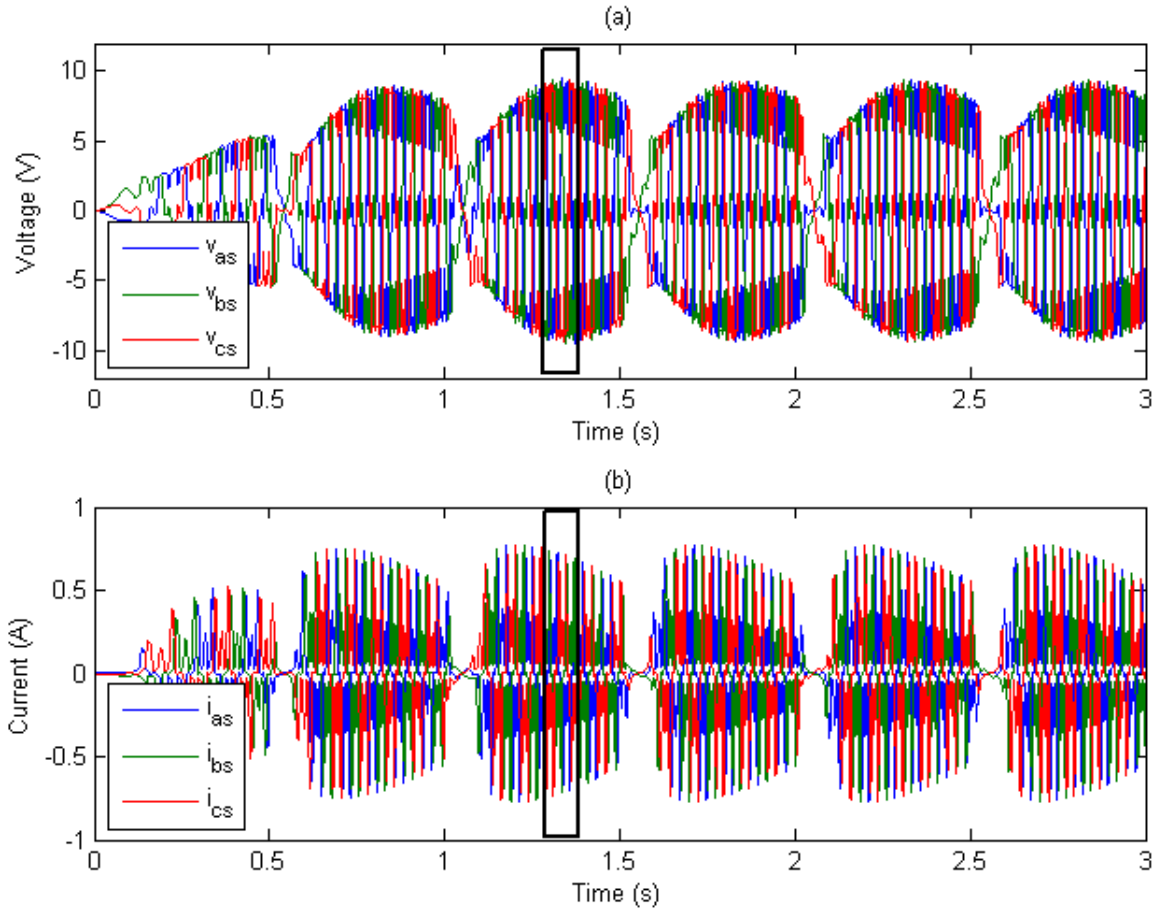

Figure 43. Stator machine variables over three periods of the square input function. (a) Stator voltages $\mathbf{v}_{abcs}$. (b) Stator currents $\mathbf{i}_{abcs}$. Black boxes show data selected for display in greater detail in Figure 44.

The dc bus voltages behave in a similar manner to the previous scenario, except that the more abrupt changes in speed result in a more distinct change from small ripples in the bus voltage to clearly riding on the capacitor as it discharges through the load according to its time constant. This is portrayed in Figure 45 and Figure 46.

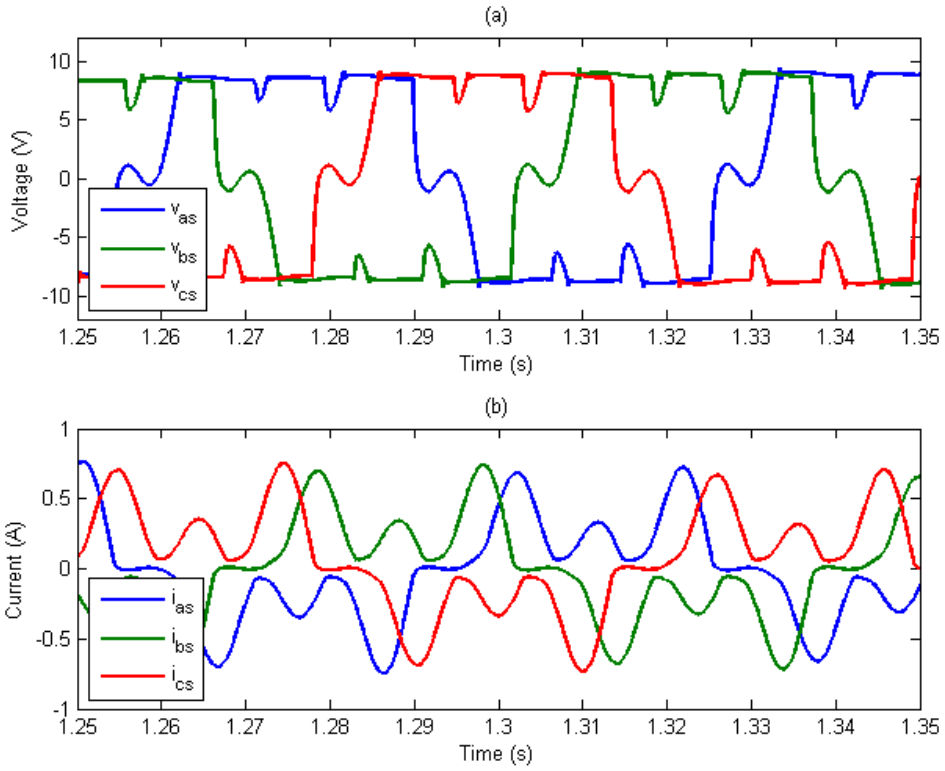

Figure 44. Stator machine variables over a fraction of a period from Figure 43. (a) Stator voltages $\mathbf{v}_{abcs}$. (b) Stator currents $\mathbf{i}_{abcs}$.

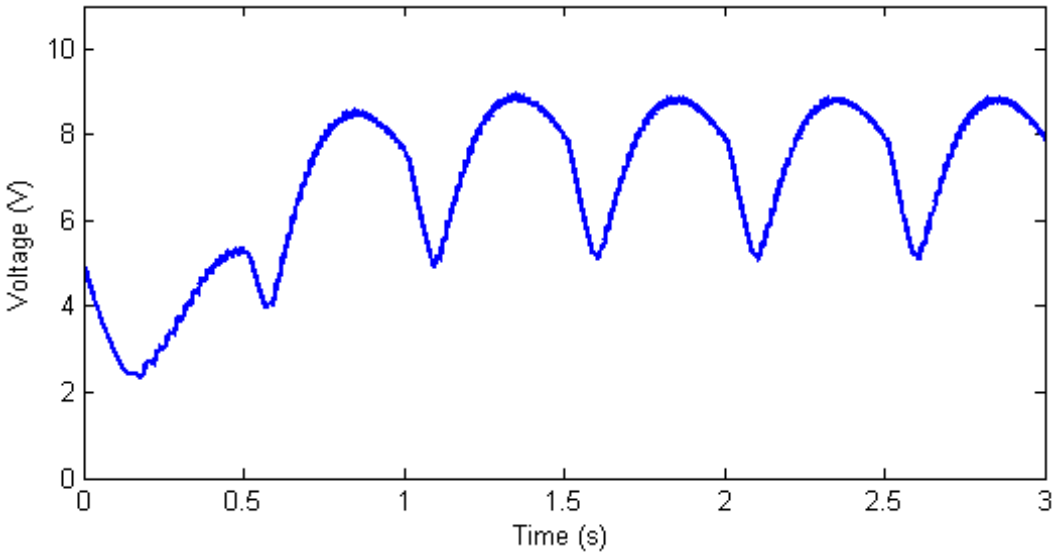

Figure 45. Voltage on the dc bus over three periods of the square input function.

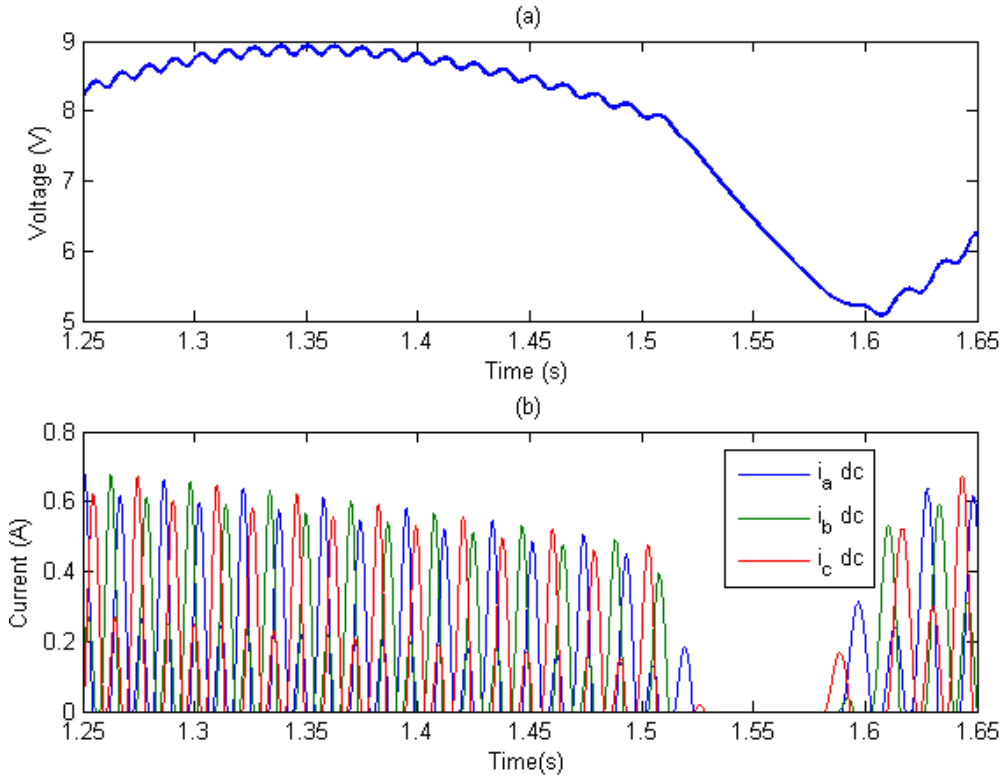

Figure 46. Demonstration of the filter capacitor's effects. (a) Voltage on the dc bus over a portion of a period. (b) Currents from individual stator phases as they pass onto the dc bus over the same elapsed time.

To determine efficiency, the energy into and out of the machine is again calculated as in the previous scenario. Here the results are that the mechanical energy into the machine is 17.45W·s while the energy delivered to the load is 9.08W·s. This leads to a similar efficiency as before of 52.0%.

3. Floating Frequency, High Amplitude Impulse Input Force Scenario

It is apparent through experimenting with various input functions, that if a fixed frequency alternating impulse is applied to the generator the machine will always stabilize so that the impulse is firing while the translator is at its maximum travel and in the direction to extend that travel. By doing so, the machine would always find its least efficient operating point, achieving efficiencies in the single digits at best.

In order to simulate a crankless internal combustion engine, it is necessary to fire the impulse at a more advantageous point in the translator travel. The impulse is triggered

to act in the direction of motion of the translator as the translator crosses the center of its travel which corresponds to zero force applied by the spring. In this way the machine will naturally achieve resonance after some time. This is quite different from how the forces act on a piston in an internal combustion engine, but the desired takeaway is to understand the operation of a linear generator that is not frequency controlled and that that has an intermittent input. In this way, this scenario explores different behaviors in linear generators than previous results and is still in the vein of a crankless internal combustion engine driven machine.

For the results shown, the input impulse force is applied for a duration of one simulation step, which is 20μs. The impulse is initially ±50kN and quickly ramps down to its final value of ±9kN. The high initial value is to aid the machine in more quickly reaching a steady state value. The steady state values of the input impulses can be seen in Figure 47. The frequency is controlled by the dynamics of the machine; it settles out at roughly 70.4Hz. If you equate this to the speed of a piston in an internal combustion engine, the engine would be operating at 4225RPM which falls within the range of nearly all automobile engines. Note that the dimensions that have been assigned to this machine are not compatible with the dimensions of an automobile engine, so the parallels between them should be filtered accordingly.

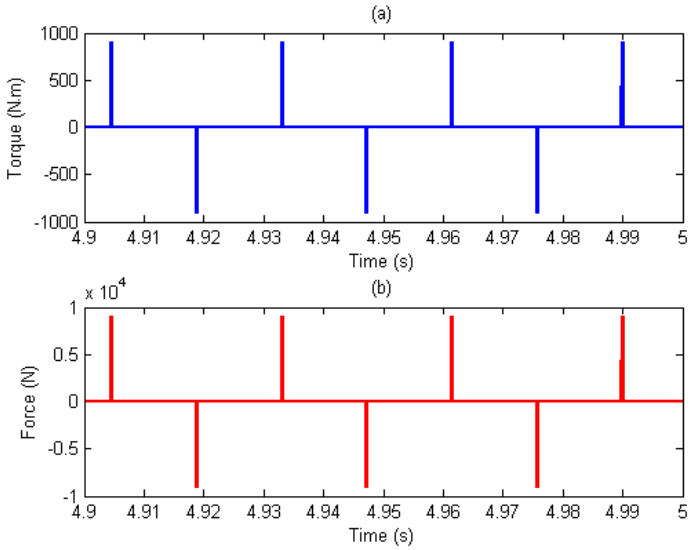

Figure 47. Applied input impulses. (a) Impulse as torque. (b) Impulse as force.

In Figure 48 the external forces acting on the translator, including the input impulse and the force of the spring, are contrasted with the motion of the translator. It is apparent that the translator is in the center of its travel when the impulse is applied. This can be seen by the position of the translator and by the force of the spring passing through zero. Some quantities in Figure 48 have been greatly down-scaled in order to more intuitively give a sense of the operation of the machine; particular attention should be paid to their multipliers in the legend.

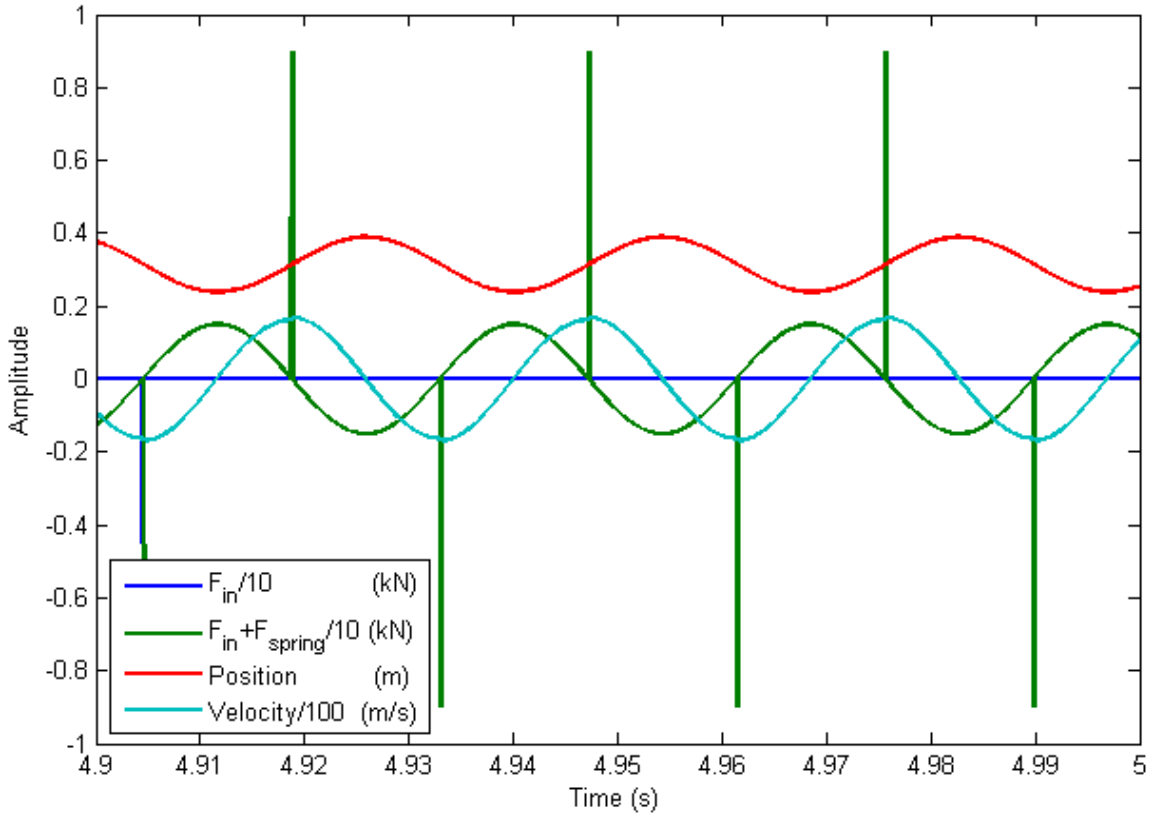

Figure 48. External forces and their relationship to translator motion.

The stator voltages and currents for the three phases can be seen in Figure 49. The voltages remain trapezoidal as before; the ringing that is visible is due to instability in the model and can be ignored. The current waveforms remain largely the same as in previous scenarios.

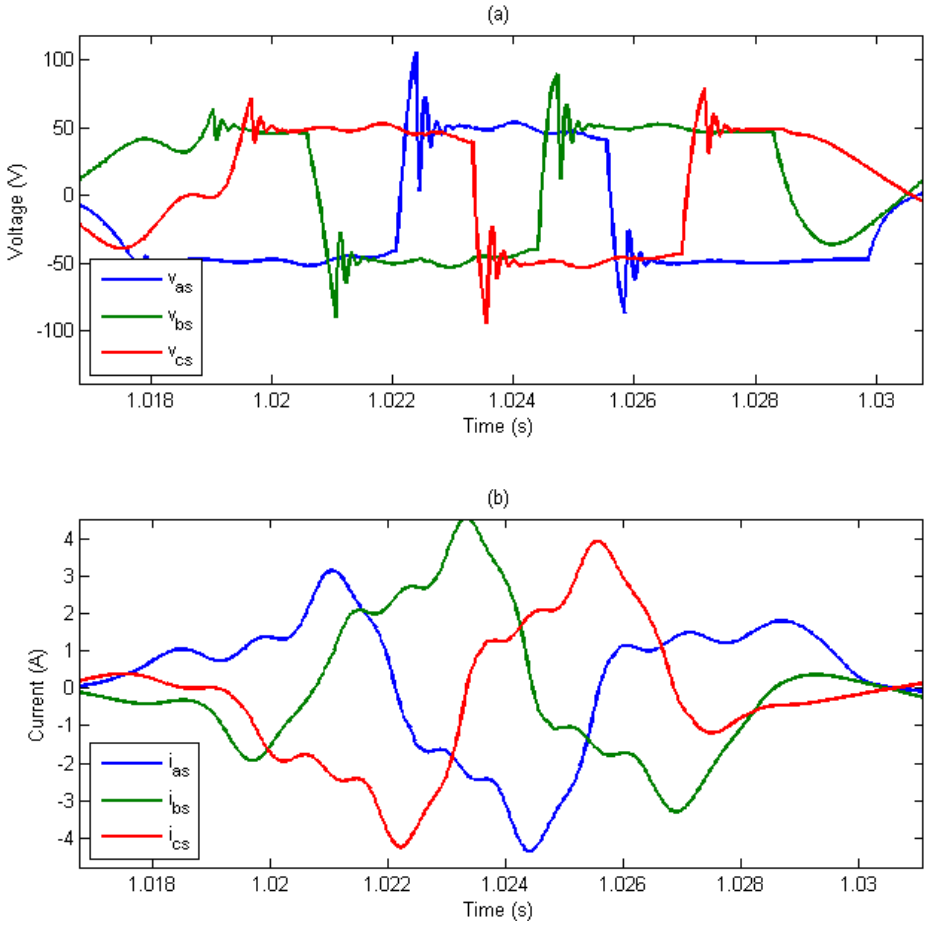

Figure 49. Stator variables over half of a translator cycle. (a) The three phases of stator voltage $\mathbf{v}_{abcs}$. (b) The three phases of stator current $\mathbf{i}_{abcs}$.

The largest change is seen in the dc bus quality. There has been a substantial increase in the quality of the power on the dc bus. This is expected at higher frequencies, where the ripple can be more easily compensated for by the capacitor. The difference in dc bus voltage quality can been seen in Figures 50 and 51. The average dc bus voltage can be seen to build up and then reach steady state at about 50V. This is much different from the previous scenarios which saw the dc bus voltage in a periodic state of flux with large transients that remained during steady state. The ripple that is visible in Figure 51 is no longer the ripple associated with the six-pulse rectifier which occur six times each electrical cycle, but rather the ripple of the translator moving over its mechanical cycle.

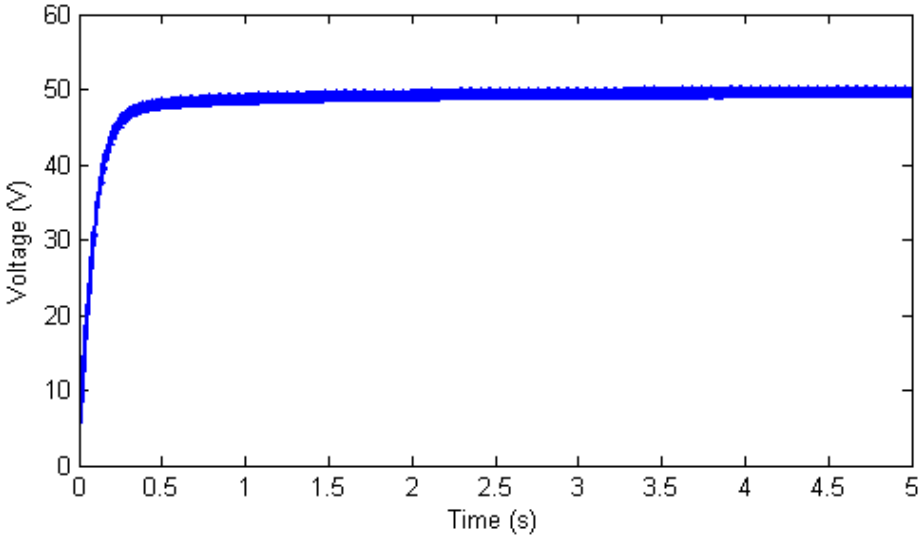

Figure 50. Transient into steady state dc bus voltage.

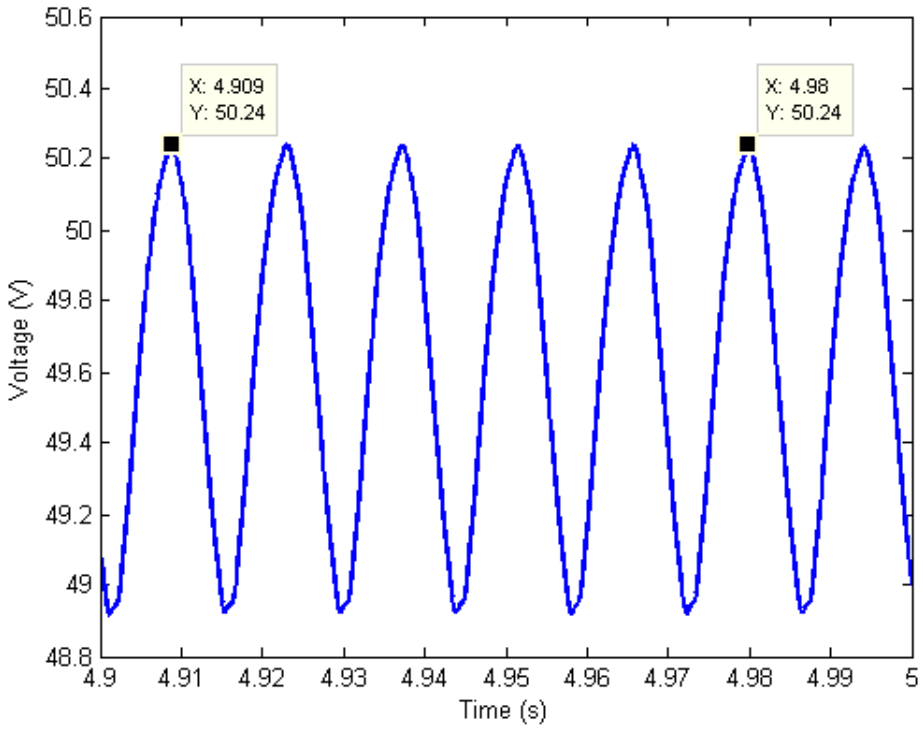

Figure 51. Steady state dc bus voltage ripple.

Here it can be measured that the total dc bus voltage ripple represents only 2.7% of the dc bus voltage. In the sinusoidal scenario it was greater than 50% of the dc bus voltage and in the square wave scenario it was roughly 44%.

The efficiency of the machine in the scenario was calculated after the machine had reached steady state to avoid the acceleration during transient portion. The final efficiency number was 71.2%. When the input impulse was administered at a fixed frequency the observed result was between 0.2–3% efficiency.

V. CONCLUSIONS AND FUTURE WORK

Chapter V will discuss the things that have been learned from this process. It will also discuss the shortcomings of the model, its assumptions and its omissions of actual phenomena. In discussing these faults, ideas for future work to address them will be injected. There is also potential for future work in imagining new ways to apply the model in its present form.

It was shown that a model for a three-phase non-sinusoidal permanent magnet synchronous machine can be developed in Simulink and that this machine can be manipulated to represent a linear machine. Both by use of the model and the physical machine, it was demonstrated that motors and generators can be used in the reverse of the operation for which they were designed.

Power quality and efficiency present large obstacles to linear machines, especially if they are going to operate at low frequencies. There is a need to explore the feasibility of better and more elaborate output filters to clean up the power quality on the dc bus. Where efficiency is concerned, there is still a great deal to learn and explore, even within the model here. There are dozens of variables that can be played with to better understand their effects on efficiency, including the spring constant, the stator resistance R_s, the leakage inductance L_{ls}, the loss coefficient B_m or the inertia of the translator J.

Major challenges in working with these variables are the second and third order effects. A change to one variable affects the overall operation of the machine making comparisons difficult. For instance, a change in *J* could make the machine run faster and the translator travel farther. This could produce more power but at lower efficiency; increased translator travel would also decrease power density in the machine.

To be truly useful, the model needs to take into account both cogging torque (especially at low speeds) and saturation. This goes back to the previous point, in order to quantify any results the state of the machine must be better understood. As a general rule of thumb, electrical machines are more efficient as they become larger and faster. The goodness factor says this, although it doesn't strictly apply to permanent magnet

machines. This is problematic if efficiency is the goal, but the saturation limit of the core is unknown.

APPENDIX A. GENERIC SIMULINK MODEL

1. Top Level View

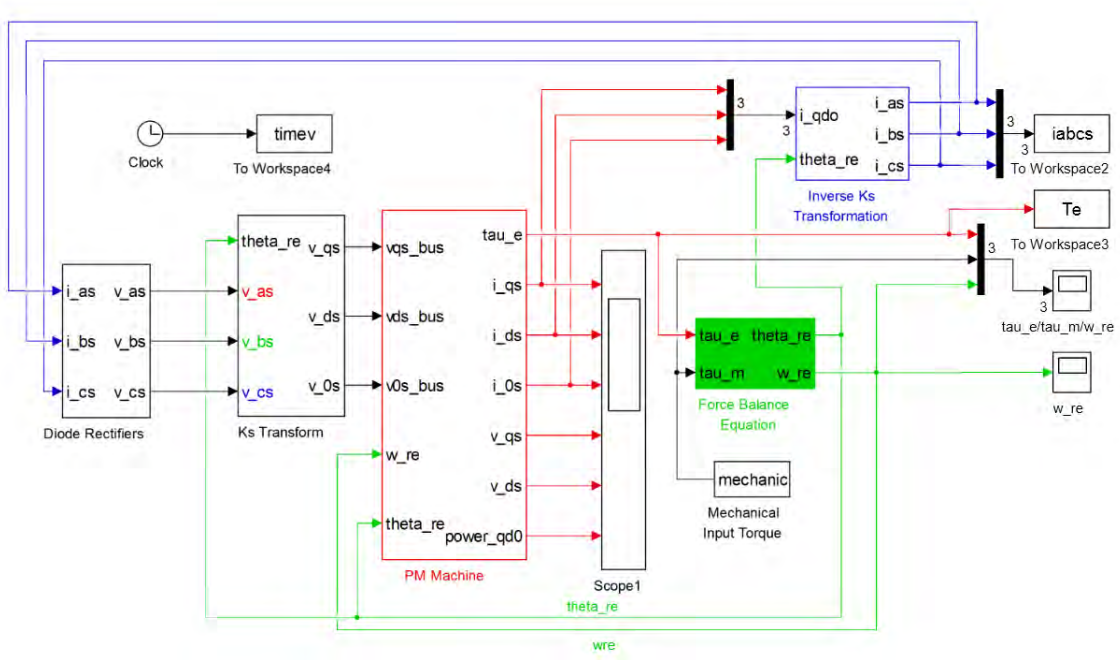

2. Permanent Magnet Machine

a. Top Level View

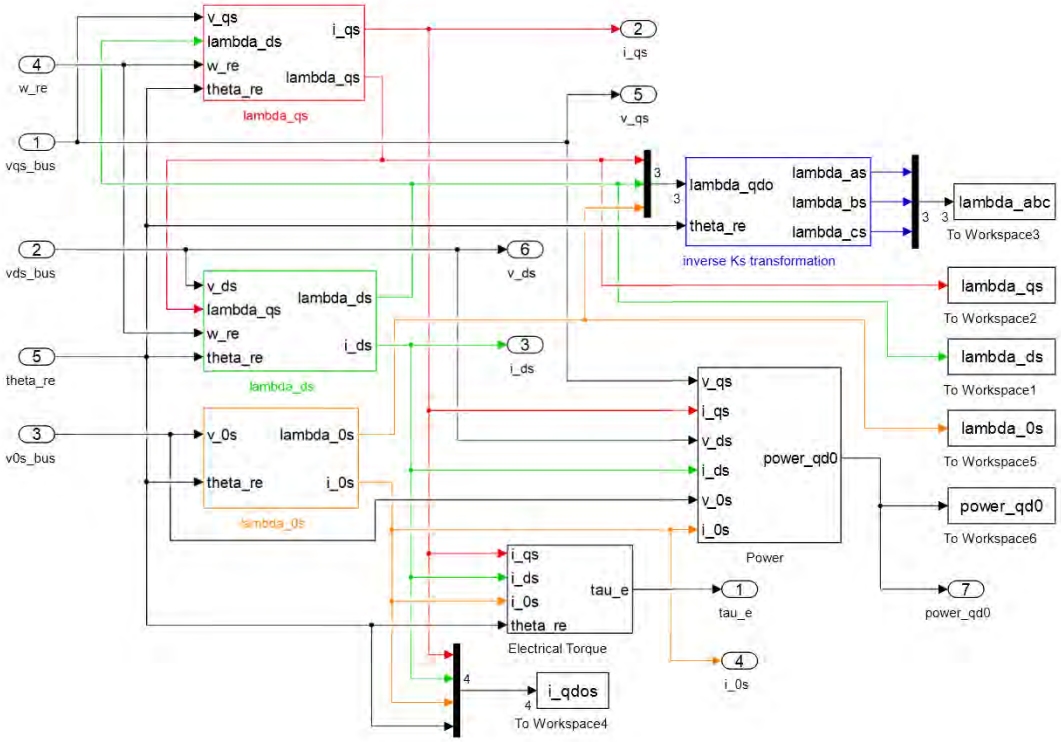

b. Flux Linkages

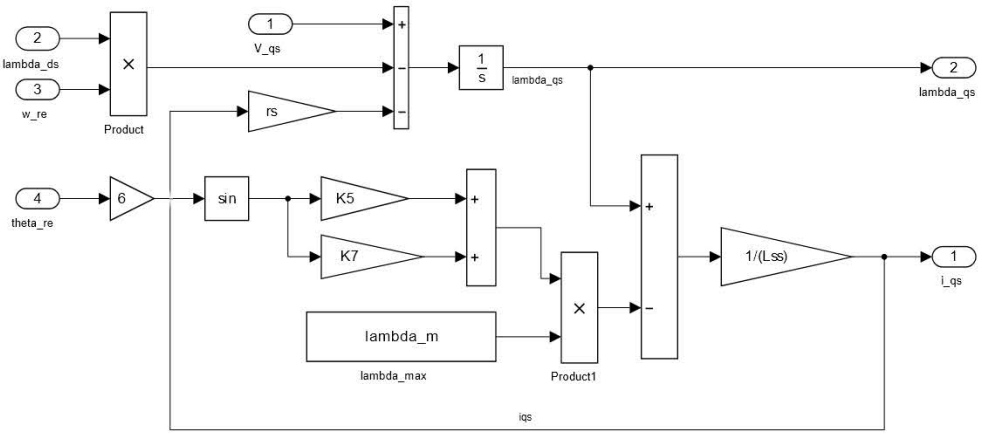

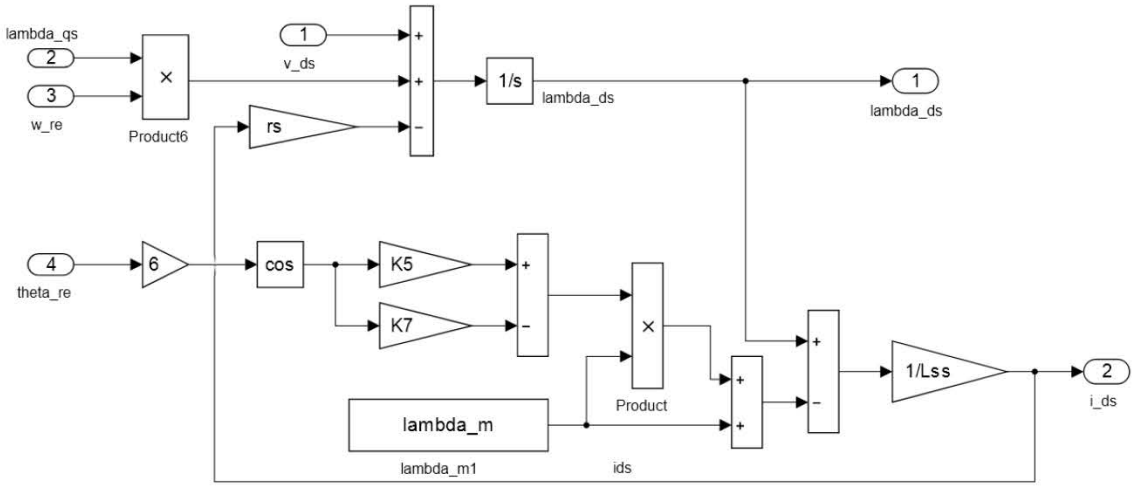

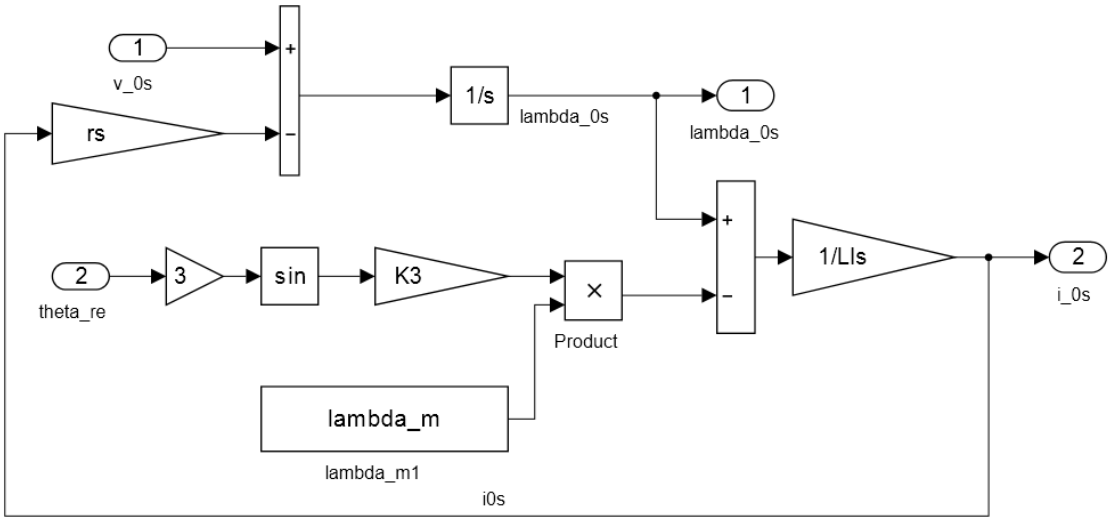

c. Electrical Torque

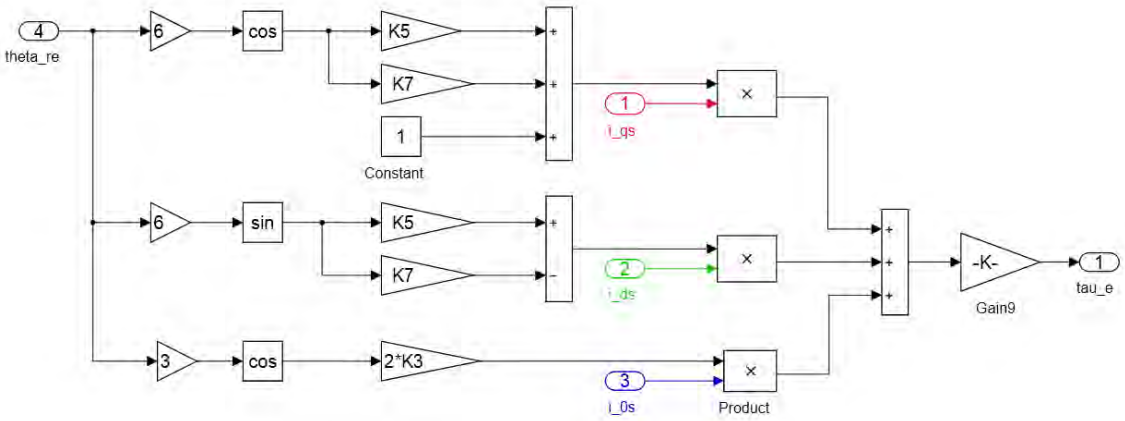

d. Electrical Power

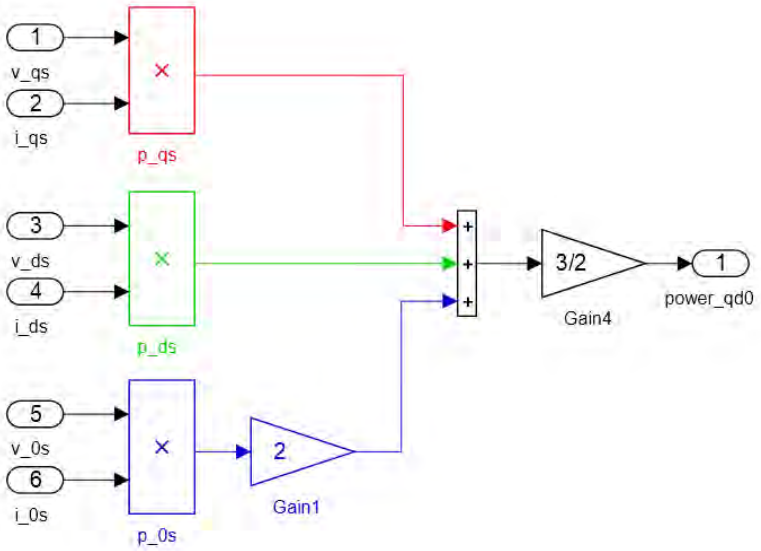

3. Ks Transform

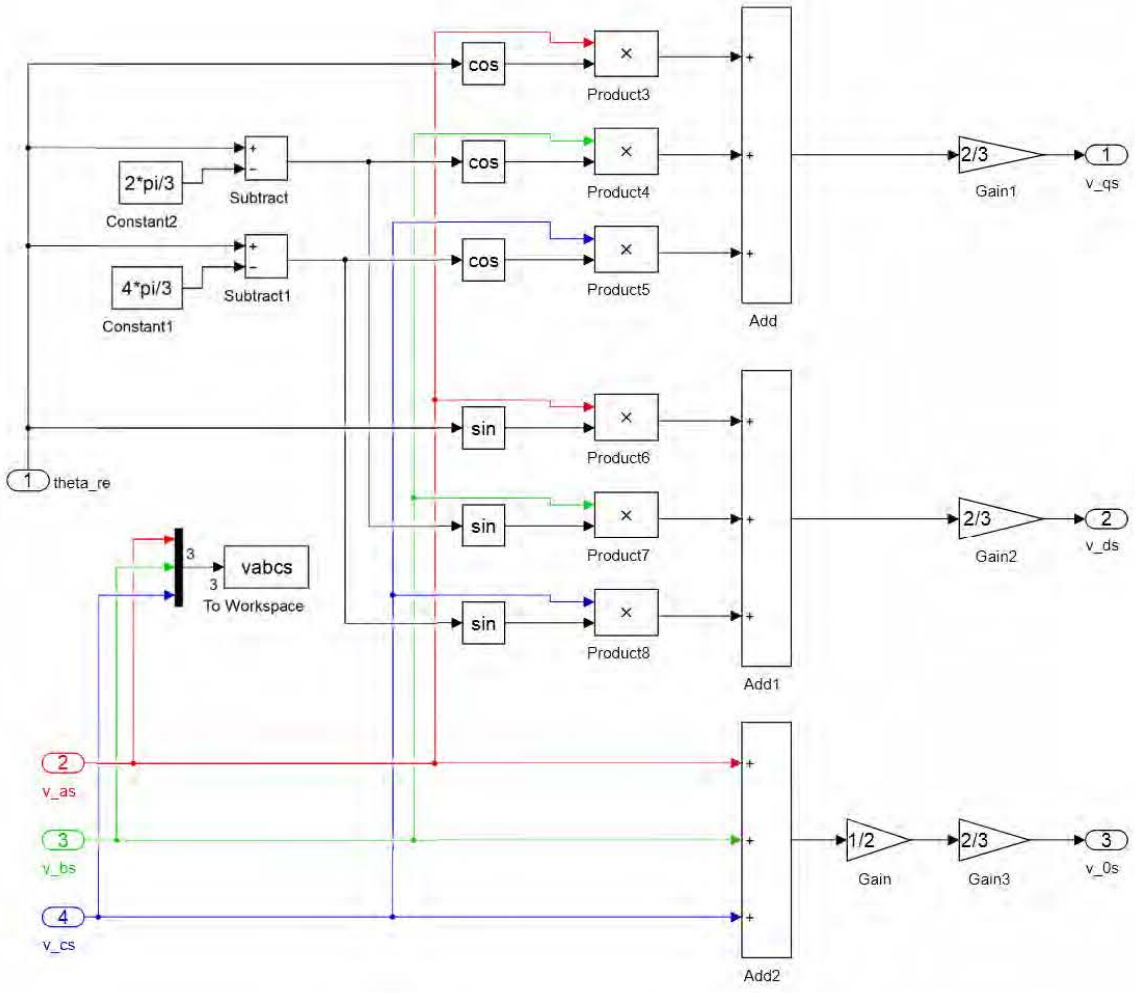

4. Inverse Ks Transform

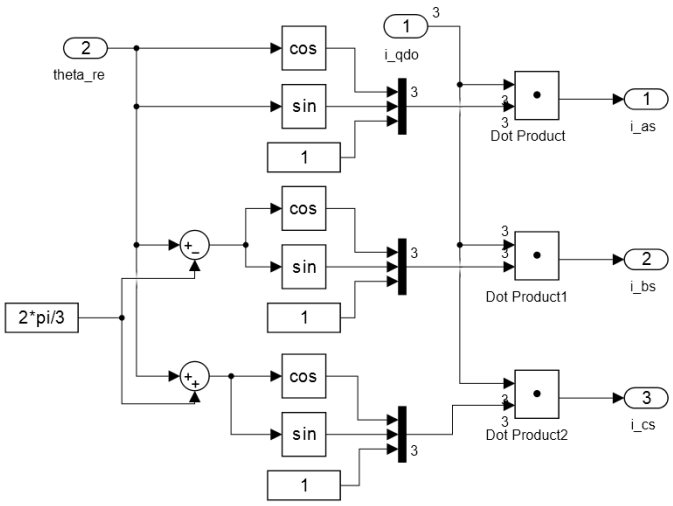

5. Balance of Forces Equation

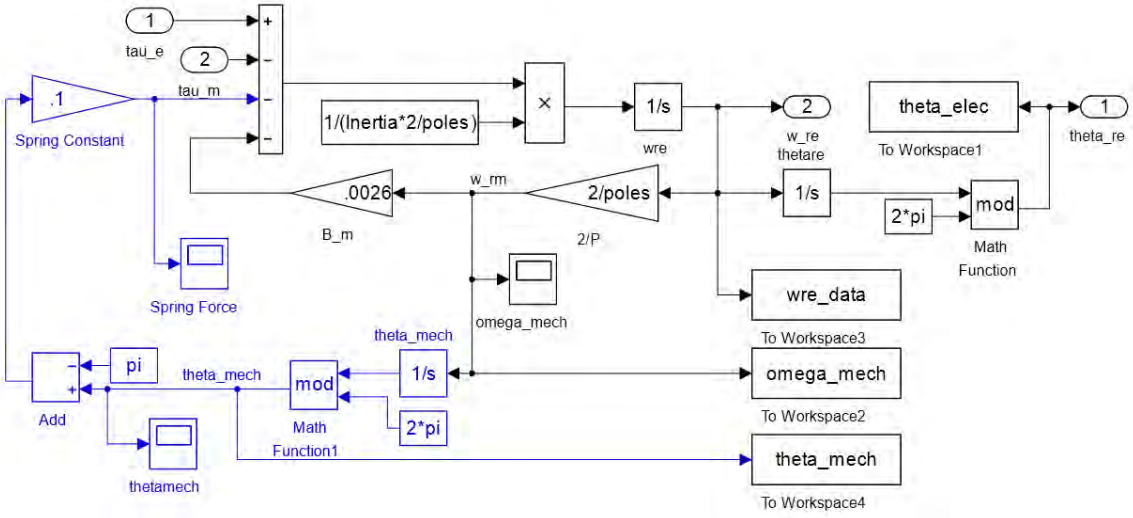

6. Diode Rectifier

a. Top Level View

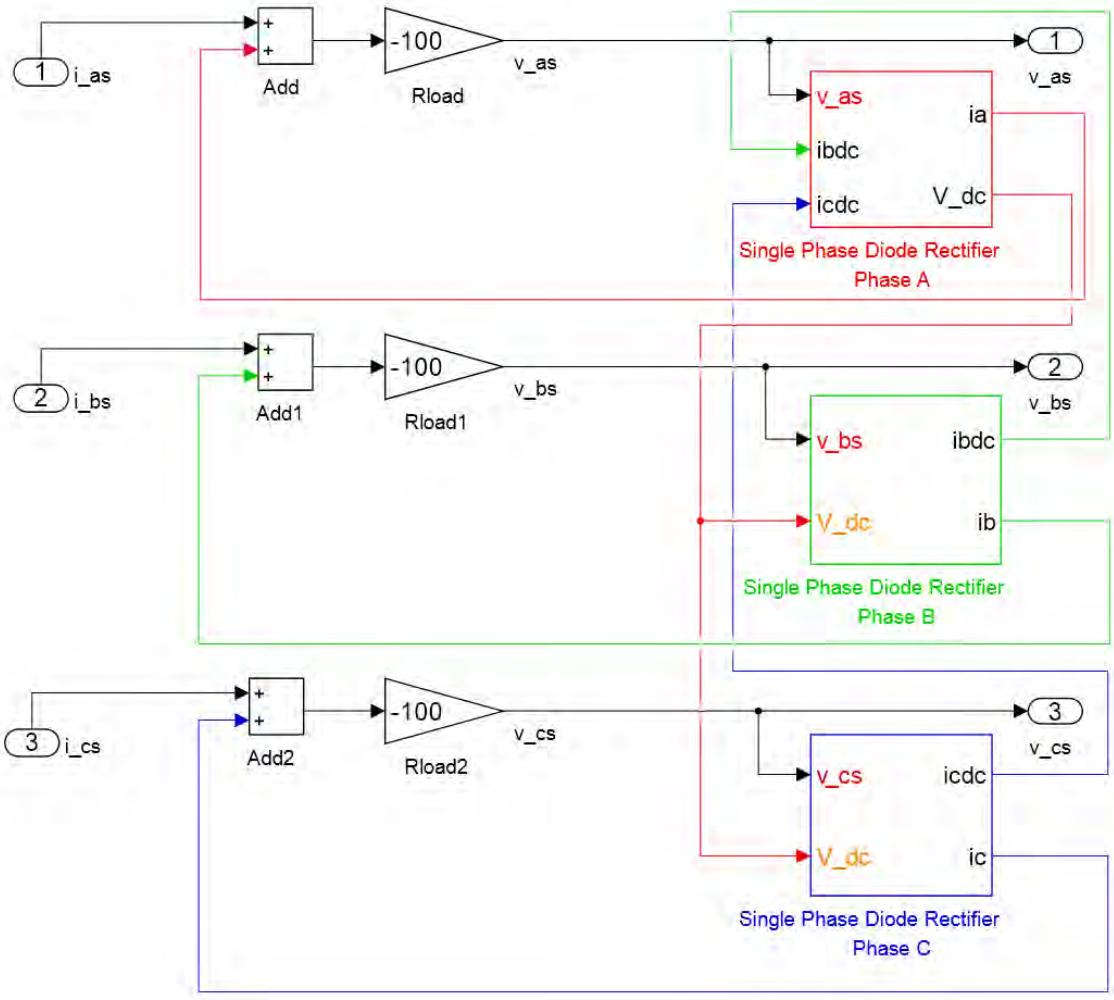

b. A-phase Rectifier

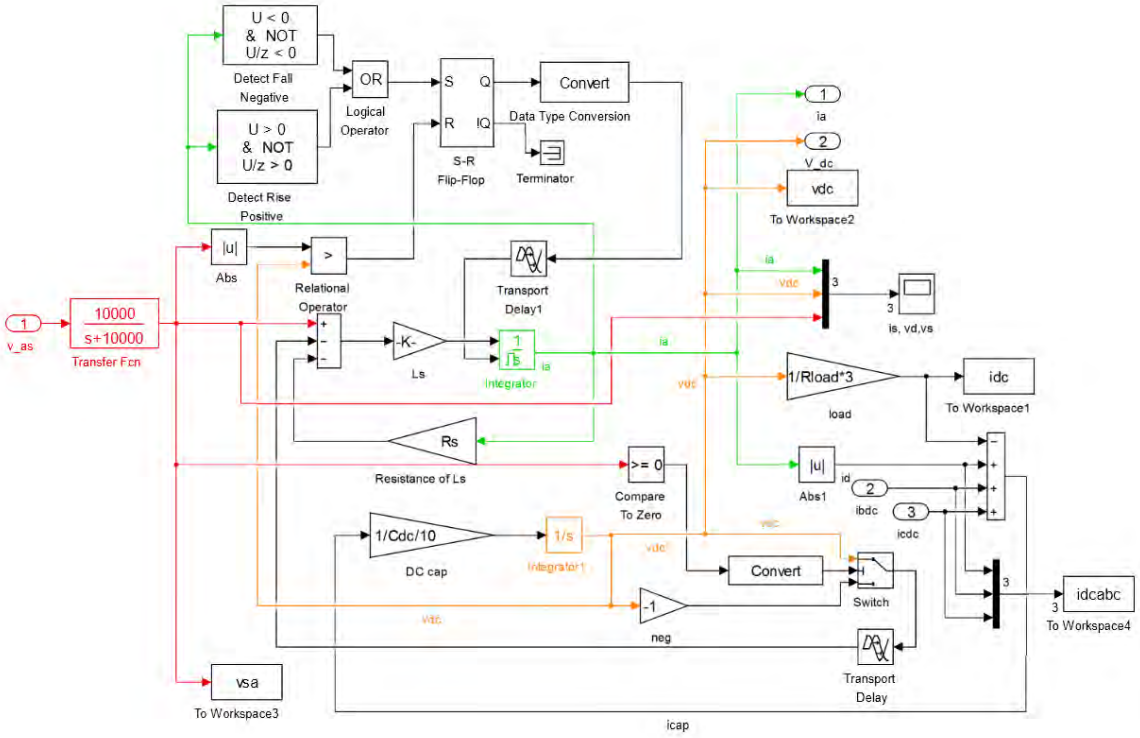

c. B-phase

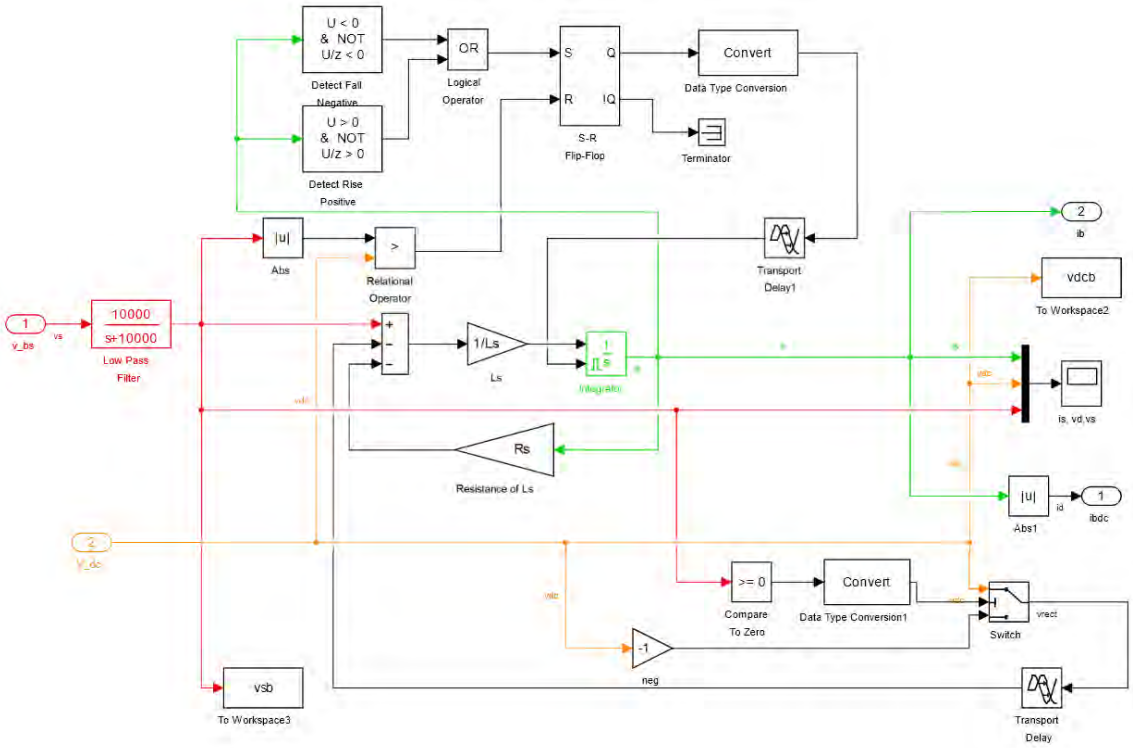
U < 0
& NOT
U/z < 0
Detect Fall
Negative
U > 0
& NOT
U/z > 0
Detect Rise
Positive
OR
Logical
Operator
S
R
Q
!Q
S-R
Flip-Flop
Convert
Data Type Conversion
Terminator
|u|
Abs
>
Relational
Operator
Transport
Delay1
2
ib
vdcb
To Workspace2
1
v_bs
vs
10000
s+10000
Low Pass
Filter
1/Ls
Ls
Rs
Resistance of Ls
is, vd, vs
|u|
Abs1
id
1
ibdc
2
V_dc
>= 0
Compare
To Zero
Convert
Data Type Conversion1
Switch
vrect
-1
neg
vsb
To Workspace3
Transport
Delay

d. C-phase

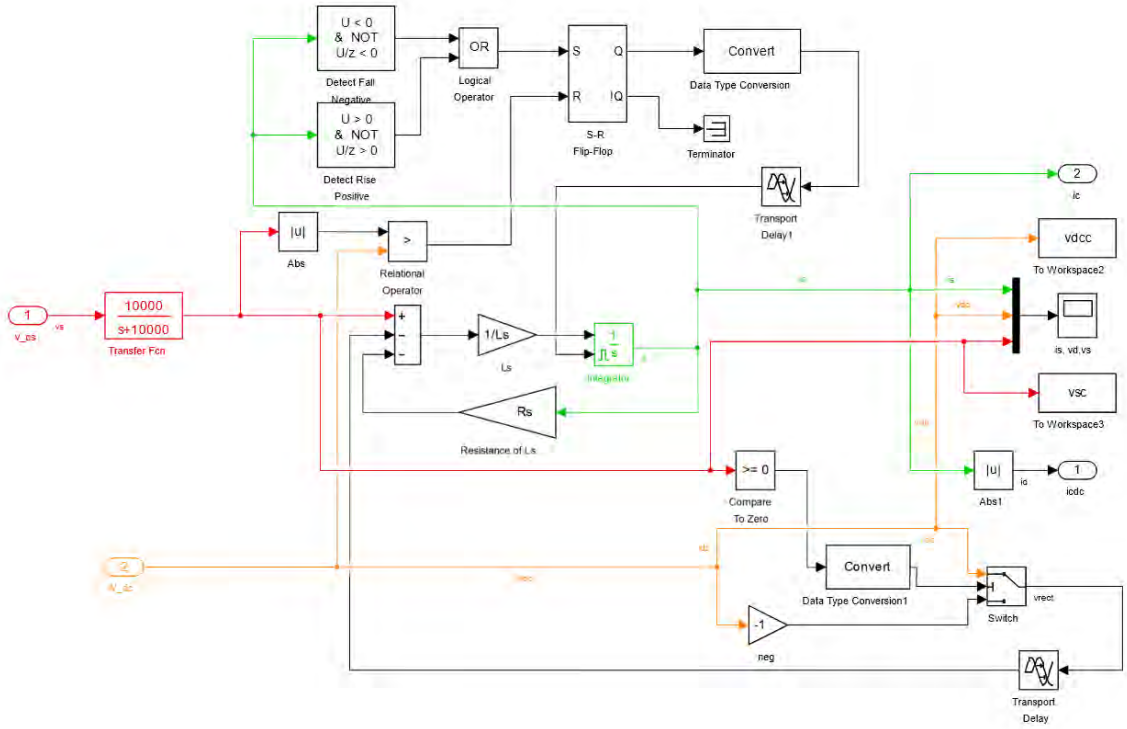
U < 0
& NOT
U/z < 0
Detect Fall
Negative
U > 0
& NOT
U/z > 0
Detect Rise
Positive
OR
Logical
Operator
S
R
Q
IQ
S-R
Flip-Flop
Convert
Data Type Conversion
Terminator
Transport
Delay1
2
ic
|u|
Abs
>
Relational
Operator
vdcc
To Workspace2
1
vs
10000
s+10000
Transfer Fcn
1/Ls
Ls
Rs
Resistance of Ls
is, vd,vs
VSC
To Workspace3
>= 0
Compare
To Zero
|u|
Abs1
ic
1
icdc
2
Convert
Data Type Conversion1
vrect
Switch
-1
neg
Transport
Delay

THIS PAGE INTENTIONALLY LEFT BLANK

APPENDIX B. LINEAR GENERATOR INITIAL CONDITIONS FILE

```
clear
close all
clc
```

1. PM Machine IC Data

```
poles = 12; %number of poles
tstop=7;
tstep=.00002;
rs=9.1;
Lms=.00412;
Bm = 0.0026;
Lls=24.5e-3;
Lss=3/2*Lms+Lls;
Inertia = .0041;
Vdc=160;
radius = 0.1; % (m)

fund_amp = 0.6;
fund_freq = 2*pi;
harmonic1 = 5;
harm1_amp = .1;
harmonic2 = 3;
harm2_amp = .1;

lambda_m = .1549;
K3=-.121;
K5=.060;
K7=-.009;
```

2. Diode Rectifier IC Data

```
Ls=1e-3;  %original
Ls1=Ls/2;
Ls2=Ls/2;
Rs=1e-3;
Rload=50;
Cdc=1100e-6;
```

Published with MATLAB® R2014a

THIS PAGE INTENTIONALLY LEFT BLANK

APPENDIX C. LOW FREQUENCY, LOW AMPLITUDE SINUSOIDAL INPUT FORCE SCENARIO

1. Simulink Input Force

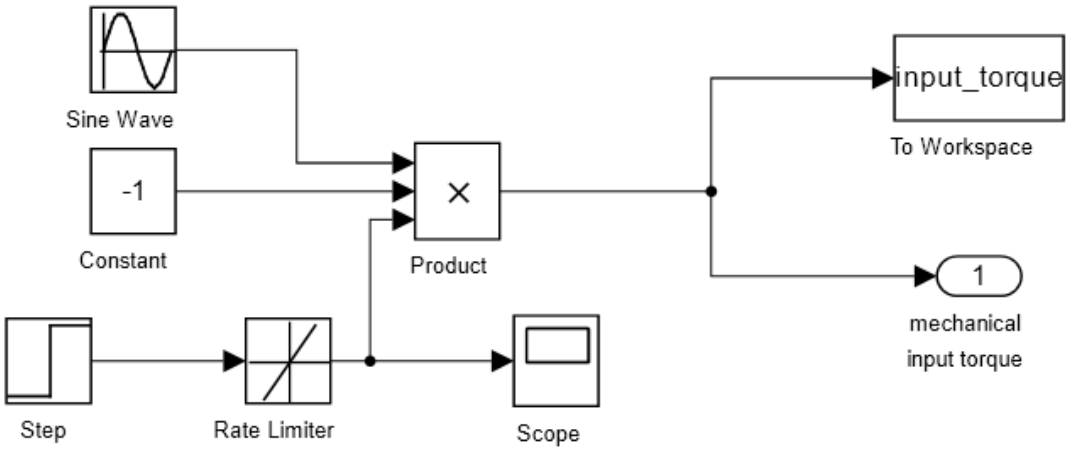

2. Defining Variables

```
% Linear Generator Post Run File
format compact
close all;
clc
fig = 0;
ias=iabcs(:,1);
ibs=iabcs(:,2);
ics=iabcs(:,3);

vas=vabcs(:,1);
vbs=vabcs(:,2);
vcs=vabcs(:,3);

power = vdc.*idc;

energy_out = sum(power)/length(timev)*max(timev)
energy_in = sum(abs(input_torque.*omega_mech))/length(timev)*max(timev)

efficiency = (energy_out / energy_in) * 100

funtime = linspace(0,2,1000);
fund = sin(2*pi*funtime);
```

```
harm3 = K3.*sin(2*pi*funtime*3);
harm5 = K5.*sin(2*pi*funtime*5);
harm7 = K7.*sin(2*pi*funtime*7);

zNormal = theta_mech ./ (2*pi); % normalized stator position

z = zNormal .* 2*pi * radius; % translator position (m)

v = omega_mech .* radius; % (m/s)

inputForce = input_torque / radius; % (N)
springForce = tau_spring / radius; % (N)
electricForce = Te / radius; % (N)
```

```
energy_out =
    9.9840
energy_in =
   18.4627
efficiency =
   54.0769
```

3. Lambdas

```
fig = fig +1;

figure(fig);
subplot(2,1,2)
plot(timev,lambda_abc(:,1),timev,lambda_abc(:,2),timev,lambda_abc(:,3),...
    'LineWidth',2)
legend('\lambda_a_s','\lambda_b_s','\lambda_c_s','Location','Southwest')
title('(b)')
xlabel('Time (s)'); ylabel('Magnetic Flux (Wb)')
% xlim([1,1.5])
xlim([1.3 1.4])
%
subplot(2,1,1)
plot(timev,lambda_abc(:,1),timev,lambda_abc(:,2),timev,lambda_abc(:,3),...
    'LineWidth',1)
title('(a)')
xlabel('Time (s)'); ylabel('Magnetic Flux (Wb)')
legend('\lambda_a_s','\lambda_b_s','\lambda_c_s','Location','Southwest')
% xlim([1,1.5])
xlim([0 3])
annotation('rectangle',...
    [0.466625 0.585461689587424 0.024625 0.335952848722982],'LineWidth',2,...
    'FaceColor','flat');
```

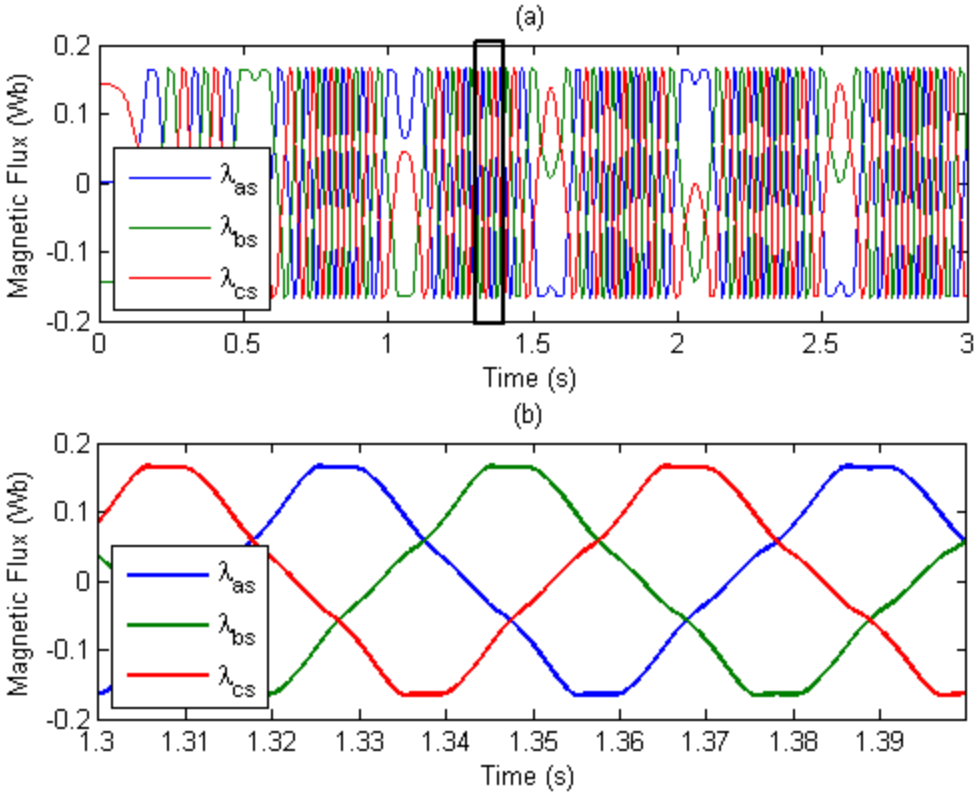

4. Forces at play

```
fig = fig+1;
figure(fig)
plot(timev,-v,timev,inputForce+springForce,'LineWidth',2)
hold on
plot(timev,-electricForce,'r')
hold off
legend('Velocity (m/s)','F_i_n+F_{spring} (N)','F_{electric}     (N)',...
    'Location','Southeast')
xlim([0 3])
ylabel('Amplitude')

fig = fig+1;
figure(fig)
plot(timev,inputForce,timev,inputForce+springForce,'LineWidth',2)
legend('F_i_n','F_i_n+F_{spring}','Location','Southwest')
xlim([0 3])
xlabel('Time (s)'); ylabel('Force (N)')
```

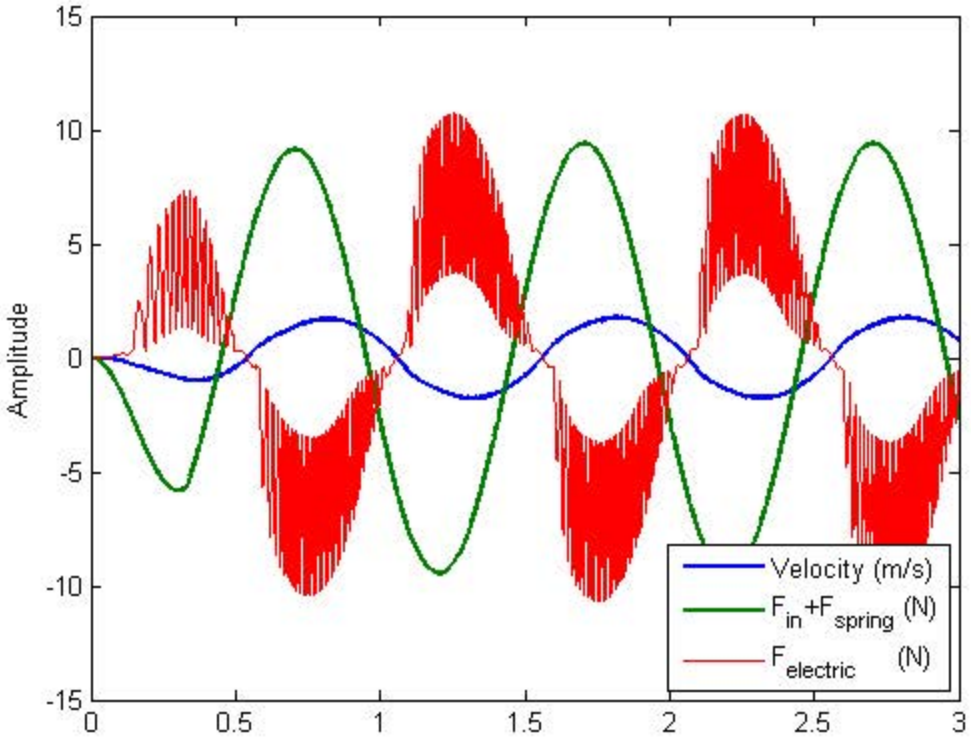
15
10
5
0
-5
-10
-15
Amplitude
0
0.5
1
1.5
2
2.5
3
Velocity (m/s)
F_in+F_spring (N)
F_electric (N)

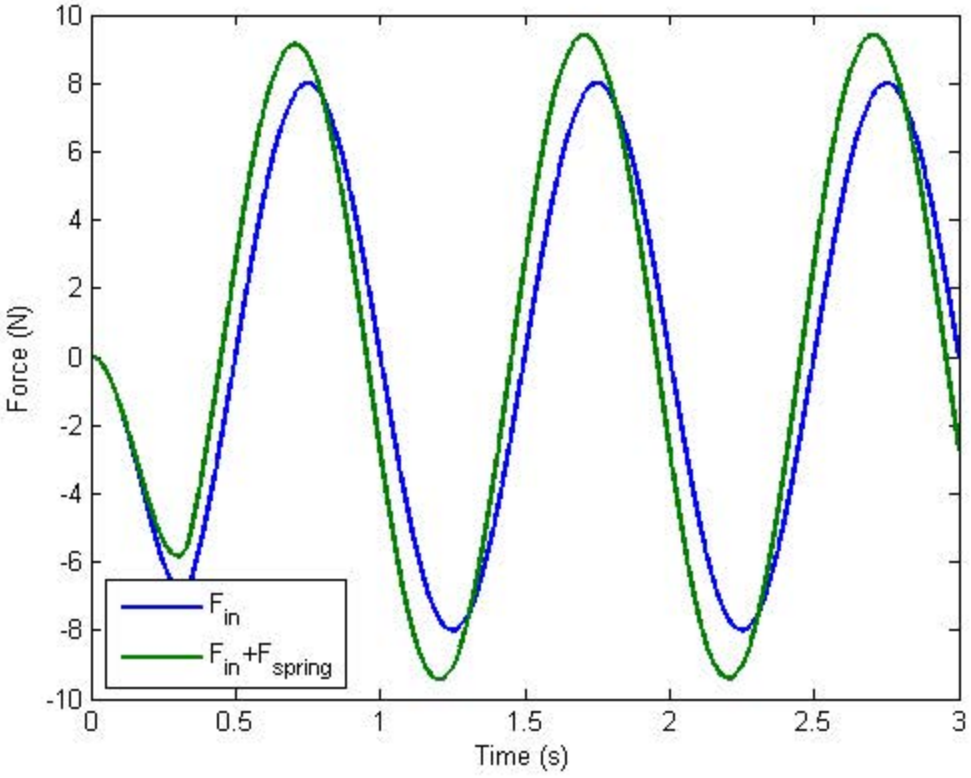
10
8
6
4
2
0
-2
-4
-6
-8
-10
Force (N)
0
0.5
1
1.5
2
2.5
3
Time (s)
F_in
F_in+F_spring

5. Position & Velocity (Mechanical)

```
fig = fig+1;
figure(fig)
plot(timev,z,timev,v,'LineWidth',2)
xlim([0 3])
ylabel('Amplitude')
xlabel('Time (s)')
legend('Position    (m)','Velocity (m/s)','Location','Northwest')
```

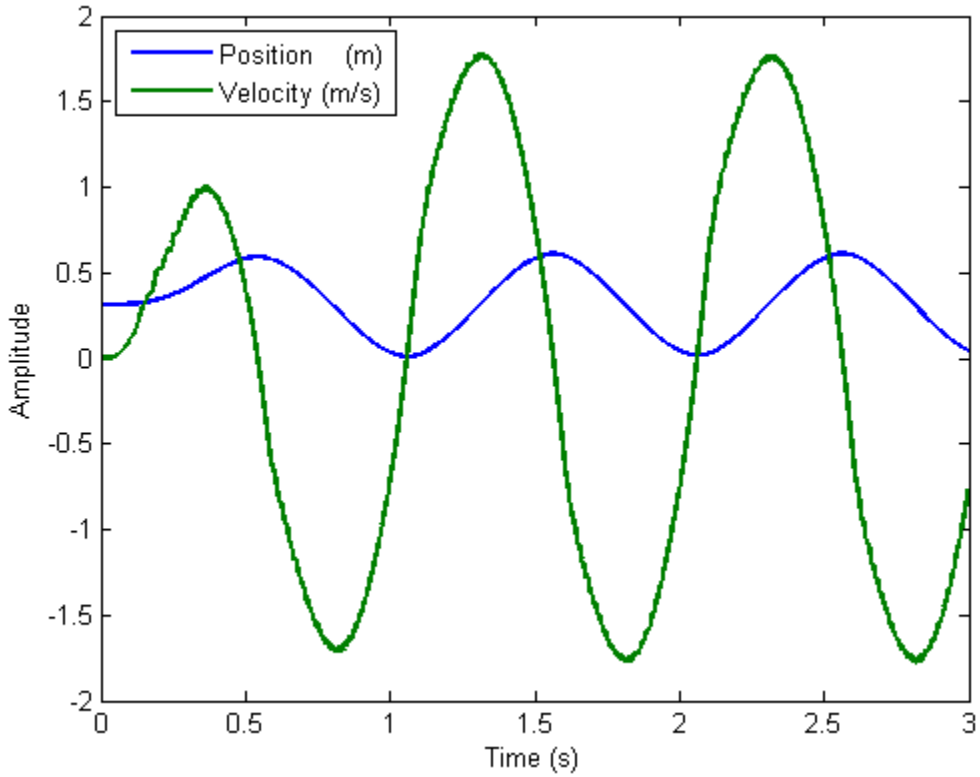

6. ABC Variables

```
fig = fig+1;

figure(fig)
subplot(2,1,1)
plot(timev,vas,timev,vbs,timev,vcs); title('(a)')
legend('v_a_s','v_b_s','v_c_s','Location','Southwest')
xlim([0 3]); ylim([-12,12])
ylabel('Voltage (V)'); xlabel('Time (s)')
annotation('rectangle',...
    [0.460625 0.587426326129664 0.026875 0.332023575638502],'LineWidth',2,...
    'FaceColor','flat');
```

```
subplot(2,1,2)
plot(timev,ias,timev,ibs,timev,ics); title('(b)')
legend('i_a_s','i_b_s','i_c_s','Location','Southwest')
xlim([0 3])
ylabel('Current (A)'); xlabel('Time (s)')
annotation('rectangle',...
    [0.4625 0.113948919449902 0.025 0.332023575638507],'LineWidth',2,...
    'FaceColor','flat');
```

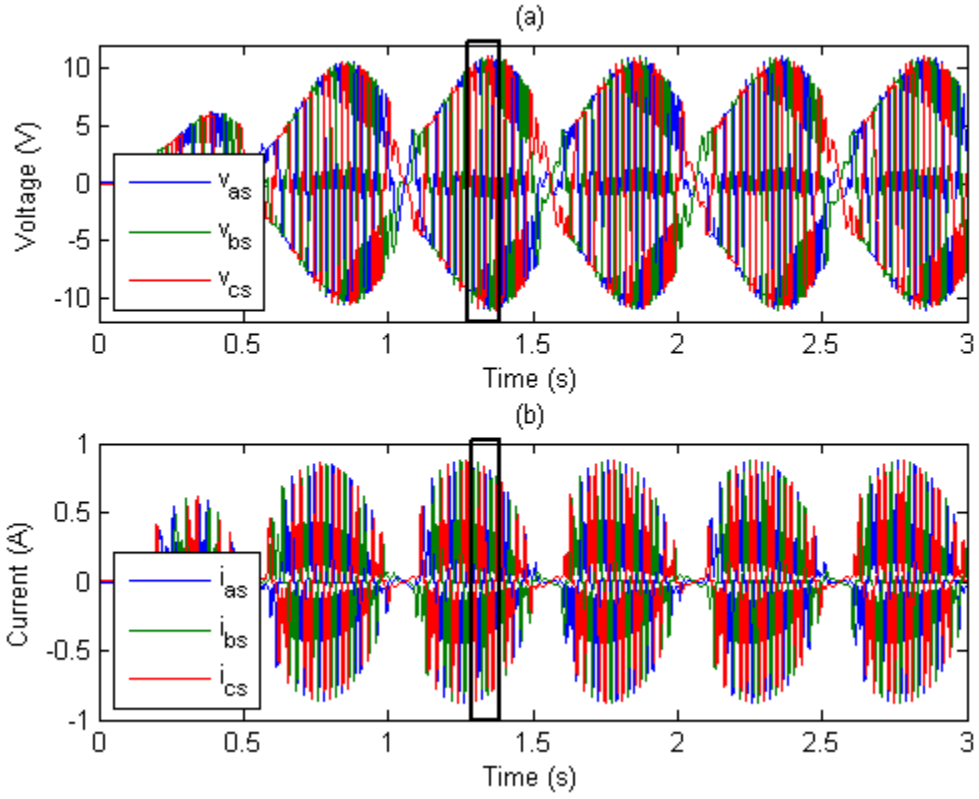

7. ABC Variables short timeframe

```
fig = fig+1;

figure(fig)
subplot(2,1,1)
plot(timev,vas,timev,vbs,timev,vcs,'LineWidth',2); title('(a)')
legend('v_a_s','v_b_s','v_c_s','Location','Southwest')
ylabel('Voltage (V)'); xlabel('Time (s)')
xlim([1.25 1.35])
ylim([-12,12])

subplot(2,1,2)
plot(timev,ias,timev,ibs,timev,ics,'LineWidth',2); title('(b)')
```

```
legend('i_a_s','i_b_s','i_c_s','Location','Southwest')
ylabel('Current (A)'); xlabel('Time (s)')
xlim([1.25 1.35])
```

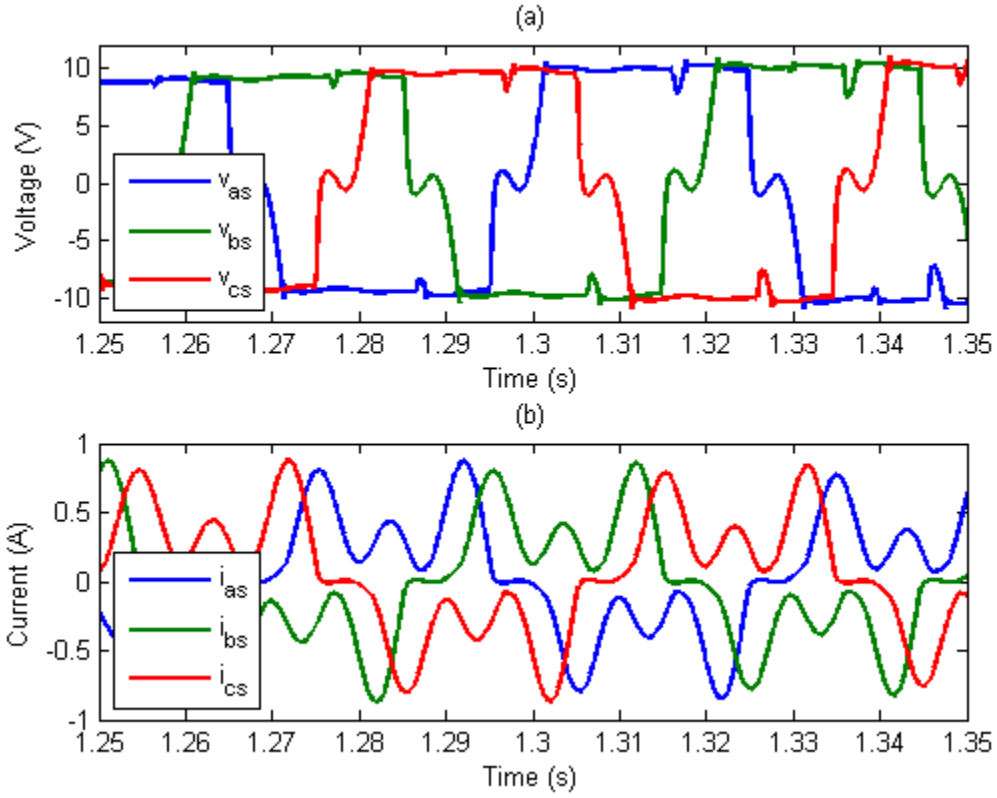

8. qd0 Variables

```
fig = fig+1;

figure(fig)
subplot(3,1,1)
plot(timev,i_qdos(:,1))
xlim([0 3])
legend('i_q')
subplot(3,1,2)
plot(timev,i_qdos(:,2))
xlim([0 3])
legend('i_d')
subplot(3,1,3)
plot(timev,i_qdos(:,3))
xlim([0 3])
legend('i_0')

iqs=i_qdos(:,1);
ids=i_qdos(:,2);
```

```
i0s=i_qdos(:,3);
theta_r=i_qdos(:,4);
iqd_angle=angle(iqs-1i*ids)*180/pi;
```

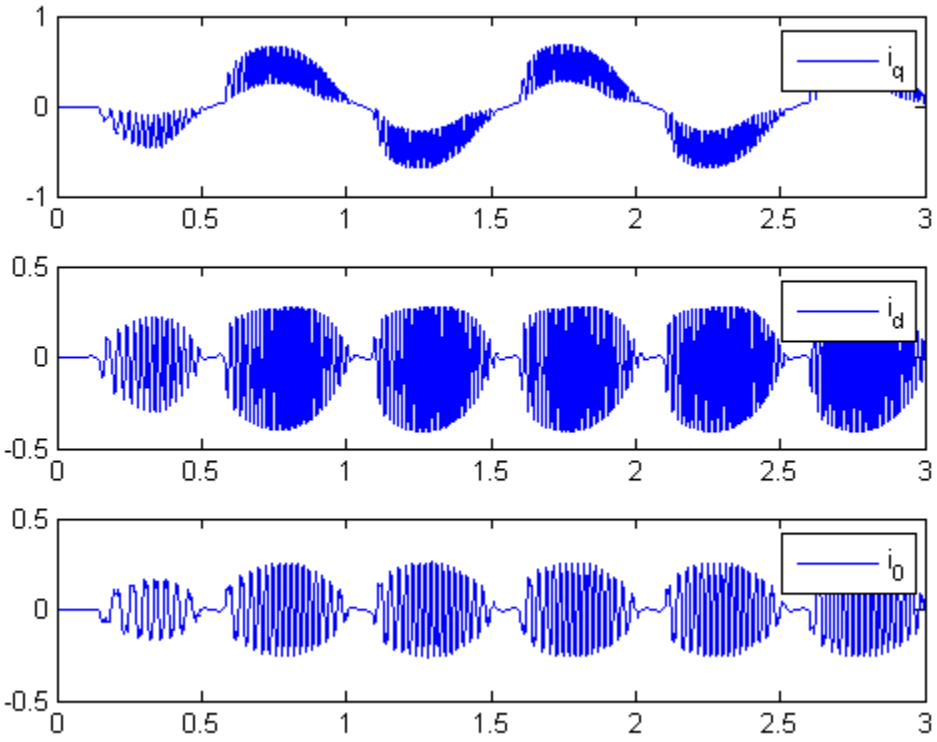

9. Velocity and Position (Electrical)

```
fig = fig+1;

figure(fig)
subplot(2,1,1)
plot(timev,wre_data,'LineWidth',2)
title('(a)')
xlabel('Time (s)'); ylabel('Angular Velocity (rad/s)')
xlim([0 3]); ylim([-125 125])
%legend('\omega_r_e')

subplot(2,1,2)
plot(timev,theta_elec,'r','LineWidth',2)
title('(b)')
xlabel('Time (s)'); ylabel('Electrical Position (rad)')
xlim([0 3])
%legend('\theta_r_e')
ylim([0,2*pi])
```

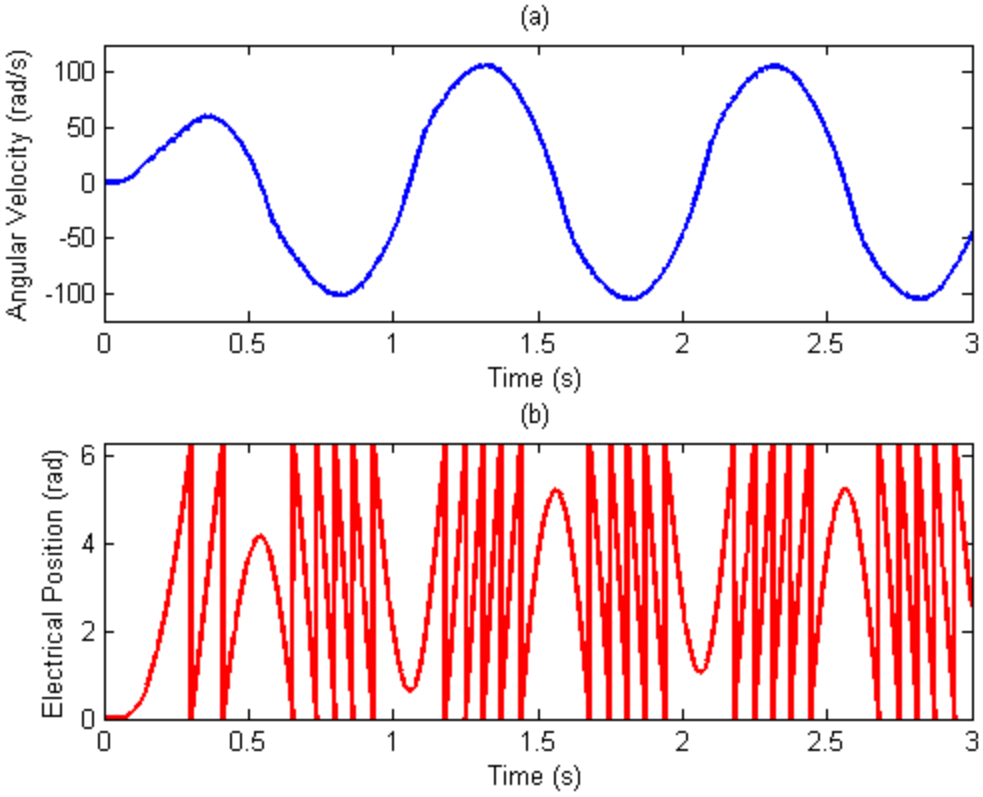

10. Velocity and Position (Mechanical)

```
fig = fig+1;

figure(fig)
subplot(2,1,1)
plot(timev,v,'LineWidth',2)
title('(a)')
xlabel('Time (s)'); ylabel('Velocity (m/s)')
xlim([0 3]);
%legend('Velocity')
xlabel('Time (s)')

subplot(2,1,2)
plot(timev,z,'r','LineWidth',2)
title('(b)')
xlim([0 3]); ylim([0 .7])
xlabel('Time (s)'); ylabel('Position (m)')
%legend('Position')
```

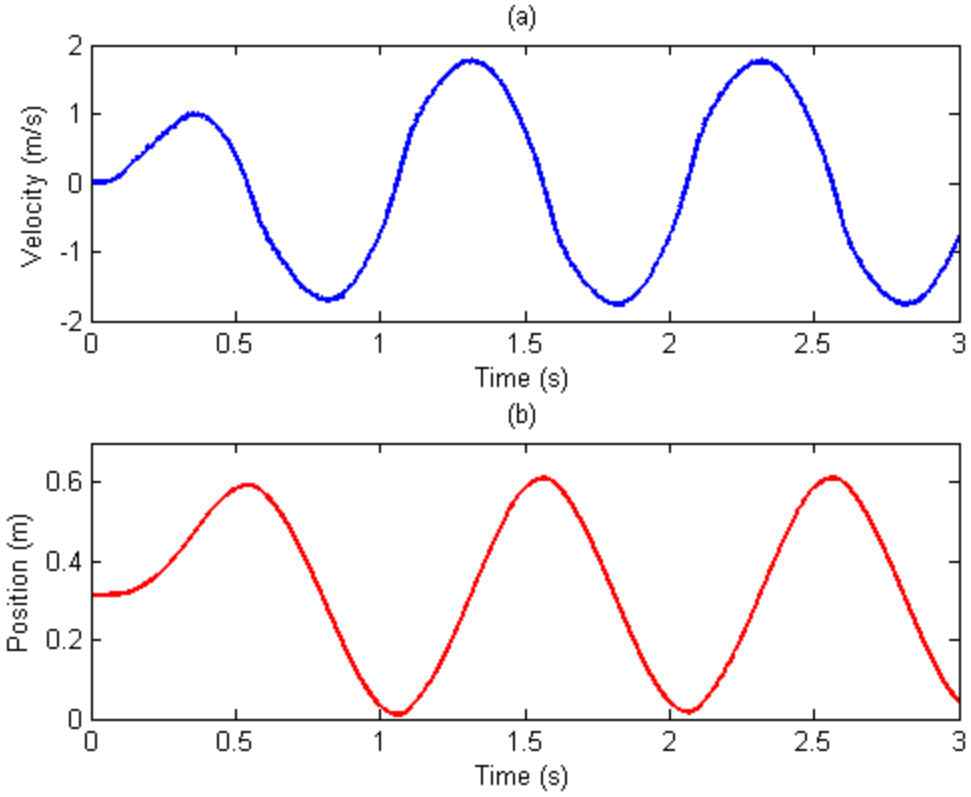

11. DC Variables

```
fig = fig+1;

figure(fig)
plot(timev,vdc,'LineWidth',2)
xlim([0 3]); ylim([0 11])
xlabel('Time (s)'); ylabel('Voltage (V)')

fig = fig+1;

figure(fig)
subplot(2,1,1)
plot(timev,vdc,'LineWidth',2); title('(a)')
xlim([1.25 1.65]); %ylim([0 11])
xlabel('Time (s)'); ylabel('Voltage (V)')

subplot(2,1,2)
figure(fig)
plot(timev,idcabc(:,1),timev,idcabc(:,2),timev,idcabc(:,3));
title('(b)')
legend('i_a dc','i_b dc','i_c dc','Location','Best')
xlim([1.25 1.65]); %ylim([-1 17])
xlabel('Time(s)'); ylabel('Current (A)')
```

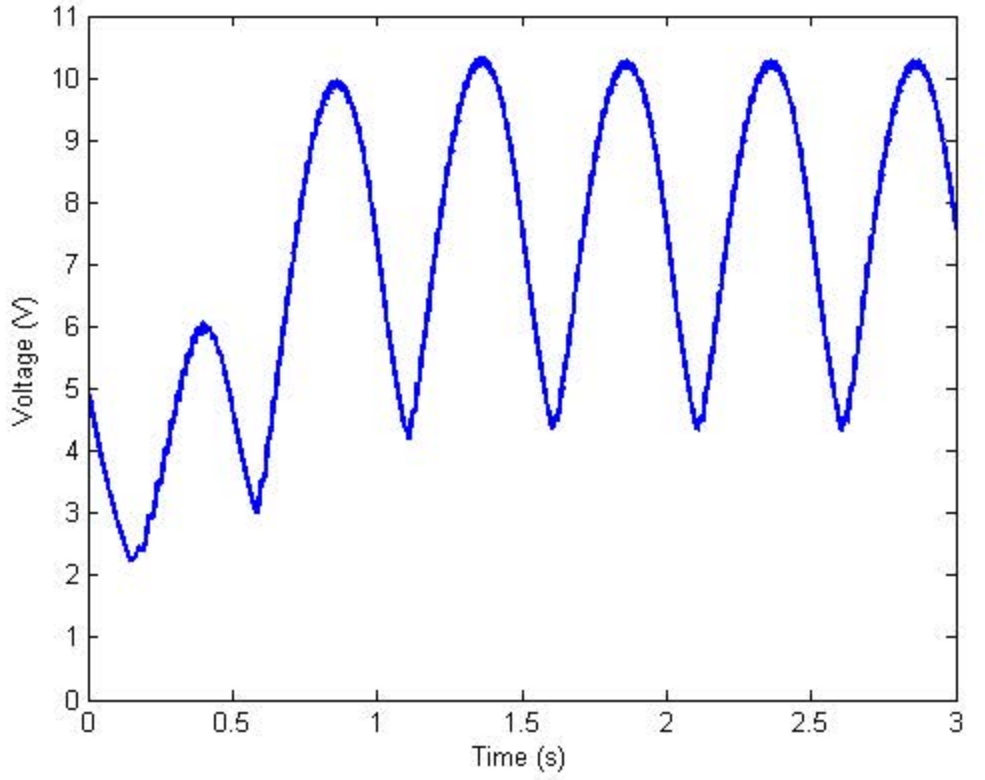
Voltage (V)
Time (s)
0
0.5
1
1.5
2
2.5
3
0
1
2
3
4
5
6
7
8
9
10
11

(a)

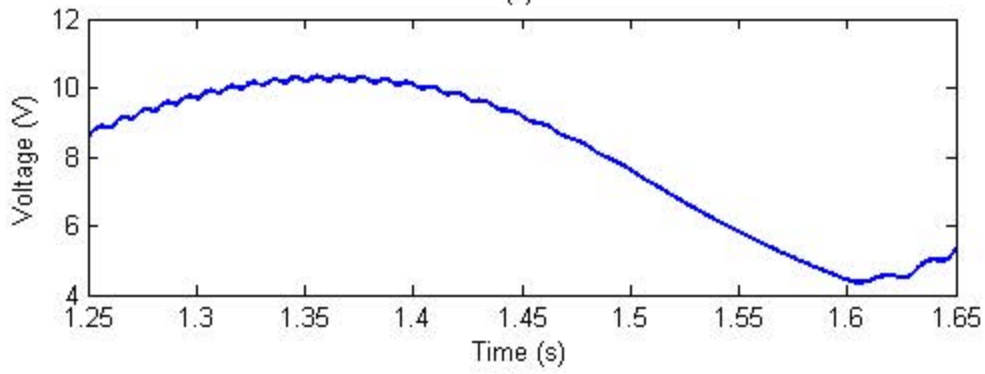
Voltage (V)
Time (s)
1.25
1.3
1.35
1.4
1.45
1.5
1.55
1.6
1.65
4
6
8
10
12

(b)

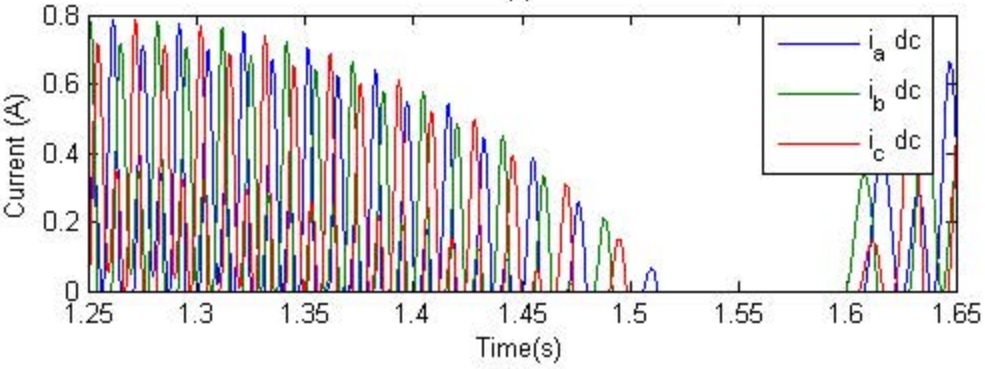
Current (A)
Time(s)
i_a dc
i_b dc
i_c dc
0
0.2
0.4
0.6
0.8
1.25
1.3
1.35
1.4
1.45
1.5
1.55
1.6
1.65

12. Lambda Harmonics

```
fig = fig+1;

figure(fig)
plot(funtime,0.1549*(fund+harm3+harm5+harm7),'LineWidth',2)
xlim([0 max(funtime)])
%legend('\lambda_P_M')
xlabel('Time (arbitrary)'); ylabel('Magnetic Flux (Wb)')
```

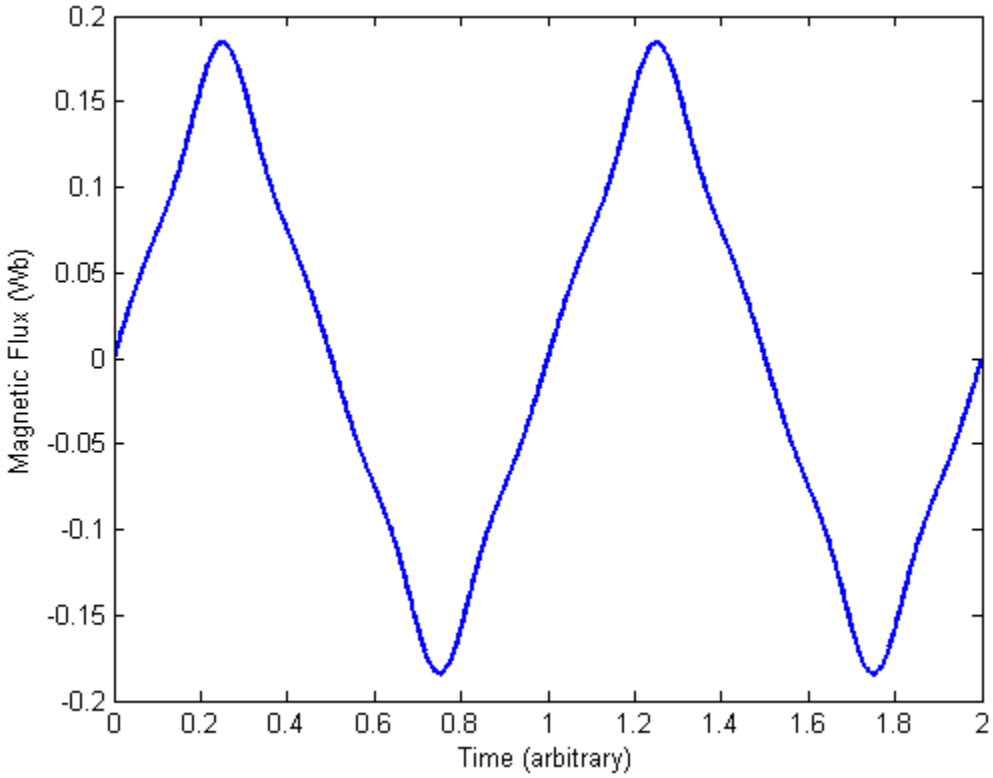

13. Input Torque and Force

```
fig = fig+1;

figure(fig)
subplot(2,1,1)
plot(timev,input_torque,'LineWidth',2)
title('(a)')
xlim([0 3]);
%legend('\tau_i_n','Location','Southeast')
ylabel('Torque (N\cdotm)')
xlabel('Time (s)')
```

```
subplot(2,1,2)
plot(timev,inputForce,'r','LineWidth',2)
title('(b)')
xlim([0 3])
%legend('F_i_n','Location','Southeast')
ylabel('Force (N)')
xlabel('Time (s)')
```

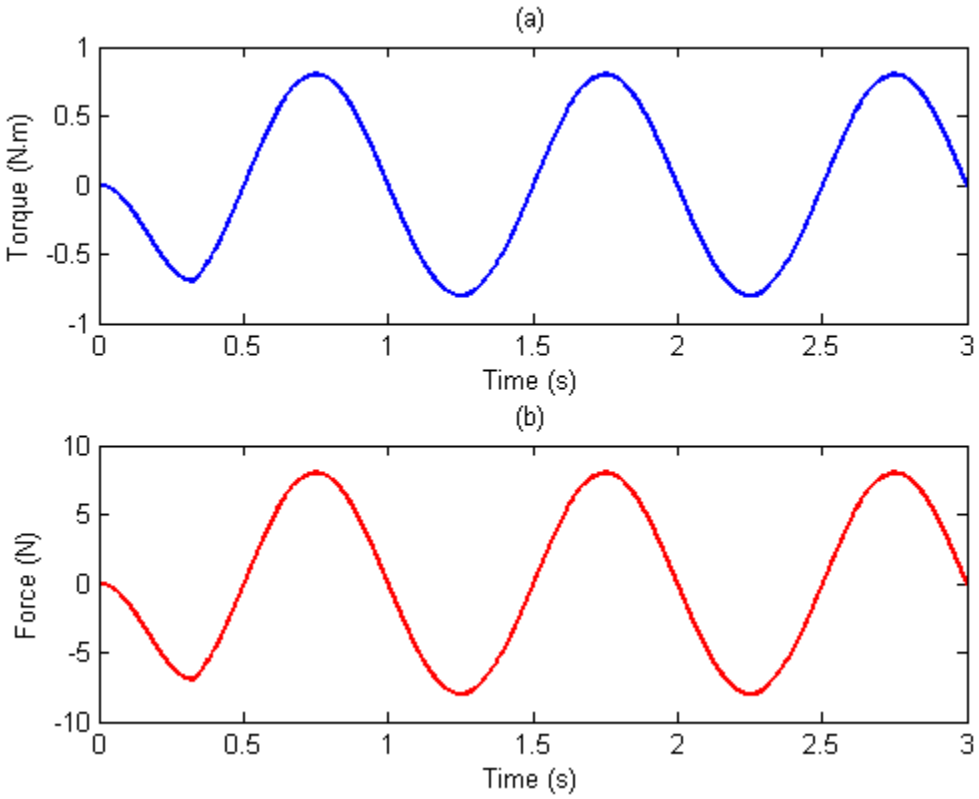

Published with MATLAB® R2014a

THIS PAGE INTENTIONALLY LEFT BLANK

APPENDIX D. LOW FREQUENCY, LOW AMPLITUDE SINE INPUT WITH MULTIPLE HARMONICS ADDED

1. Simulink Input Force

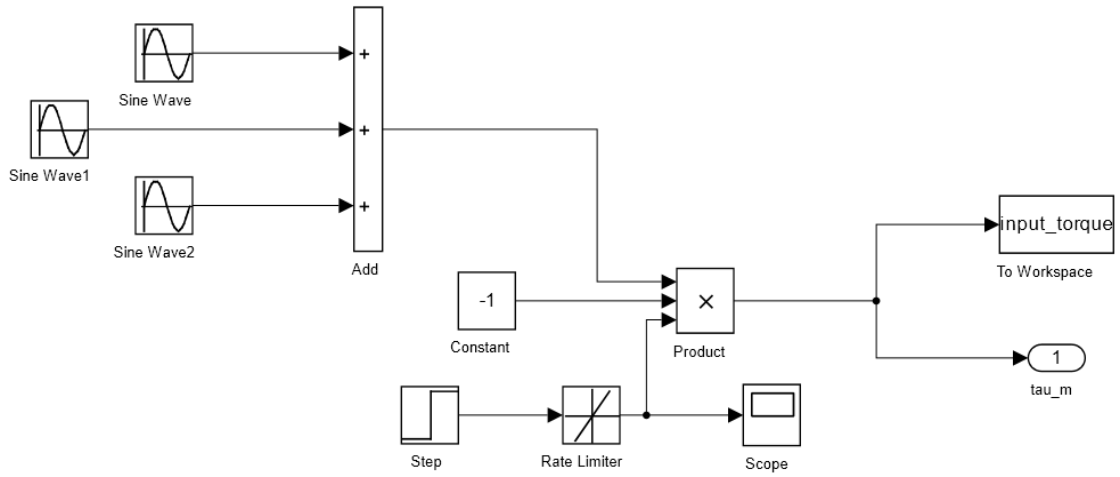

2. Defining Variables

```
% Linear Generator Post Run File
format compact
close all;
clc
fig = 0;
ias=iabcs(:,1);
ibs=iabcs(:,2);
ics=iabcs(:,3);

vas=vabcs(:,1);
vbs=vabcs(:,2);
vcs=vabcs(:,3);

power = vdc.*idc;

energy_out = sum(power)/length(timev)*max(timev)
energy_in = sum(abs(input_torque.*omega_mech))/length(timev)*max(timev)

efficiency = (energy_out / energy_in) * 100

funtime = linspace(0,2,1000);
fund = sin(2*pi*funtime);
harm3 = K3.*sin(2*pi*funtime*3);
harm5 = K5.*sin(2*pi*funtime*5);
```

```
harm7 = K7.*sin(2*pi*funtime*7);

zNormal = theta_mech ./ (2*pi); % normalized stator position

z = zNormal .* 2*pi * radius; % translator position (m)

v = omega_mech .* radius; % (m/s)

inputForce = input_torque / radius; % (N)
springForce = tau_spring / radius; % (N)
electricForce = Te / radius; % (N)
```

```
energy_out =
    5.8314
energy_in =
   10.2244
efficiency =
   57.0341
```

3. Lambdas

```
fig = fig +1;

figure(fig);
subplot(2,1,2)
plot(timev,lambda_abc(:,1),timev,lambda_abc(:,2),timev,lambda_abc(:,3),...
    'LineWidth',2)
legend('\lambda_a_s','\lambda_b_s','\lambda_c_s','Location','Southwest')
title('(b)')
xlabel('Time (s)'); ylabel('Magnetic Flux (Wb)')
% xlim([1,1.5])
xlim([1.3 1.4])
%
subplot(2,1,1)
plot(timev,lambda_abc(:,1),timev,lambda_abc(:,2),timev,lambda_abc(:,3),...
    'LineWidth',1)
title('(a)')
xlabel('Time (s)'); ylabel('Magnetic Flux (Wb)')
legend('\lambda_a_s','\lambda_b_s','\lambda_c_s','Location','Southwest')
% xlim([1,1.5])
xlim([0 3])
annotation('rectangle',...
    [0.466625 0.585461689587424 0.024625 0.335952848722982],'LineWidth',2,...
    'FaceColor','flat');
```

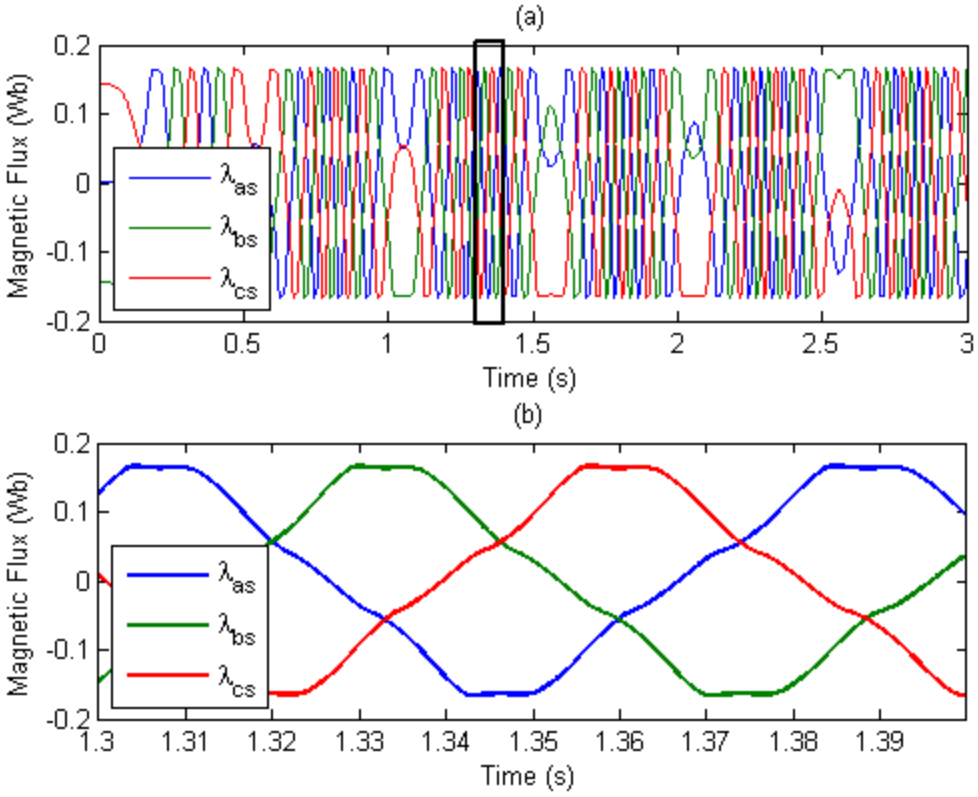

4. Forces at play

```
fig = fig+1;
figure(fig)
plot(timev,-v,timev,inputForce+springForce,'LineWidth',2)
hold on
plot(timev,-electricForce,'r')
hold off
legend('Velocity (m/s)','F_i_n+F_{spring} (N)','F_{electric}     (N)',...
    'Location','Southeast')
xlim([0 3])
ylabel('Amplitude')

fig = fig+1;
figure(fig)
plot(timev,inputForce,timev,inputForce+springForce,'LineWidth',2)
legend('F_i_n','F_i_n+F_{spring}','Location','Southwest')
xlim([0 3])
xlabel('Time (s)'); ylabel('Force (N)')
```

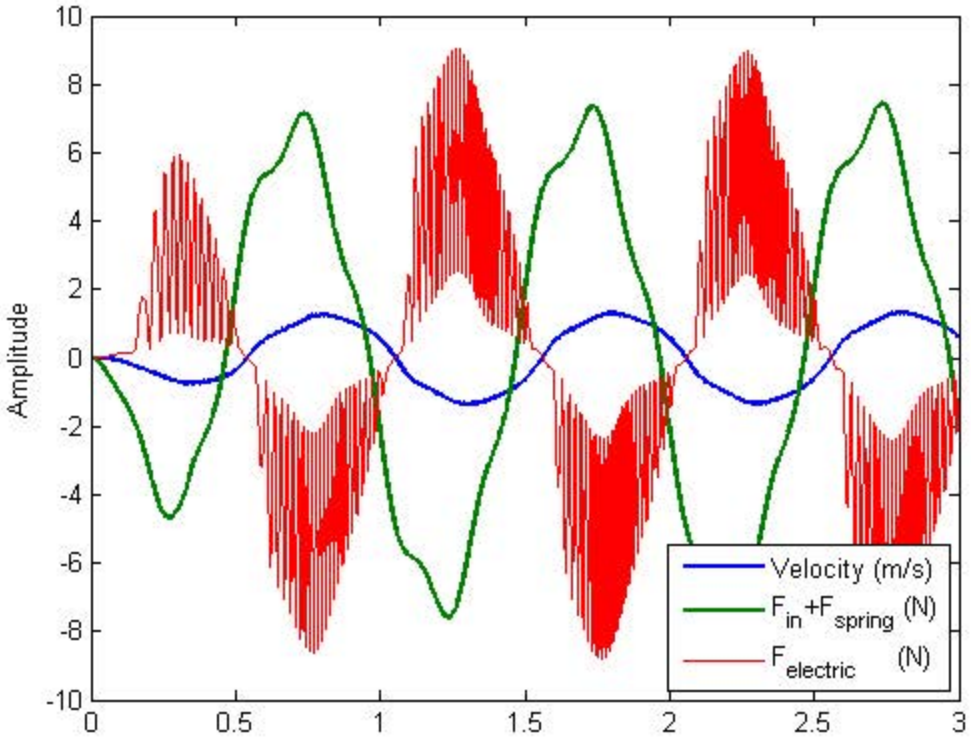
Amplitude
Velocity (m/s)
F_in+F_spring (N)
F_electric (N)

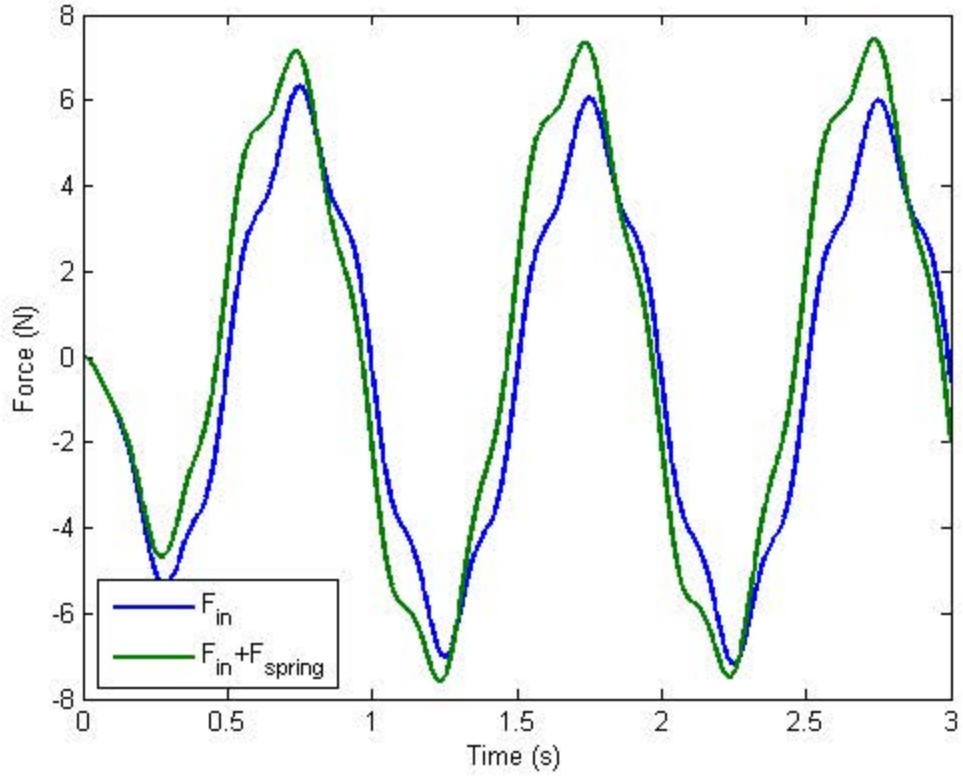
Force (N)
F_in
F_in+F_spring
Time (s)

5. Position & Velocity (Mechanical)

```
fig = fig+1;
figure(fig)
plot(timev,z,timev,v,'LineWidth',2)
xlim([0 3])
ylabel('Amplitude')
xlabel('Time (s)')
legend('Position    (m)','Velocity (m/s)','Location','Northwest')
```

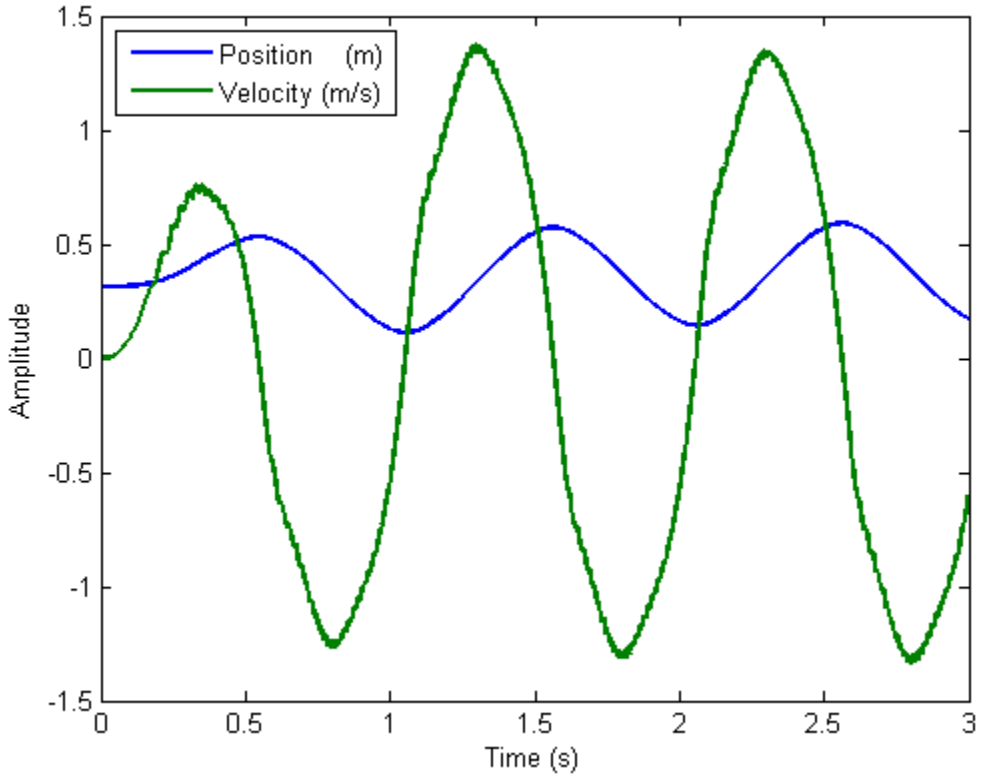

6. ABC Variables

```
fig = fig+1;

figure(fig)
subplot(2,1,1)
plot(timev,vas,timev,vbs,timev,vcs); title('(a)')
legend('v_a_s','v_b_s','v_c_s','Location','Southwest')
xlim([0 3]); ylim([-12,12])
ylabel('Voltage (V)'); xlabel('Time (s)')
annotation('rectangle',...
    [0.460625 0.587426326129664 0.026875 0.332023575638502],'LineWidth',2,...
    'FaceColor','flat');
```

```
subplot(2,1,2)
plot(timev,ias,timev,ibs,timev,ics); title('(b)')
legend('i_a_s','i_b_s','i_c_s','Location','Southwest')
xlim([0 3])
ylabel('Current (A)'); xlabel('Time (s)')
annotation('rectangle',...
    [0.4625 0.113948919449902 0.025 0.332023575638507],'LineWidth',2,...
    'FaceColor','flat');
```

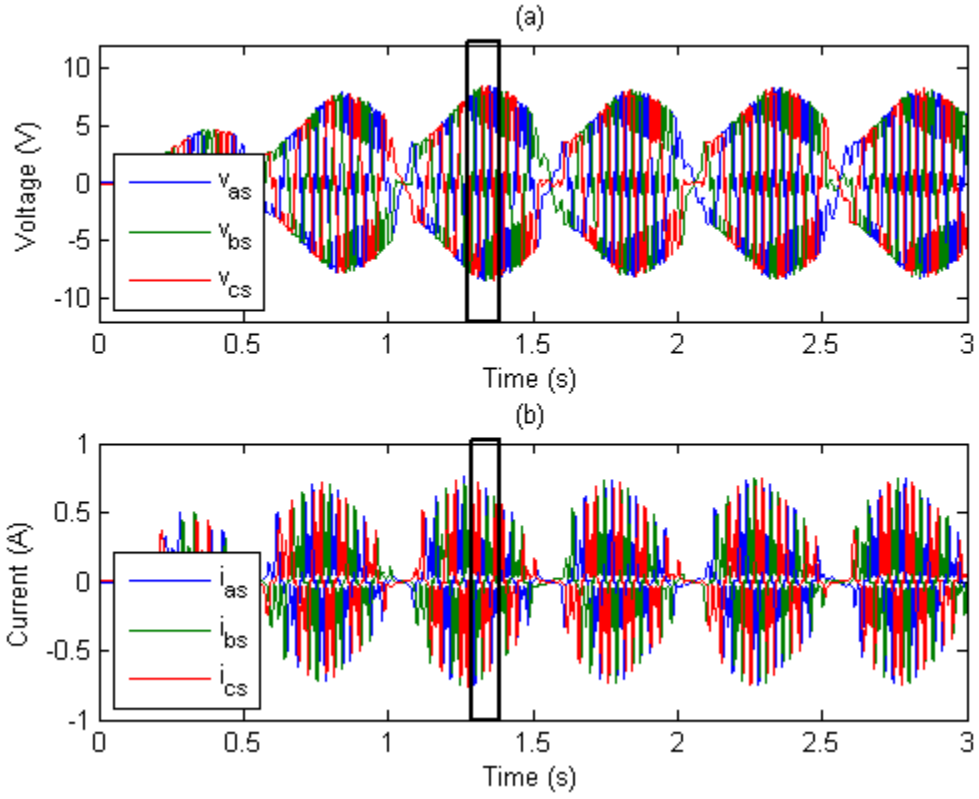

7. ABC Variables short timeframe

```
fig = fig+1;

figure(fig)
subplot(2,1,1)
plot(timev,vas,timev,vbs,timev,vcs,'LineWidth',2); title('(a)')
legend('v_a_s','v_b_s','v_c_s','Location','Southwest')
ylabel('Voltage (V)'); xlabel('Time (s)')
xlim([1.25 1.35])
ylim([-12,12])

subplot(2,1,2)
plot(timev,ias,timev,ibs,timev,ics,'LineWidth',2); title('(b)')
```

```
legend('i_a_s','i_b_s','i_c_s','Location','Southwest')
ylabel('Current (A)'); xlabel('Time (s)')
xlim([1.25 1.35])
```

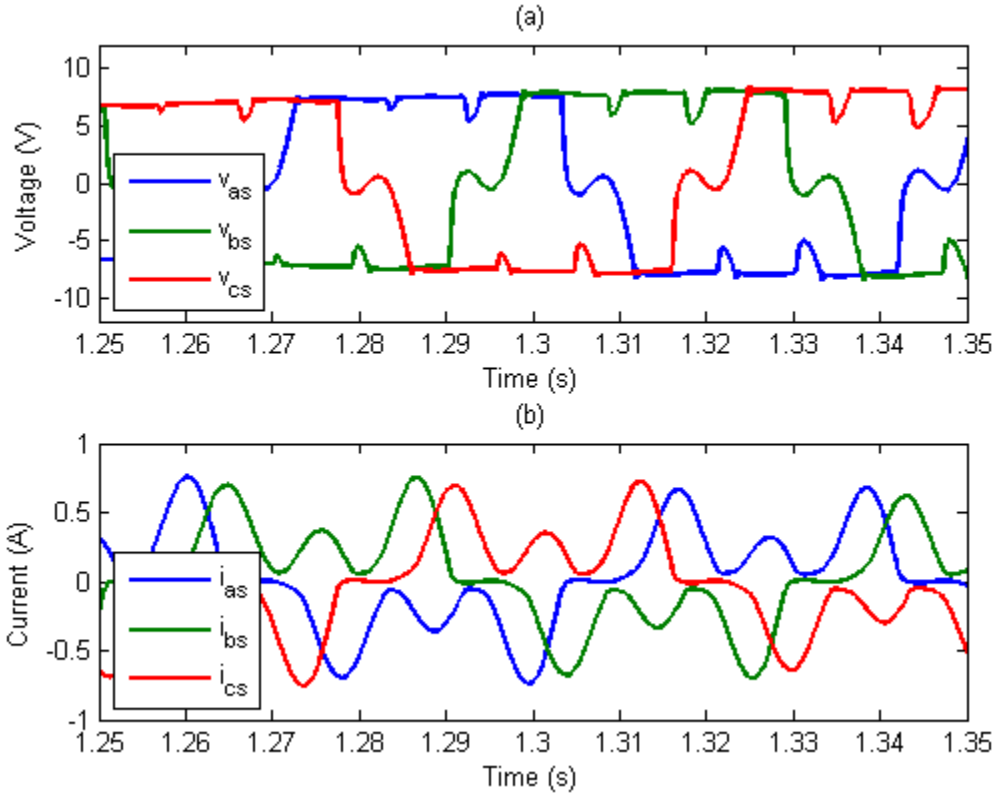

8. qd0 Variables

```
fig = fig+1;

figure(fig)
subplot(3,1,1)
plot(timev,i_qdos(:,1))
xlim([0 3])
legend('i_q')
subplot(3,1,2)
plot(timev,i_qdos(:,2))
xlim([0 3])
legend('i_d')
subplot(3,1,3)
plot(timev,i_qdos(:,3))
xlim([0 3])
legend('i_0')

iqs=i_qdos(:,1);
ids=i_qdos(:,2);
```

```
i0s=i_qdos(:,3);
theta_r=i_qdos(:,4);
iqd_angle=angle(iqs-1i*ids)*180/pi;
```

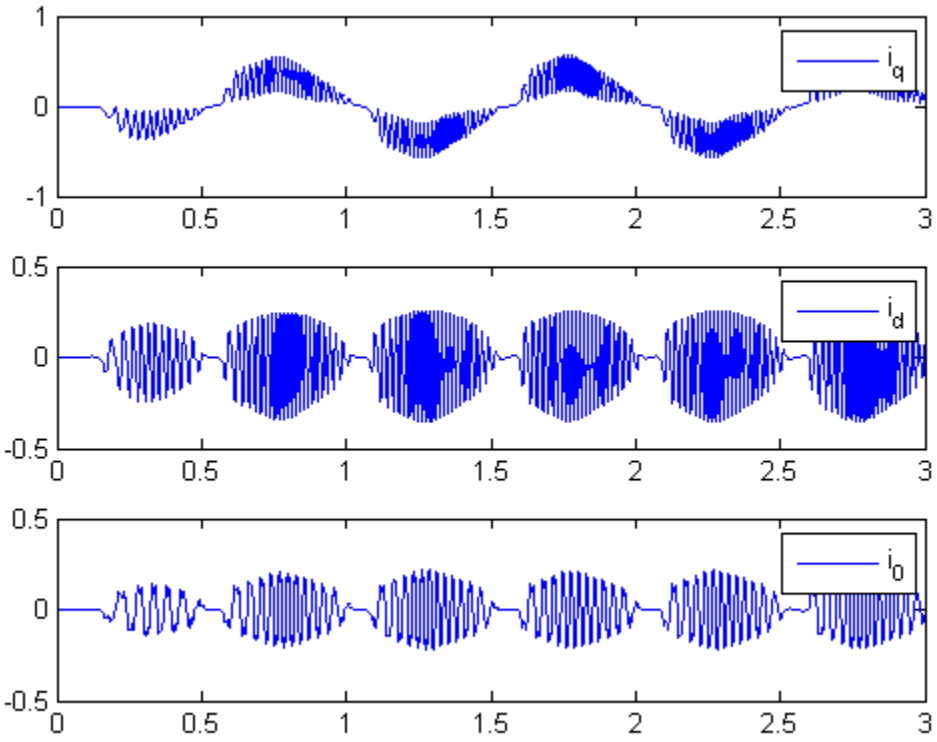

9. Velocity and Position (Electrical)

```
fig = fig+1;

figure(fig)
subplot(2,1,1)
plot(timev,wre_data,'LineWidth',2)
title('(a)')
xlabel('Time (s)'); ylabel('Angular Velocity (rad/s)')
xlim([0 3]); ylim([-125 125])
%legend('\omega_r_e')

subplot(2,1,2)
plot(timev,theta_elec,'r','LineWidth',2)
title('(b)')
xlabel('Time (s)'); ylabel('Electrical Position (rad)')
xlim([0 3])
%legend('\theta_r_e')
ylim([0,2*pi])
```

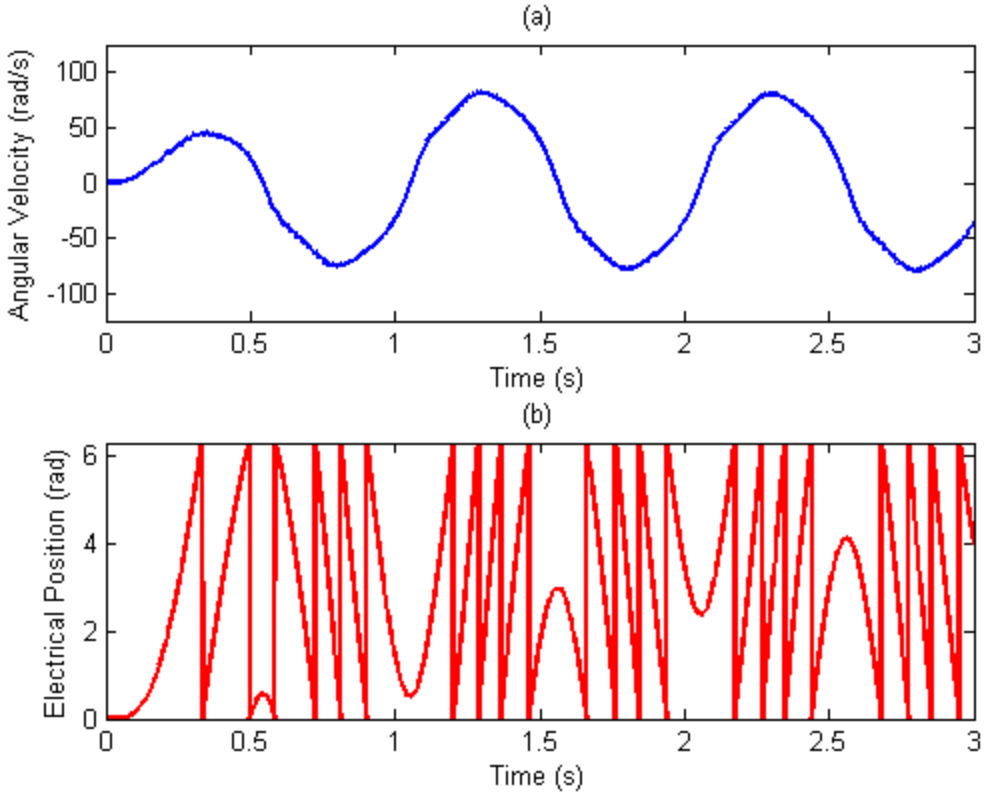

10. Velocity and Position (Mechanical)

```
fig = fig+1;

figure(fig)
subplot(2,1,1)
plot(timev,v,'LineWidth',2)
title('(a)')
xlabel('Time (s)'); ylabel('Velocity (m/s)')
xlim([0 3]);
%legend('Velocity')
xlabel('Time (s)')

subplot(2,1,2)
plot(timev,z,'r','LineWidth',2)
title('(b)')
xlim([0 3]); ylim([0 .7])
xlabel('Time (s)'); ylabel('Position (m)')
%legend('Position')
```

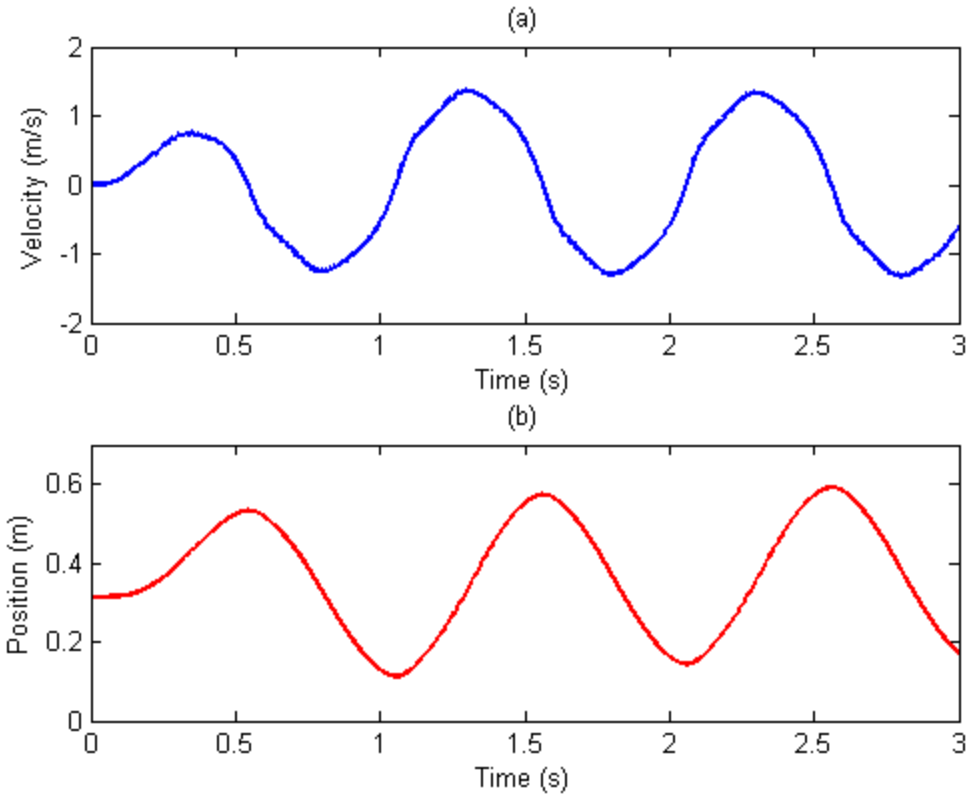

11. DC Variables

```
fig = fig+1;

figure(fig)
plot(timev,vdc,'LineWidth',2)
xlim([0 3]); ylim([0 11])
xlabel('Time (s)'); ylabel('Voltage (V)')

fig = fig+1;

figure(fig)
subplot(2,1,1)
plot(timev,vdc,'LineWidth',2); title('(a)')
xlim([1.25 1.65]); %ylim([0 11])
xlabel('Time (s)'); ylabel('Voltage (V)')

subplot(2,1,2)
figure(fig)
plot(timev,idcabc(:,1),timev,idcabc(:,2),timev,idcabc(:,3));
title('(b)')
legend('i_a dc','i_b dc','i_c dc','Location','Best')
xlim([1.25 1.65]); %ylim([-1 17])
xlabel('Time(s)'); ylabel('Current (A)')
```

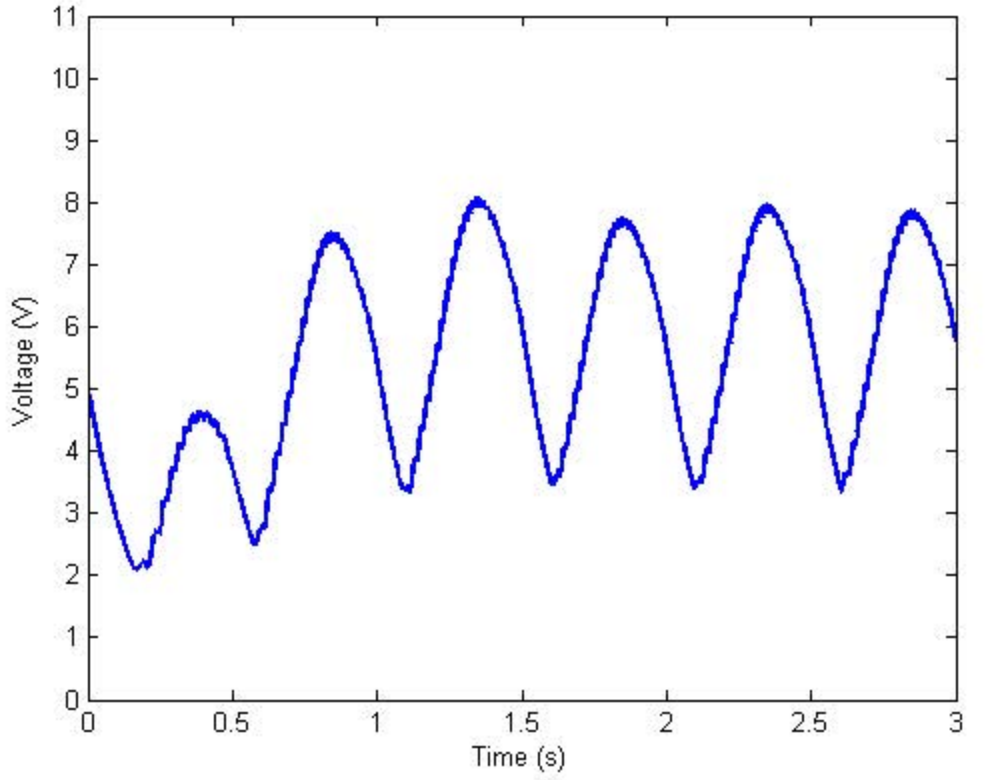
Voltage (V)
Time (s)
0
0.5
1
1.5
2
2.5
3
0
1
2
3
4
5
6
7
8
9
10
11

(a)

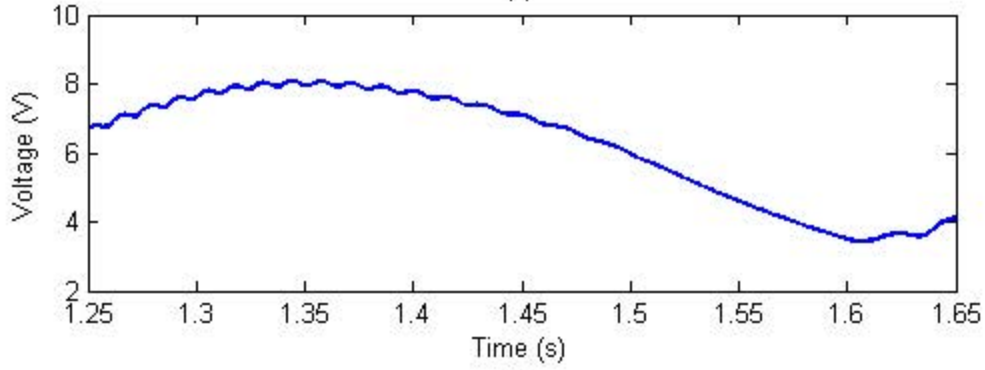
Voltage (V)
Time (s)
1.25
1.3
1.35
1.4
1.45
1.5
1.55
1.6
1.65
2
4
6
8
10

(b)

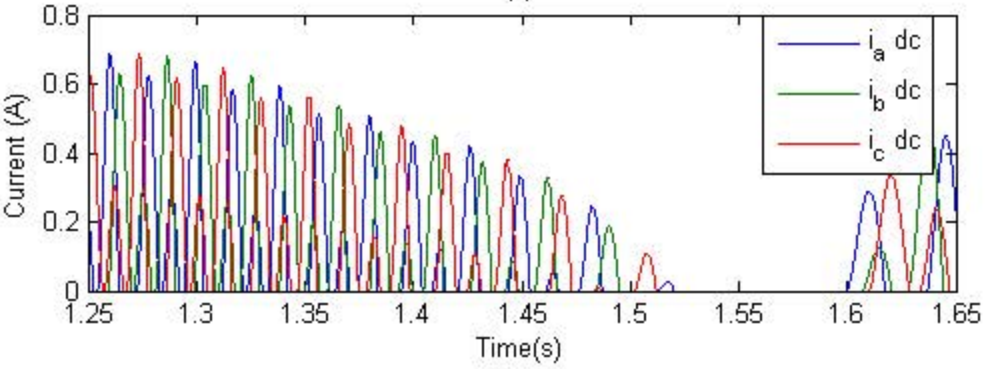
Current (A)
Time(s)
i_a dc
i_b dc
i_c dc
0
0.2
0.4
0.6
0.8
1.25
1.3
1.35
1.4
1.45
1.5
1.55
1.6
1.65

12. Lambda Harmonics

```
fig = fig+1;

figure(fig)
plot(funtime,0.1549*(fund+harm3+harm5+harm7),'LineWidth',2)
xlim([0 max(funtime)])
%legend('\lambda_P_M')
xlabel('Time (arbitrary)'); ylabel('Magnetic Flux (Wb)')
```

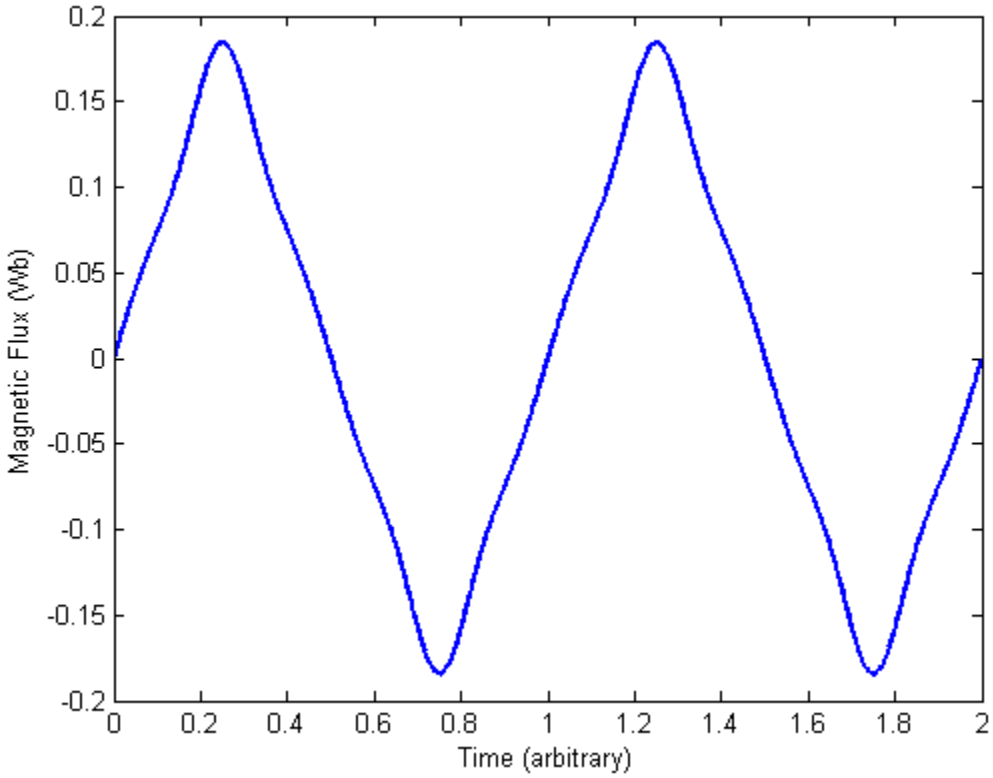

13. Input Torque and Force

```
fig = fig+1;

figure(fig)
subplot(2,1,1)
plot(timev,input_torque,'LineWidth',2)
title('(a)')
xlim([0 3]);
%legend('\tau_i_n','Location','Southeast')
ylabel('Torque (N\cdotm)')
xlabel('Time (s)')
```

```
subplot(2,1,2)
plot(timev,inputForce,'r','LineWidth',2)
title('(b)')
xlim([0 3])
%legend('F_i_n','Location','Southeast')
ylabel('Force (N)')
xlabel('Time (s)')
```

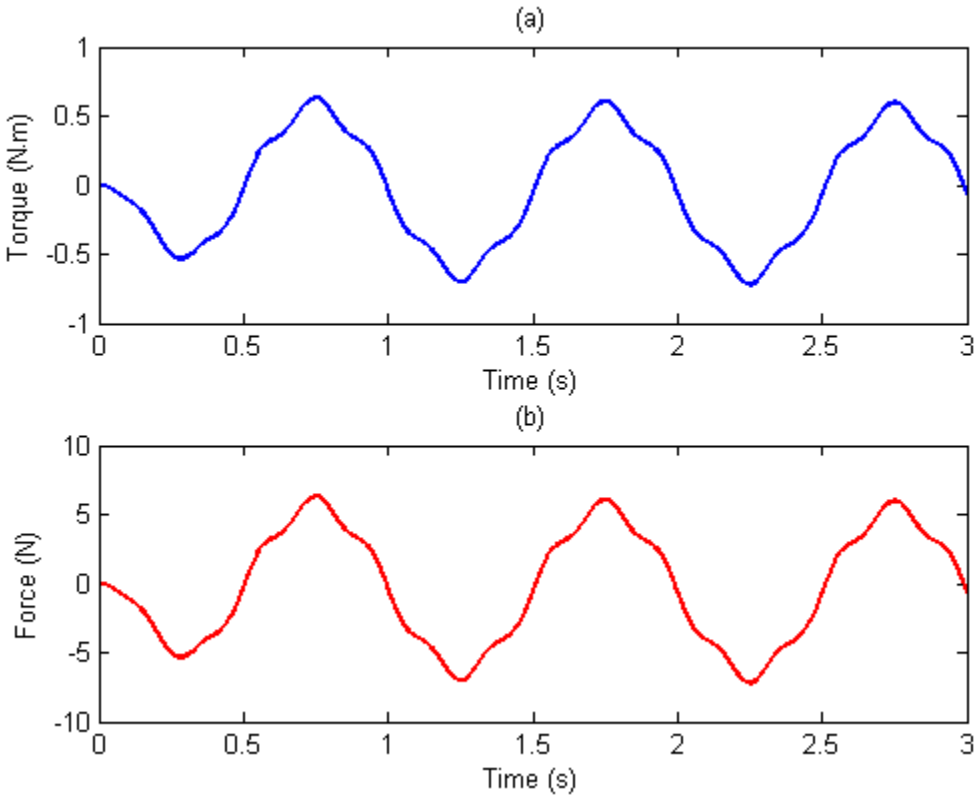

Published with MATLAB® R2014a

THIS PAGE INTENTIONALLY LEFT BLANK

APPENDIX E. LOW FREQUENCY, LOW AMPLITUDE SQUARE INPUT FORCE SCENARIO

1. Simulink Input Force

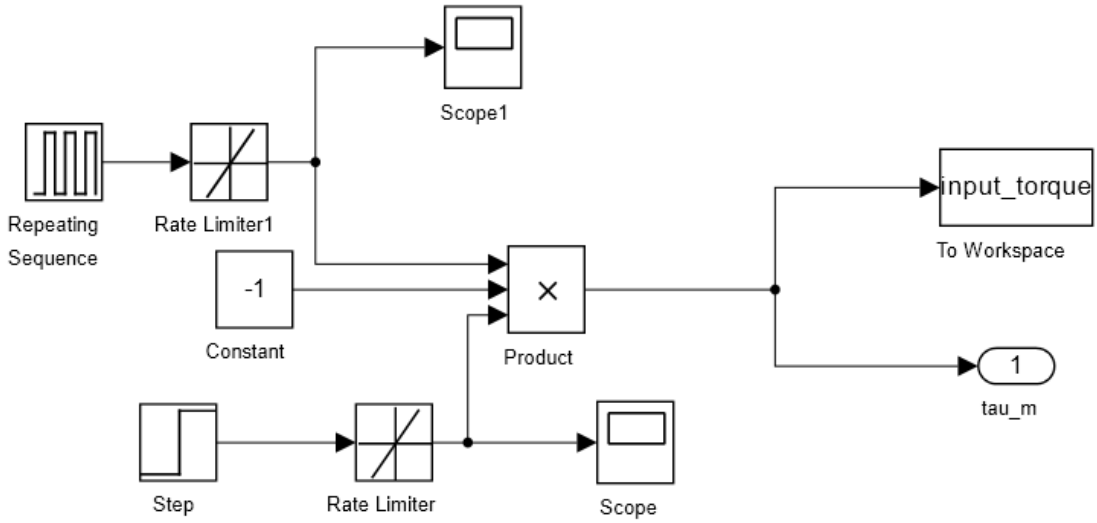

2. Defining Variables

```
% Linear Generator Post Run File
format compact
close all;
clc
fig = 0;
ias=iabcs(:,1);
ibs=iabcs(:,2);
ics=iabcs(:,3);

vas=vabcs(:,1);
vbs=vabcs(:,2);
vcs=vabcs(:,3);

power = vdc.*idc;

energy_out = sum(power)/length(timev)*max(timev)
energy_in = sum(abs(input_torque.*omega_mech))/length(timev)*max(timev)

efficiency = (energy_out / energy_in) * 100

funtime = linspace(0,2,1000);
fund = sin(2*pi*funtime);
```

```
harm3 = K3.*sin(2*pi*funtime*3);
harm5 = K5.*sin(2*pi*funtime*5);
harm7 = K7.*sin(2*pi*funtime*7);

zNormal = theta_mech ./ (2*pi); % normalized stator position

z = zNormal .* 2*pi * radius; % translator position (m)

v = omega_mech .* radius; % (m/s)

inputForce = input_torque / radius; % (N)
springForce = tau_spring / radius; % (N)
electricForce = Te / radius; % (N)
```

```
energy_out =
    9.0774
energy_in =
   17.4520
efficiency =
   52.0135
```

3. Lambdas

```
fig = fig +1;

figure(fig);
subplot(2,1,2)
plot(timev,lambda_abc(:,1),timev,lambda_abc(:,2),timev,lambda_abc(:,3),...
    'LineWidth',2)
legend('\lambda_a_s','\lambda_b_s','\lambda_c_s','Location','Southwest')
title('(b)')
xlabel('Time (s)'); ylabel('Magnetic Flux (Wb)')
% xlim([1,1.5])
xlim([1.3 1.4])
%
subplot(2,1,1)
plot(timev,lambda_abc(:,1),timev,lambda_abc(:,2),timev,lambda_abc(:,3),...
    'LineWidth',1)
title('(a)')
xlabel('Time (s)'); ylabel('Magnetic Flux (Wb)')
legend('\lambda_a_s','\lambda_b_s','\lambda_c_s','Location','Southwest')
% xlim([1,1.5])
xlim([0 3])
annotation('rectangle',...
    [0.466625 0.585461689587424 0.024625 0.335952848722982],'LineWidth',2,...
    'FaceColor','flat');
```

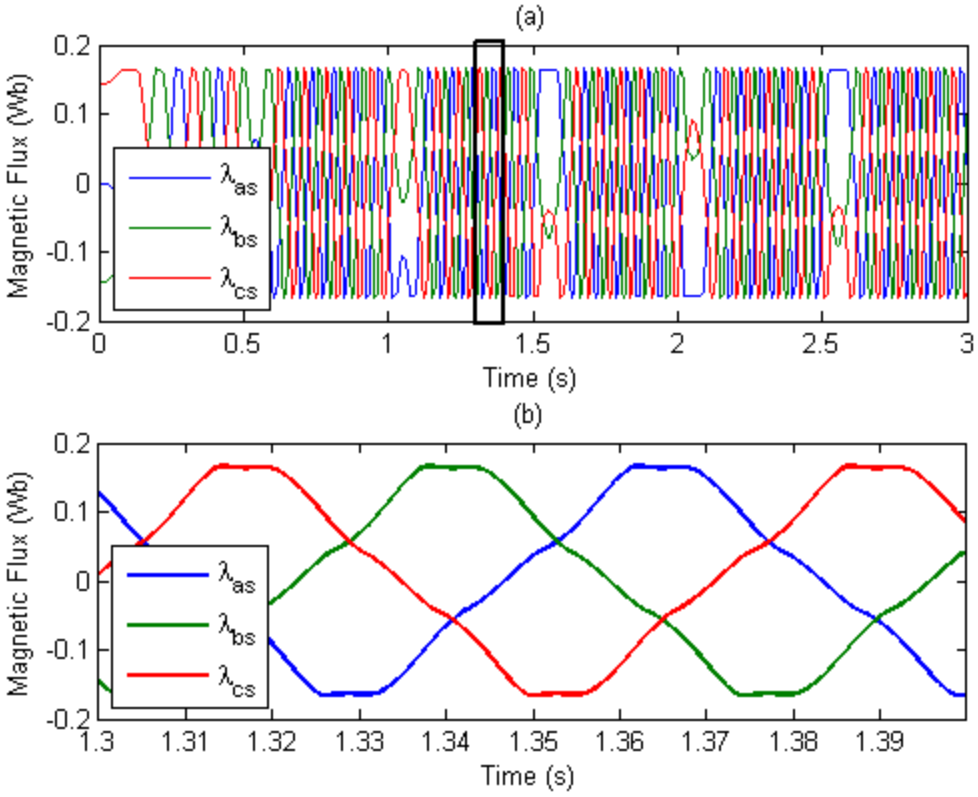

4. Forces at play

```
fig = fig+1;
figure(fig)
plot(timev,-v,timev,inputForce+springForce,'LineWidth',2)
hold on
plot(timev,-electricForce,'r')
hold off
legend('Velocity (m/s)','F_i_n+F_{spring} (N)','F_{electric}     (N)',...
    'Location','Southeast')
xlim([0 3])
ylabel('Amplitude')

fig = fig+1;
figure(fig)
plot(timev,inputForce,timev,inputForce+springForce,'LineWidth',2)
legend('F_i_n','F_i_n+F_{spring}','Location','Southwest')
xlim([0 3])
xlabel('Time (s)'); ylabel('Force (N)')
```

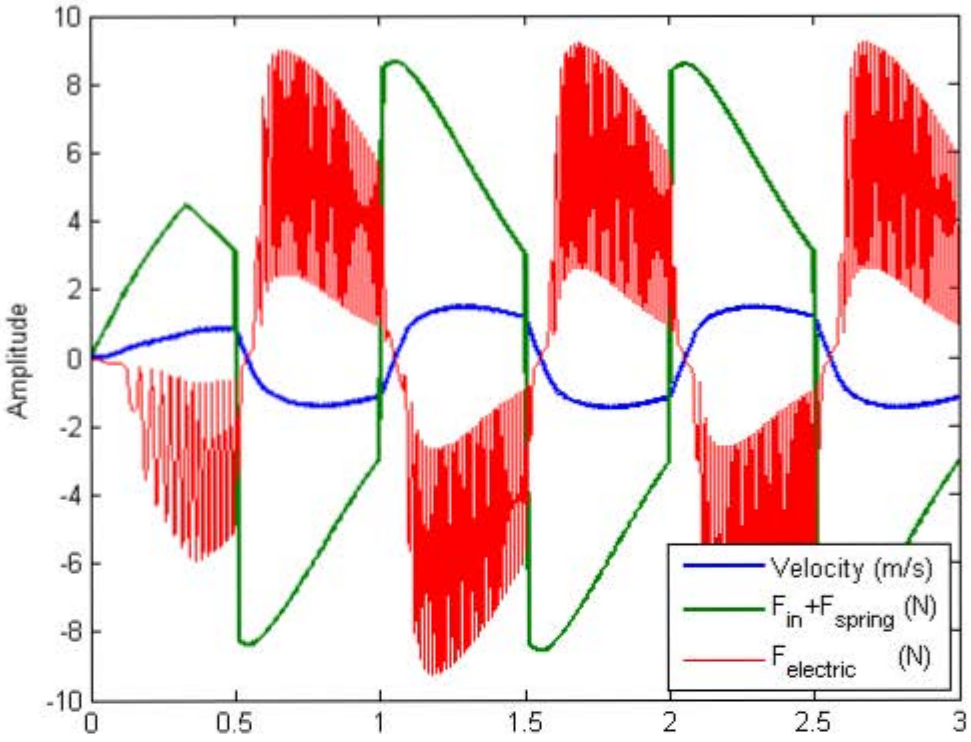
Amplitude
Velocity (m/s)
F_in+F_spring (N)
F_electric (N)

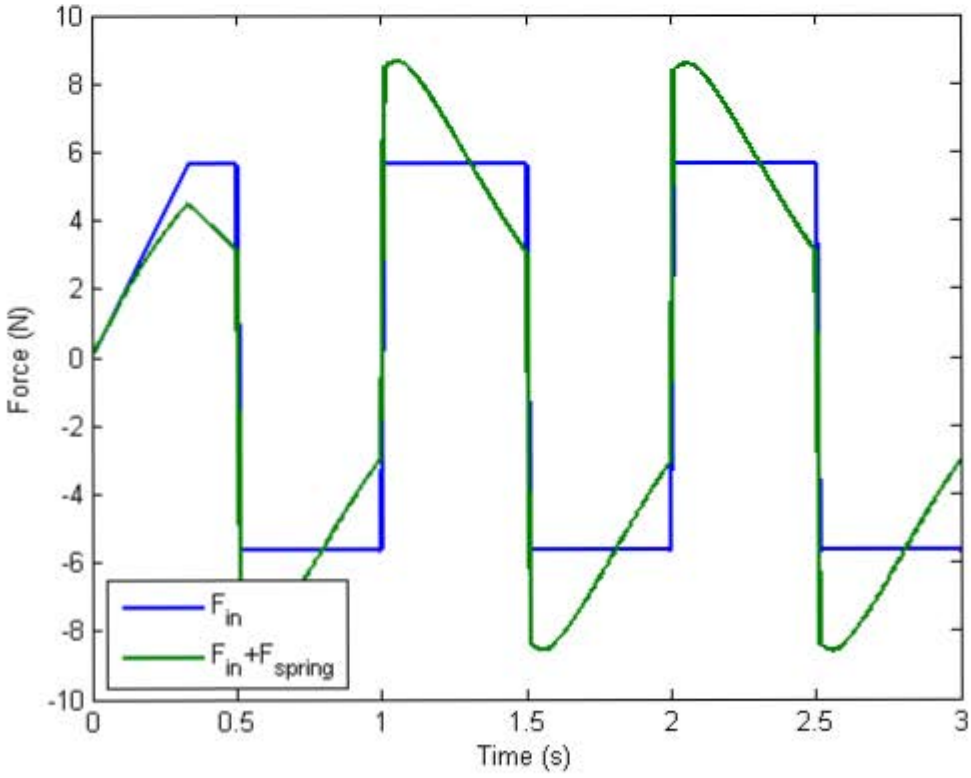
Force (N)
F_in
F_in+F_spring
Time (s)

5. Position & Velocity (Mechanical)

```
fig = fig+1;
figure(fig)
plot(timev,z,timev,v,'LineWidth',2)
xlim([0 3])
ylabel('Amplitude')
xlabel('Time (s)')
legend('Position    (m)','Velocity (m/s)','Location','Northwest')
```

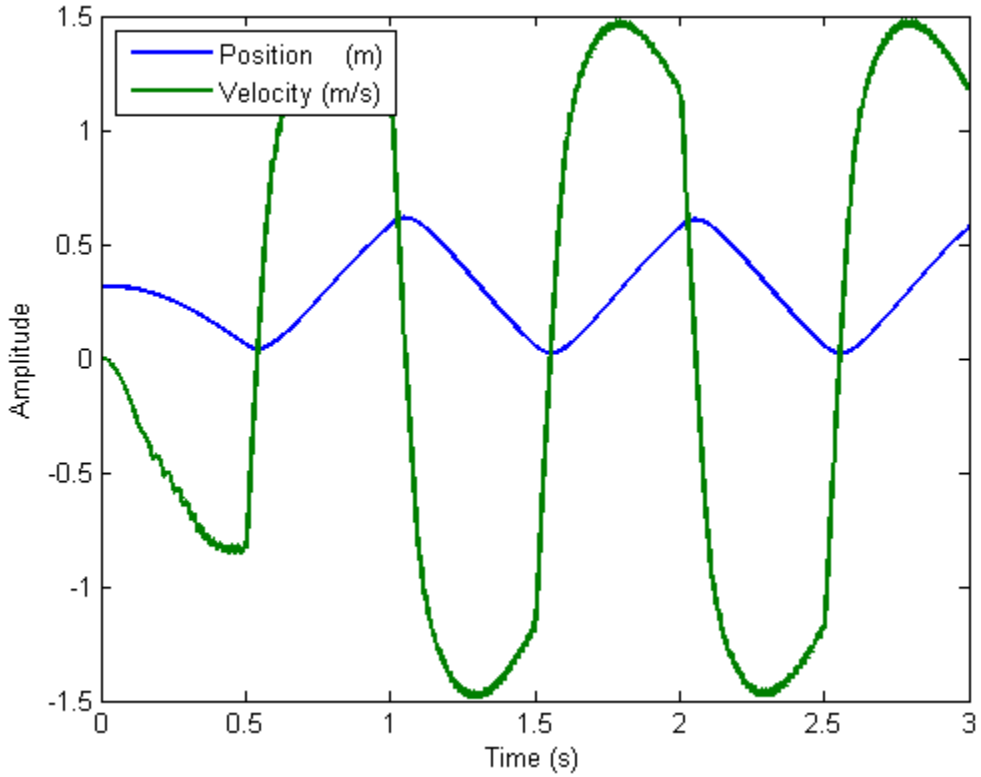

6. ABC Variables

```
fig = fig+1;

figure(fig)
subplot(2,1,1)
plot(timev,vas,timev,vbs,timev,vcs); title('(a)')
legend('v_a_s','v_b_s','v_c_s','Location','Southwest')
xlim([0 3]); ylim([-12,12])
ylabel('Voltage (V)'); xlabel('Time (s)')
annotation('rectangle',...
    [0.460625 0.587426326129664 0.026875 0.332023575638502],'LineWidth',2,...
    'FaceColor','flat');
```

```
subplot(2,1,2)
plot(timev,ias,timev,ibs,timev,ics); title('(b)')
legend('i_a_s','i_b_s','i_c_s','Location','Southwest')
xlim([0 3])
ylabel('Current (A)'); xlabel('Time (s)')
annotation('rectangle',...
    [0.4625 0.113948919449902 0.025 0.332023575638507],'LineWidth',2,...
    'FaceColor','flat');
```

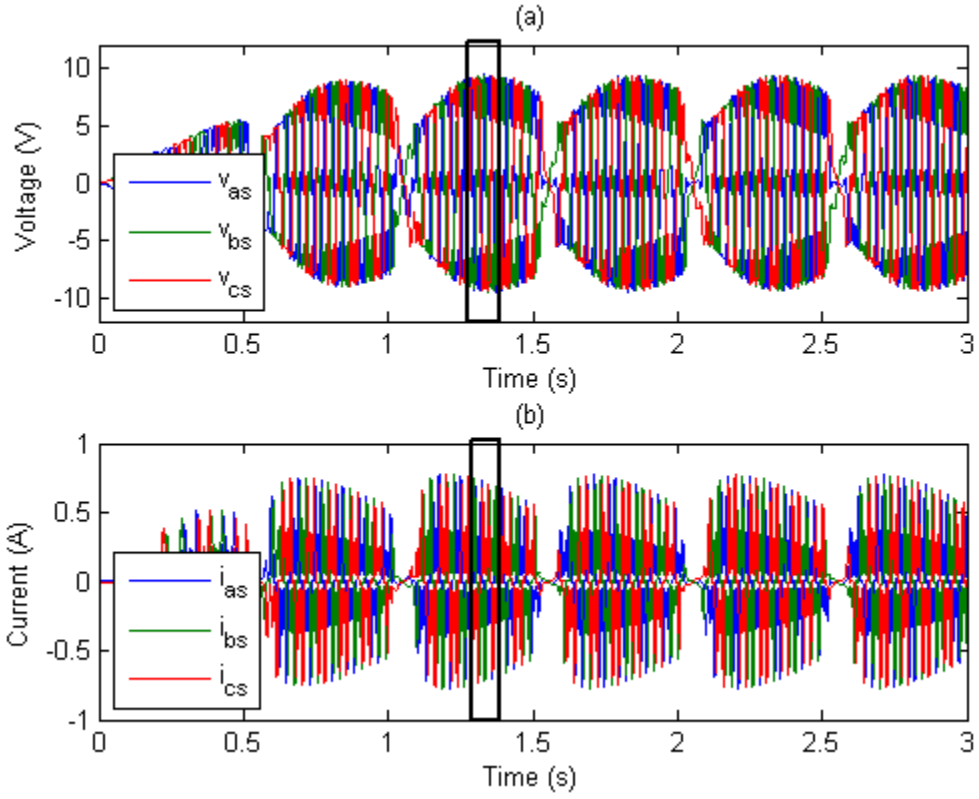

7. ABC Variables short timeframe

```
fig = fig+1;

figure(fig)
subplot(2,1,1)
plot(timev,vas,timev,vbs,timev,vcs,'LineWidth',2); title('(a)')
legend('v_a_s','v_b_s','v_c_s','Location','Southwest')
ylabel('Voltage (V)'); xlabel('Time (s)')
xlim([1.25 1.35])
ylim([-12,12])

subplot(2,1,2)
plot(timev,ias,timev,ibs,timev,ics,'LineWidth',2); title('(b)')
```

```
legend('i_a_s','i_b_s','i_c_s','Location','Southwest')
ylabel('Current (A)'); xlabel('Time (s)')
xlim([1.25 1.35])
```

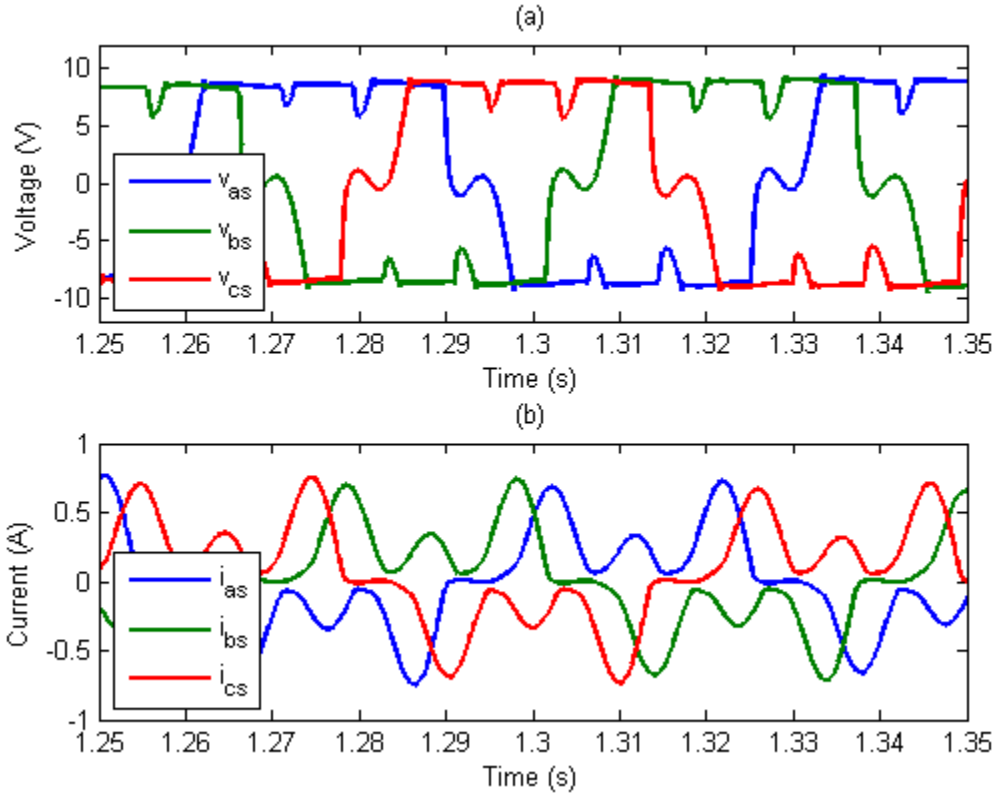

8. qd0 Variables

```
fig = fig+1;

figure(fig)
subplot(3,1,1)
plot(timev,i_qdos(:,1))
xlim([0 3])
legend('i_q')
subplot(3,1,2)
plot(timev,i_qdos(:,2))
xlim([0 3])
legend('i_d')
subplot(3,1,3)
plot(timev,i_qdos(:,3))
xlim([0 3])
legend('i_0')

iqs=i_qdos(:,1);
ids=i_qdos(:,2);
```

```
i0s=i_qdos(:,3);
theta_r=i_qdos(:,4);
iqd_angle=angle(iqs-1i*ids)*180/pi;
```

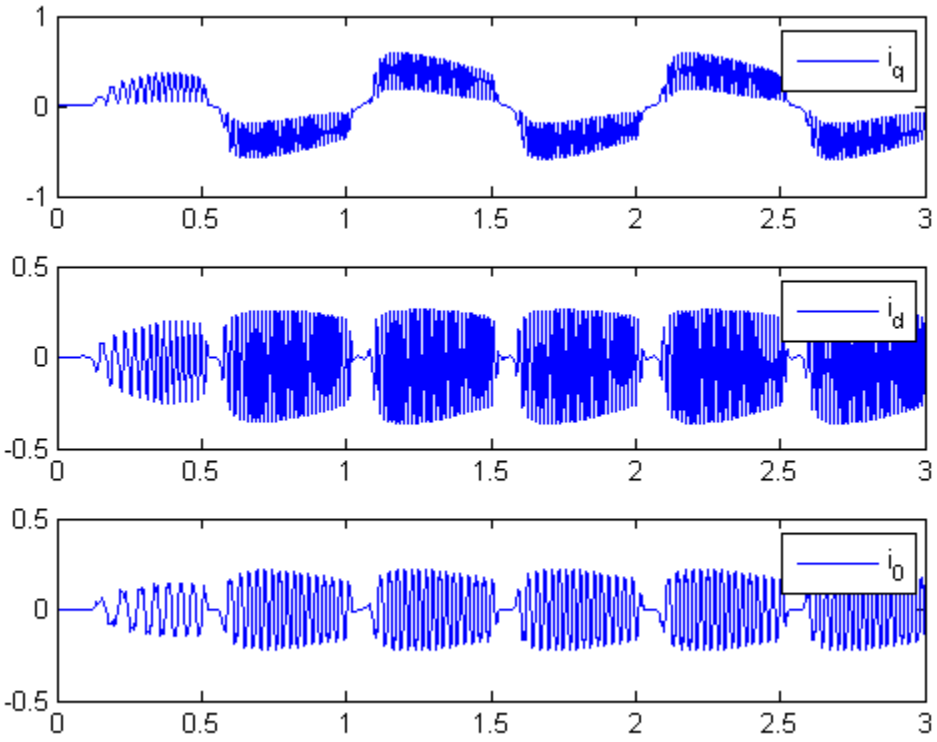

9. Velocity and Position (Electrical)

```
fig = fig+1;

figure(fig)
subplot(2,1,1)
plot(timev,wre_data,'LineWidth',2)
title('(a)')
xlabel('Time (s)'); ylabel('Angular Velocity (rad/s)')
xlim([0 3]); ylim([-125 125])
%legend('\omega_r_e')

subplot(2,1,2)
plot(timev,theta_elec,'r','LineWidth',2)
title('(b)')
xlabel('Time (s)'); ylabel('Electrical Position (rad)')
xlim([0 3])
%legend('\theta_r_e')
ylim([0,2*pi])
```

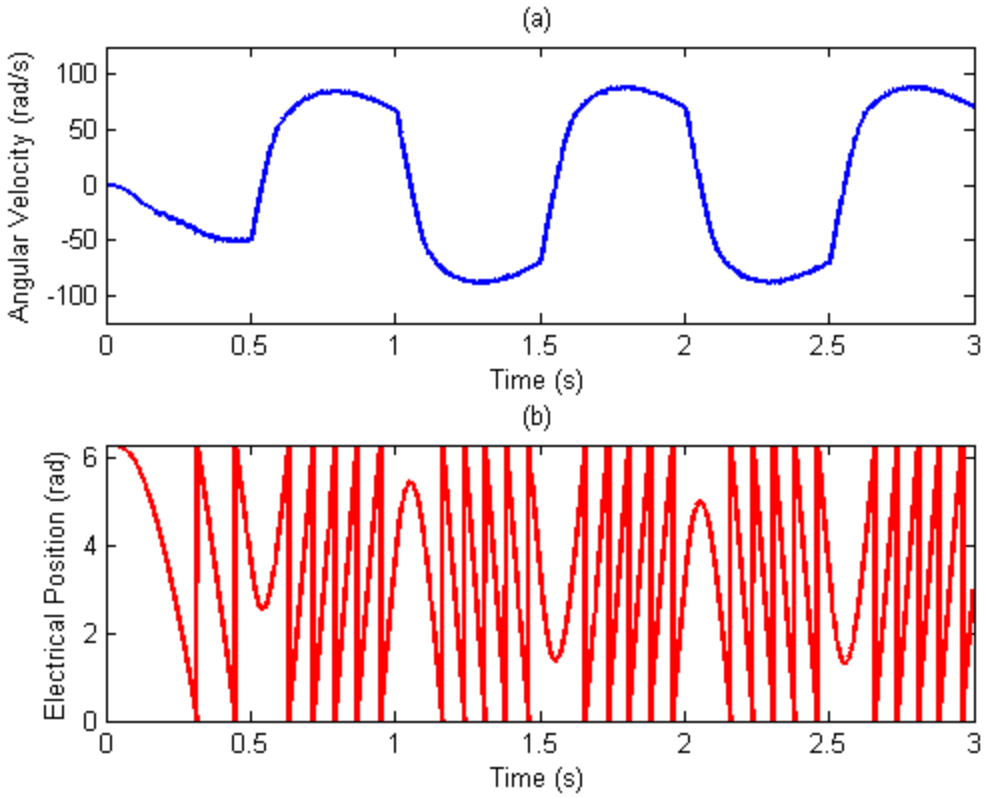

10. Velocity and Position (Mechanical)

```
fig = fig+1;

figure(fig)
subplot(2,1,1)
plot(timev,v,'LineWidth',2)
title('(a)')
xlabel('Time (s)'); ylabel('Velocity (m/s)')
xlim([0 3]);
%legend('Velocity')
xlabel('Time (s)')

subplot(2,1,2)
plot(timev,z,'r','LineWidth',2)
title('(b)')
xlim([0 3]); ylim([0 .7])
xlabel('Time (s)'); ylabel('Position (m)')
%legend('Position')
```

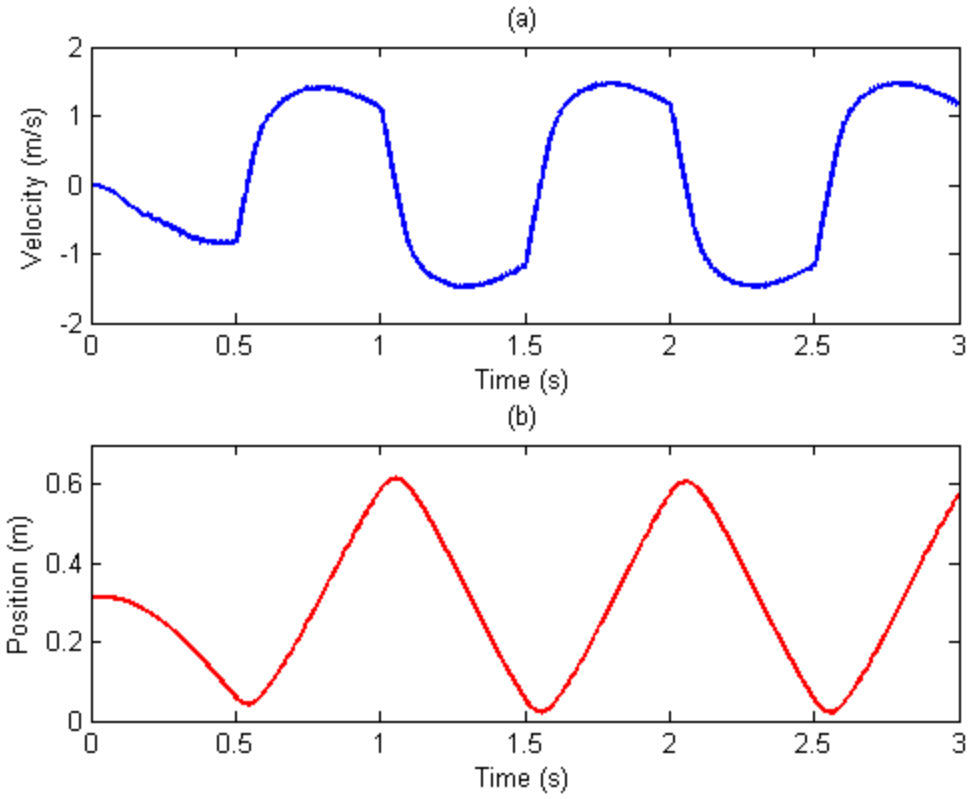

11. DC Variables

```
fig = fig+1;

figure(fig)
plot(timev,vdc,'LineWidth',2)
xlim([0 3]); ylim([0 11])
xlabel('Time (s)'); ylabel('Voltage (V)')

fig = fig+1;

figure(fig)
subplot(2,1,1)
plot(timev,vdc,'LineWidth',2); title('(a)')
xlim([1.25 1.65]); %ylim([0 11])
xlabel('Time (s)'); ylabel('Voltage (V)')

subplot(2,1,2)
figure(fig)
plot(timev,idcabc(:,1),timev,idcabc(:,2),timev,idcabc(:,3));
title('(b)')
legend('i_a dc','i_b dc','i_c dc','Location','Best')
xlim([1.25 1.65]); %ylim([-1 17])
xlabel('Time(s)'); ylabel('Current (A)')
```

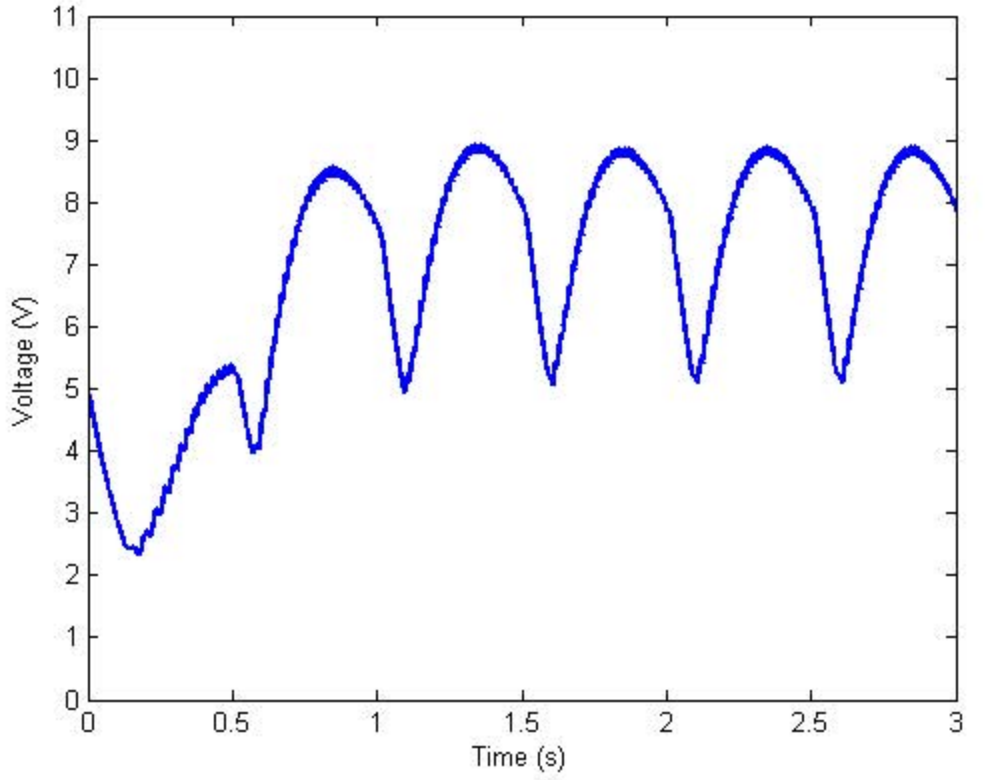
Voltage (V)
Time (s)

(a)

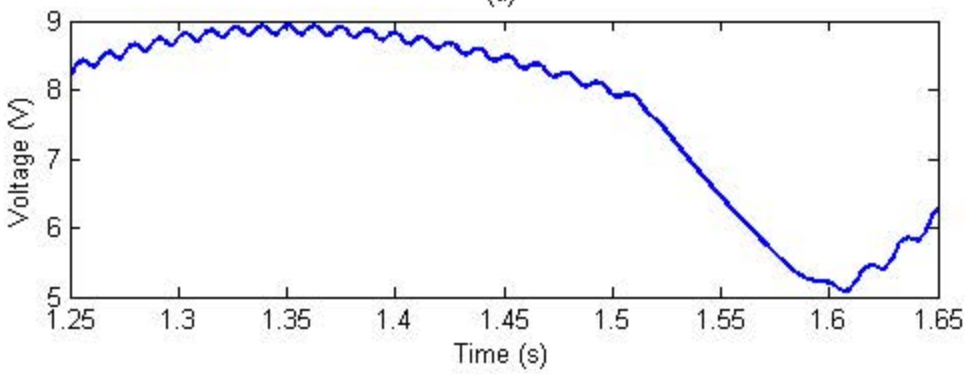
Voltage (V)
Time (s)

(b)

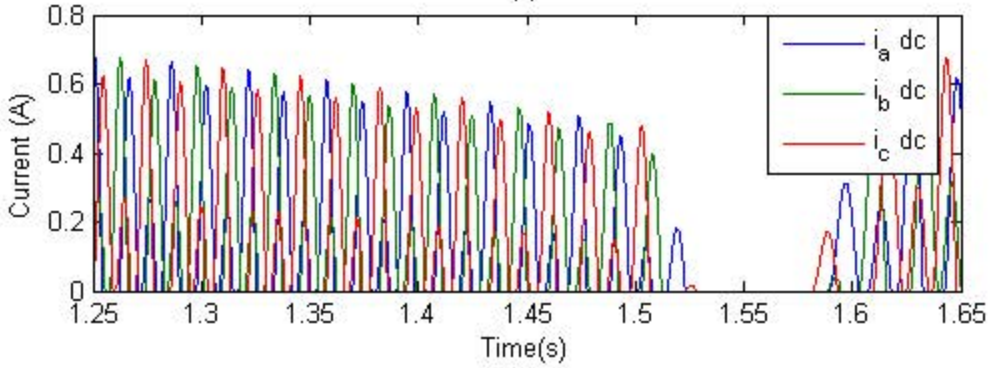
Current (A)
Time(s)
i_a dc
i_b dc
i_c dc

12. Lambda Harmonics

```
fig = fig+1;

figure(fig)
plot(funtime,0.1549*(fund+harm3+harm5+harm7),'LineWidth',2)
xlim([0 max(funtime)])
%legend('\lambda_P_M')
xlabel('Time (arbitrary)'); ylabel('Magnetic Flux (Wb)')
```

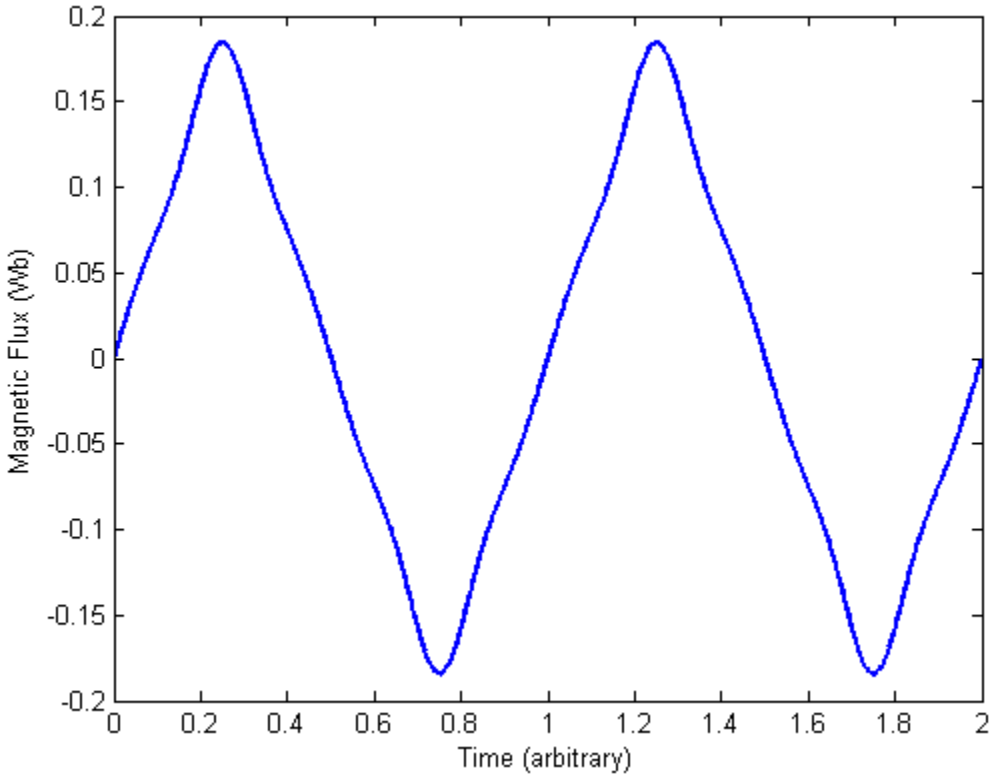

13. Input Torque and Force

```
fig = fig+1;

figure(fig)
subplot(2,1,1)
plot(timev,input_torque,'LineWidth',2)
title('(a)')
xlim([0 3]);
%legend('\tau_i_n','Location','Southeast')
ylabel('Torque (N\cdotm)')
xlabel('Time (s)')
```

```
subplot(2,1,2)
plot(timev,inputForce,'r','LineWidth',2)
title('(b)')
xlim([0 3])
%legend('F_i_n','Location','Southeast')
ylabel('Force (N)')
xlabel('Time (s)')
```

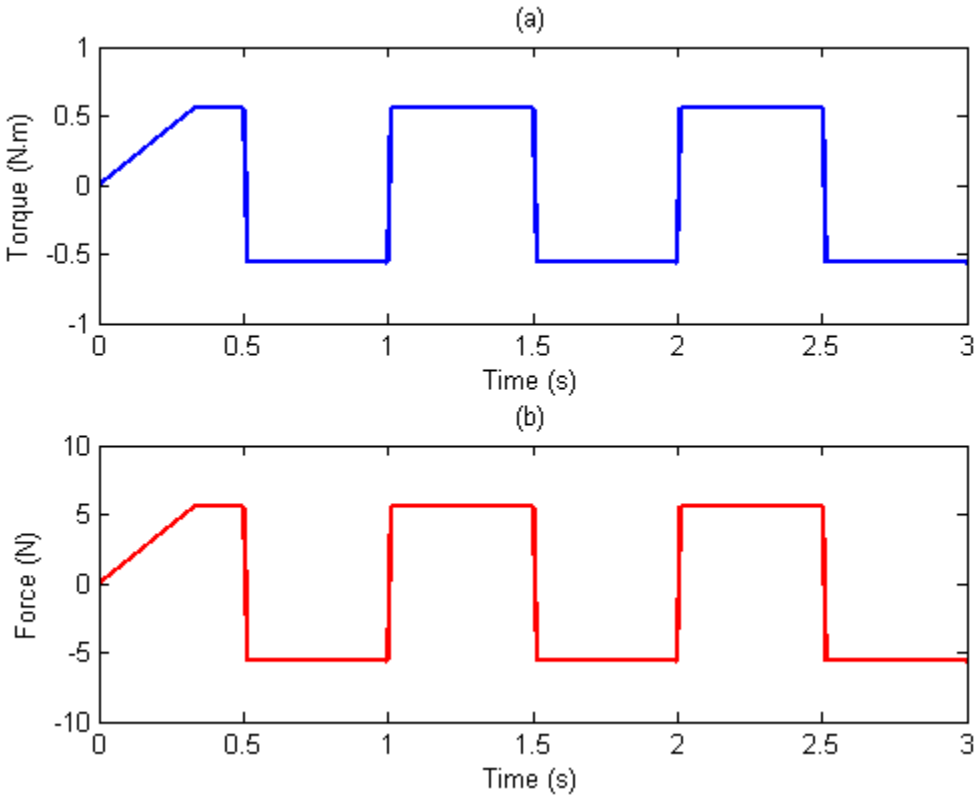

Published with MATLAB® R2014a

THIS PAGE INTENTIONALLY LEFT BLANK

APPENDIX F. HIGH FREQUENCY, HIGH AMPLITUDE SQUARE INPUT FORCE SCENARIO

1. Simulink Input Force

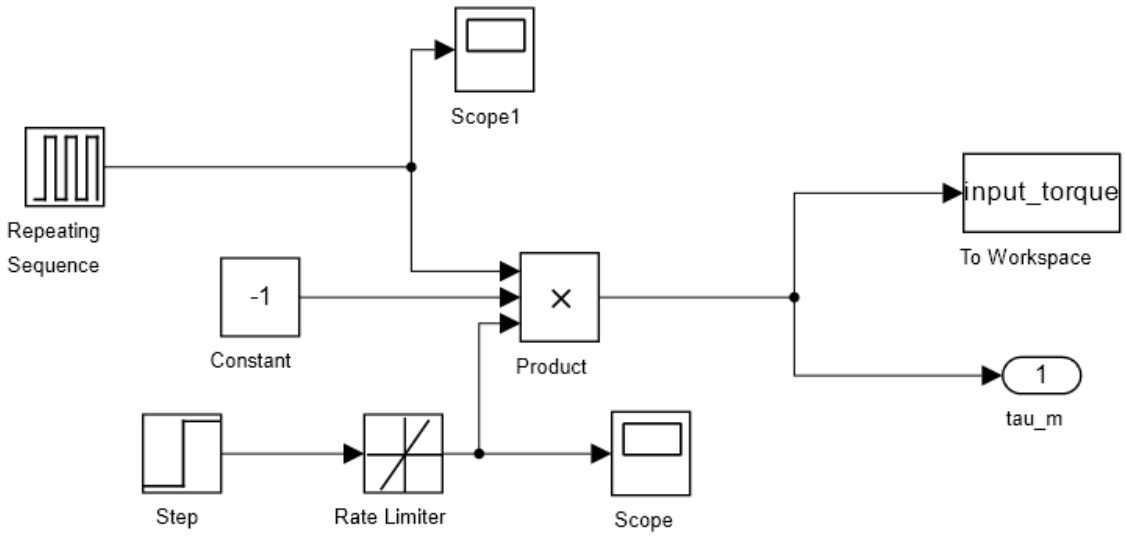

2. Defining Variables

```
format compact
close all;
clc
fig = 0;
ias=iabcs(:,1);
ibs=iabcs(:,2);
ics=iabcs(:,3);

vas=vabcs(:,1);
vbs=vabcs(:,2);
vcs=vabcs(:,3);

power = vdc.*idc;

energy_sum = (sum(abs(input_torque.*omega_mech))-sum(power)...
    -sum(Bm*omega_mech))/length(timev)

energy_out = sum(power(length(timev)-50000:length(timev)))/50000
energy_in = sum(abs(input_torque(length(timev)-50000:length(timev))...
    .*omega_mech(length(timev)-50000:length(timev))))/50000
```

```
efficiency = (energy_out / energy_in) * 100

funtime = linspace(0,2,1000);
fund = sin(2*pi*funtime);
harm3 = K3.*sin(2*pi*funtime*3);
harm5 = K5.*sin(2*pi*funtime*5);
harm7 = K7.*sin(2*pi*funtime*7);

zNormal = theta_mech ./ (2*pi); % normalized stator position

z = zNormal .* 2*pi * radius; % translator position (m)

v = omega_mech .* radius; % (m/s)
tau_frict = omega_mech*.0026;

frictionForce = tau_frict / radius;
inputForce = input_torque / radius; % (N)
springForce = tau_spring / radius; % (N)
electricForce = Te / radius; % (N)
```

```
energy_sum =
   1.4912e+05
energy_out =
  326.0576
energy_in =
   1.5638e+05
efficiency =
    0.2085
```

3. Lambda

```
fig = fig +1;

figure(fig);
plot(timev,lambda_abc(:,1),timev,lambda_abc(:,2),timev,lambda_abc(:,3),...
    'LineWidth',1)
xlabel('Time (s)'); ylabel('Magnetic Flux (Wb)')
legend('\lambda_a_s','\lambda_b_s','\lambda_c_s','Location','Southwest')
% xlim([1,1.5])
xlim([4.9 5])
```

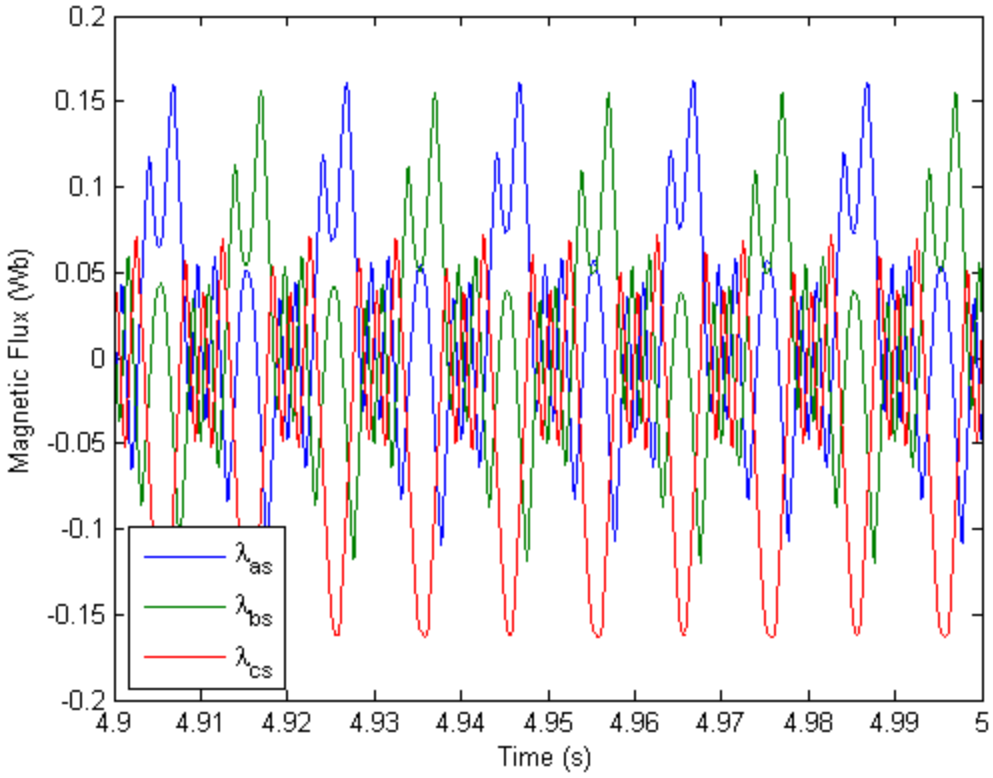

4. Forces at play

```
fig = fig+1;
figure(fig)
plot(timev,-inputForce/10000,timev,-(inputForce+springForce)/10000,...
    timev,z,timev,v/100,'LineWidth',2)
legend('F_i_n/10             (kN)','F_i_n+F_{spring}/10 (kN)',...
    'Position          (m)','Velocity/100  (m/s)','Location','Southwest')
xlim([max(timev)-.1 max(timev)])
xlabel('Time (s)'); ylabel('Amplitude')
```

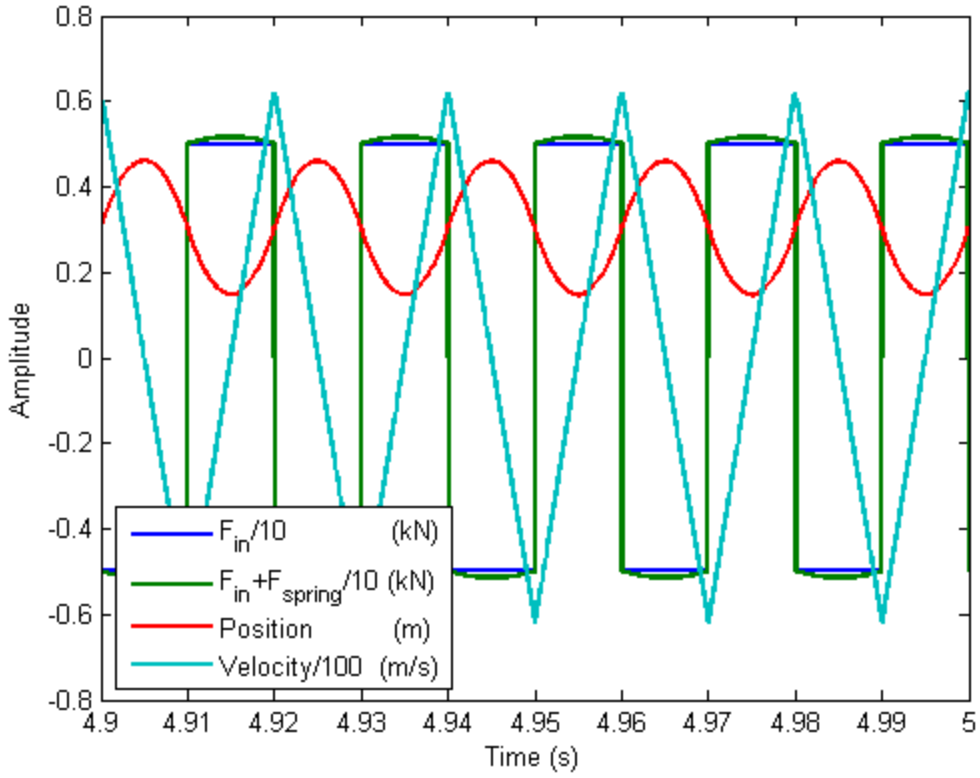

5. ABC Variables

```
fig = fig+1;
figure(fig)
subplot(2,1,1)
plot(timev,vas,timev,vbs,timev,vcs); title('(a)')
legend('v_a_s','v_b_s','v_c_s','Location','Southwest')
ylabel('Voltage (V)'); xlabel('Time (s)')

subplot(2,1,2)
plot(timev,ias,timev,ibs,timev,ics); title('(b)')
legend('i_a_s','i_b_s','i_c_s','Location','Southwest')
ylabel('Current (A)'); xlabel('Time (s)')
```

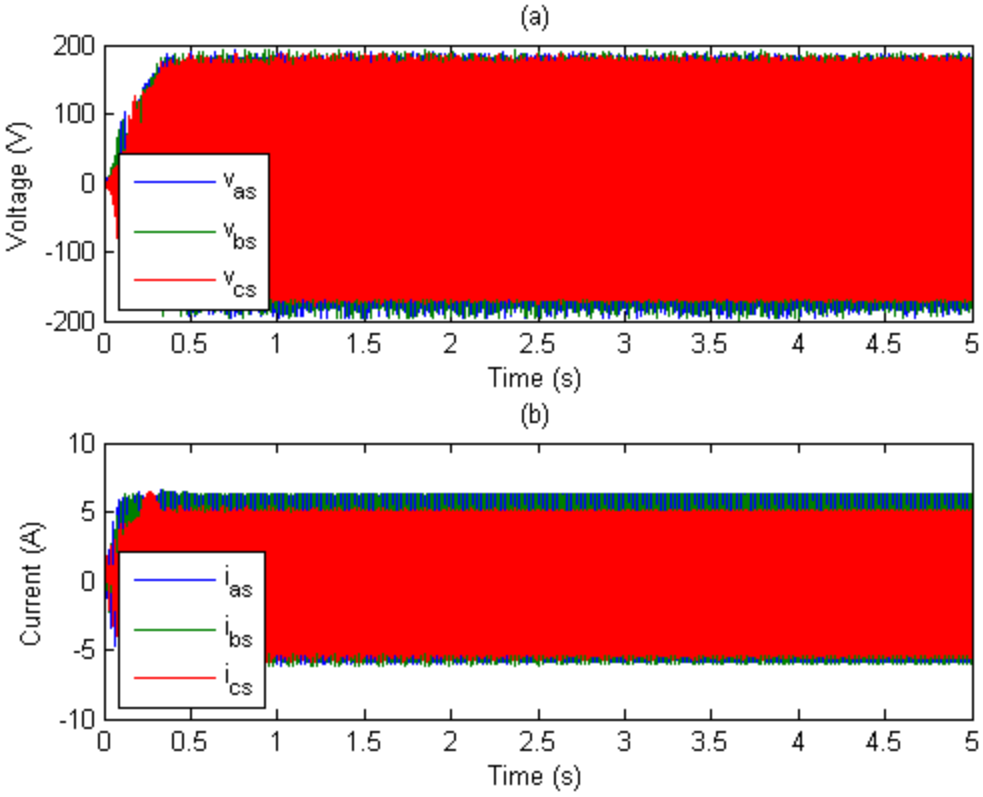

6. ABC Variables short timeframe

```
fig = fig+1;
figure(fig)
subplot(2,1,1)
plot(timev,vas,timev,vbs,timev,vcs,'LineWidth',2); title('(a)')
legend('v_a_s','v_b_s','v_c_s','Location','Southwest')
ylabel('Voltage (V)'); xlabel('Time (s)')
xlim([max(timev)-.1 max(timev)])

subplot(2,1,2)
plot(timev,ias,timev,ibs,timev,ics,'LineWidth',2); title('(b)')
legend('i_a_s','i_b_s','i_c_s','Location','Southwest')
ylabel('Current (A)'); xlabel('Time (s)')
xlim([max(timev)-.1 max(timev)])
```

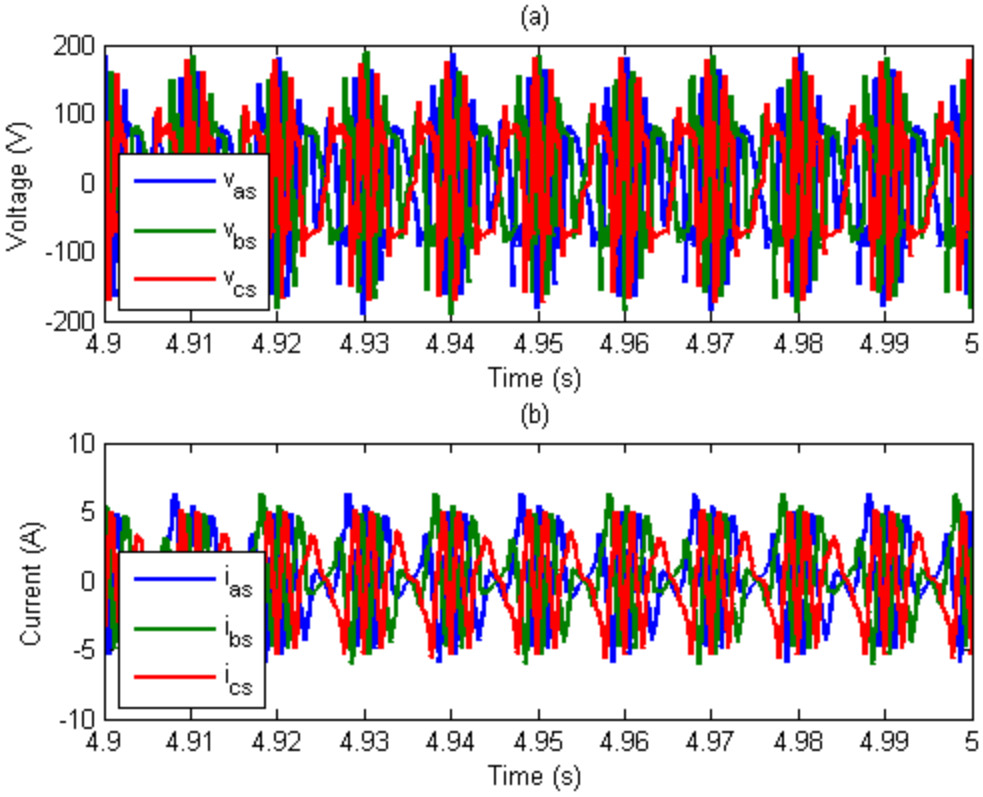

7. qd0 Variables

```
fig = fig+1;

figure(fig)
subplot(3,1,1)
plot(timev,i_qdos(:,1))
xlim([4.9 5])
legend('i_q')
subplot(3,1,2)
plot(timev,i_qdos(:,2))
xlim([4.9 5])
legend('i_d')
subplot(3,1,3)
plot(timev,i_qdos(:,3))
xlim([4.9 5])
legend('i_0')

iqs=i_qdos(:,1);
ids=i_qdos(:,2);
i0s=i_qdos(:,3);
theta_r=i_qdos(:,4);
iqd_angle=angle(iqs-1i*ids)*180/pi;
```

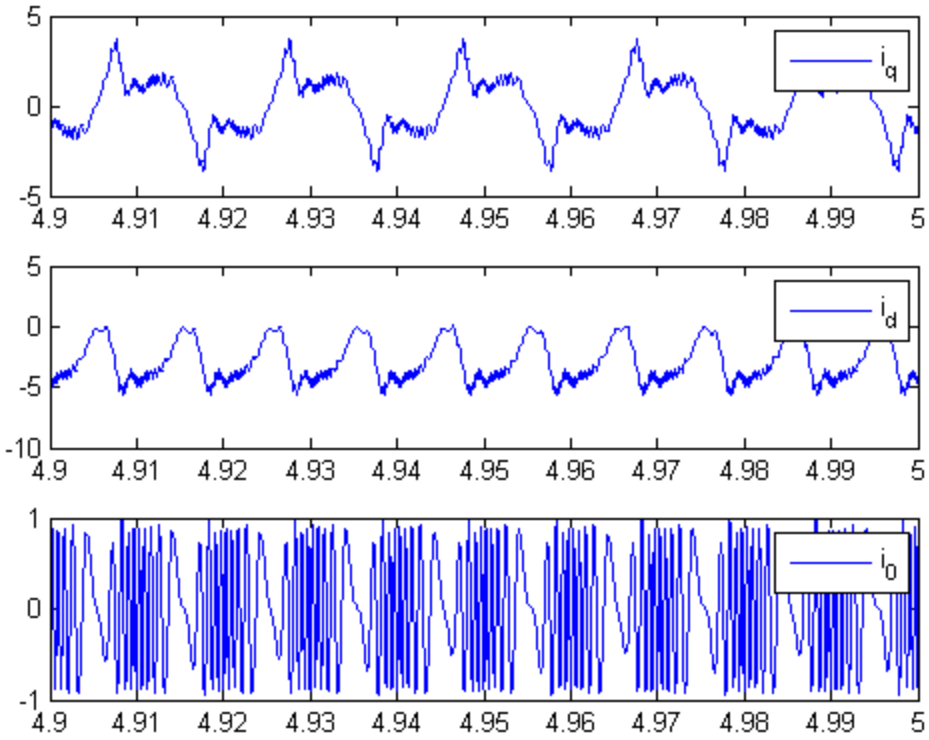

8. Velocity and Position (Electrical)

```
fig = fig+1;

figure(fig)
subplot(2,1,1)
plot(timev,wre_data,'LineWidth',2)
title('(a)')
xlabel('Time (s)'); ylabel('Angular Velocity (rad/s)')
xlim([4.9 5]); %ylim([-125 125])
%legend('\omega_r_e')

subplot(2,1,2)
plot(timev,theta_elec,'r','LineWidth',2)
title('(b)')
xlabel('Time (s)'); ylabel('Electrical Position (rad)')
xlim([4.9 5])
%legend('\theta_r_e')
%ylim([0,2*pi])
```

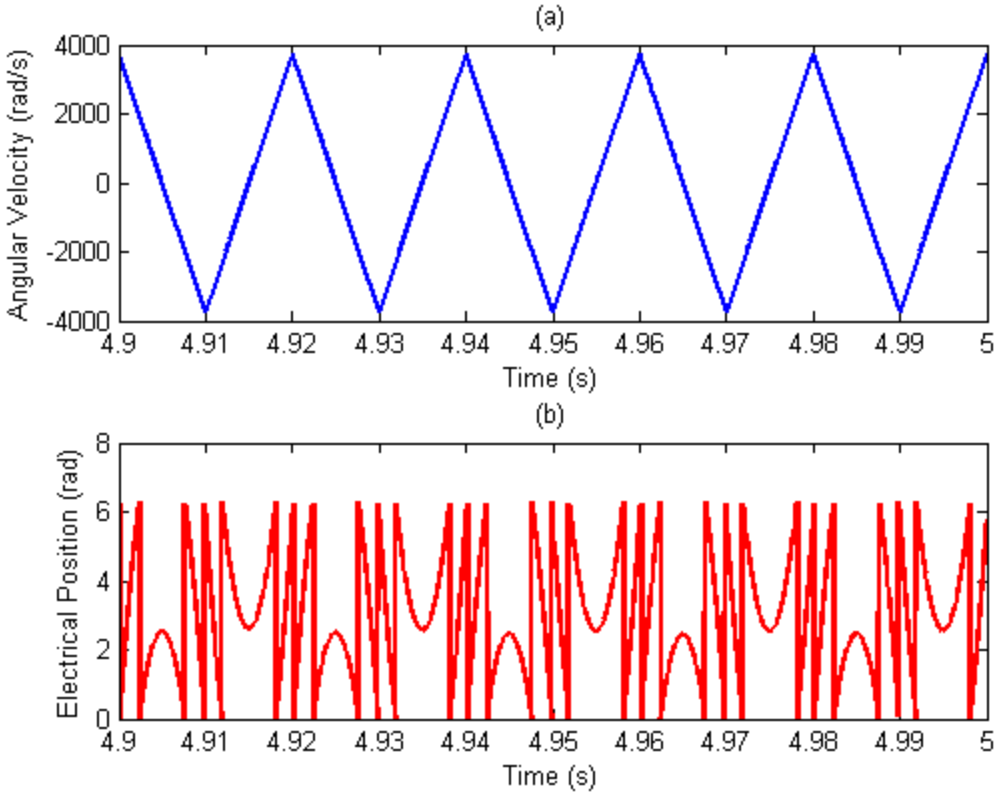

9. Velocity and Position (Mechanical)

```
fig = fig+1;

figure(fig)
subplot(2,1,1)
plot(timev,v,'LineWidth',2)
title('(a)')
xlabel('Time (s)'); ylabel('Velocity (m/s)')
xlim([4.9 5]);
%legend('Velocity')
xlabel('Time (s)')

subplot(2,1,2)
plot(timev,z,'r','LineWidth',2)
title('(b)')
xlim([4.9 5]); ylim([0 2*pi/10])
xlabel('Time (s)'); ylabel('Position (m)')
%legend('Position')
```

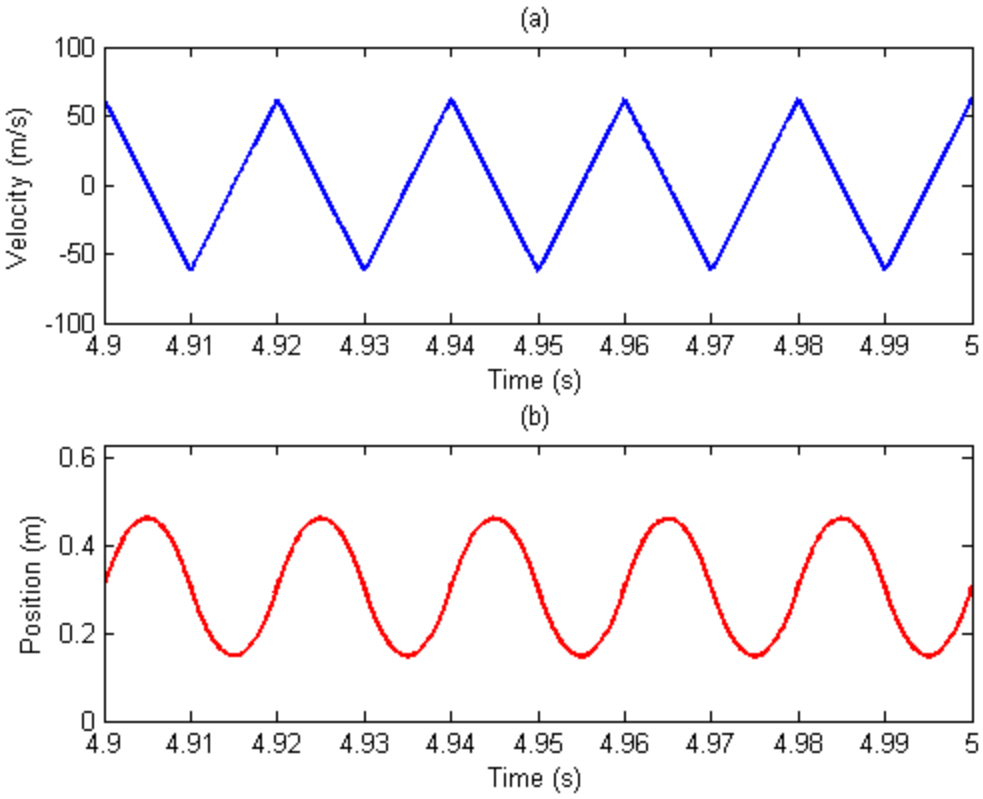

10. DC Variables

```
fig = fig+1;

figure(fig)
plot(timev,vdc,'LineWidth',2)
xlim([4.9 5]); %ylim([0 11])
xlabel('Time (s)'); ylabel('Voltage (V)')

fig = fig+1;

figure(fig)

plot(timev,vdc,'LineWidth',2); %title('(a)')
%xlim([0.5 0.6]); %%ylim([0 11])
xlabel('Time (s)'); ylabel('Voltage (V)')

fig=fig+1
figure(fig)
plot(timev,idcabc(:,1),timev,idcabc(:,2),timev,idcabc(:,3));
%title('(b)')
legend('i_a dc','i_b dc','i_c dc','Location','Best')
xlim([2.34 2.367]); %%ylim([-1 17])
xlabel('Time(s)'); ylabel('Current (A)')
```

```
% %% Lambda Harmonics
% fig = fig+1;
%
% figure(fig)
% plot(funtime,0.1549*(fund+harm3+harm5+harm7),'LineWidth',2)
% xlim([0 max(funtime)])
% %legend('\lambda_P_M')
% xlabel('Time (arbitrary)'); ylabel('Magnetic Flux (Wb)')
```

```
fig =
    10
```

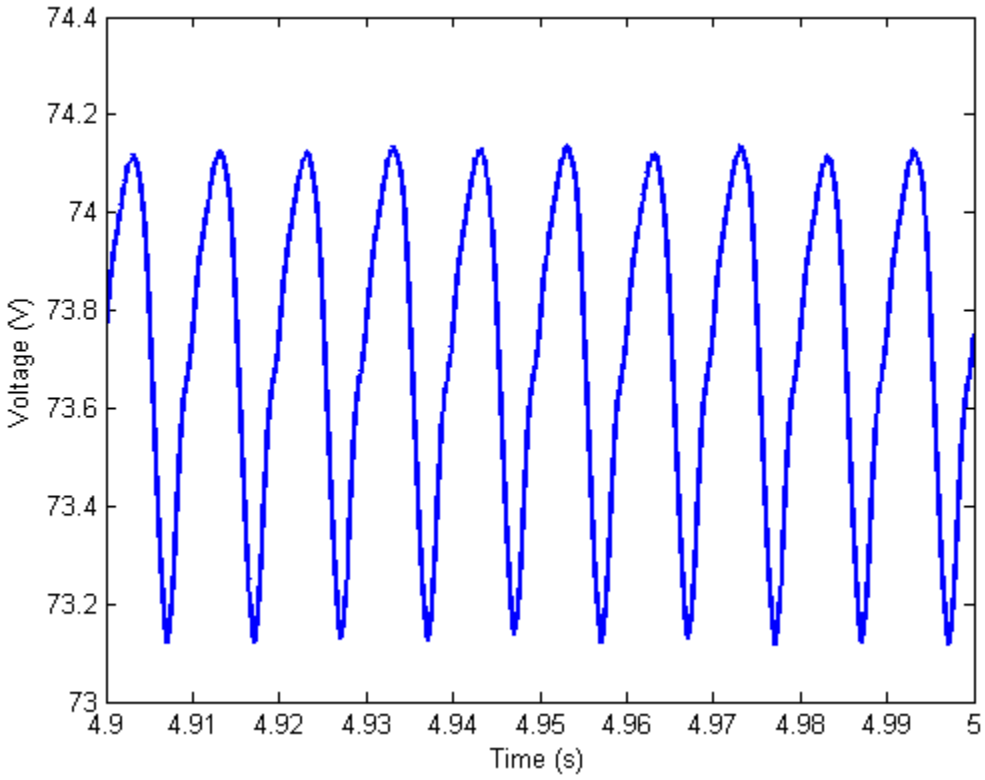

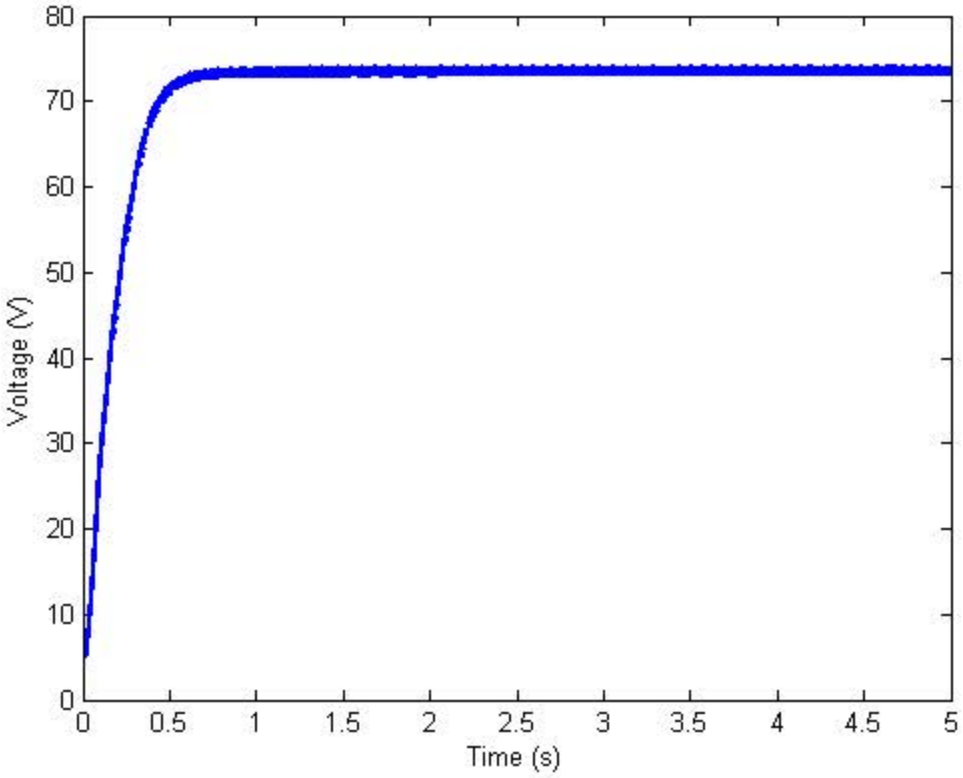
Voltage (V)
Time (s)
0
10
20
30
40
50
60
70
80
0
0.5
1
1.5
2
2.5
3
3.5
4
4.5
5

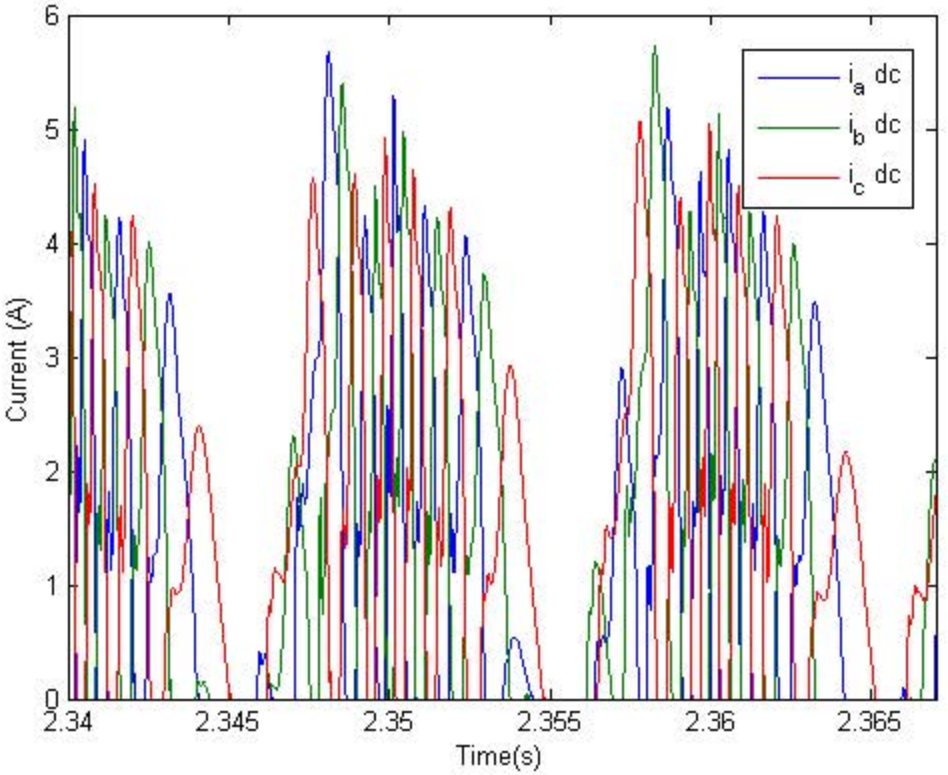
Current (A)
Time(s)
i_a dc
i_b dc
i_c dc
0
1
2
3
4
5
6
2.34
2.345
2.35
2.355
2.36
2.365

11. Input Torque and Force

```
fig = fig+1;

figure(fig)
subplot(2,1,1)
plot(timev,input_torque,'LineWidth',2)
title('(a)')
xlim([4.9 5]);
%legend('\tau_i_n','Location','Southeast')
ylabel('Torque (N\cdotm)')
xlabel('Time (s)')

subplot(2,1,2)
plot(timev,inputForce,'r','LineWidth',2)
title('(b)')
xlim([4.9 5])
%legend('F_i_n','Location','Southeast')
ylabel('Force (N)')
xlabel('Time (s)')
```

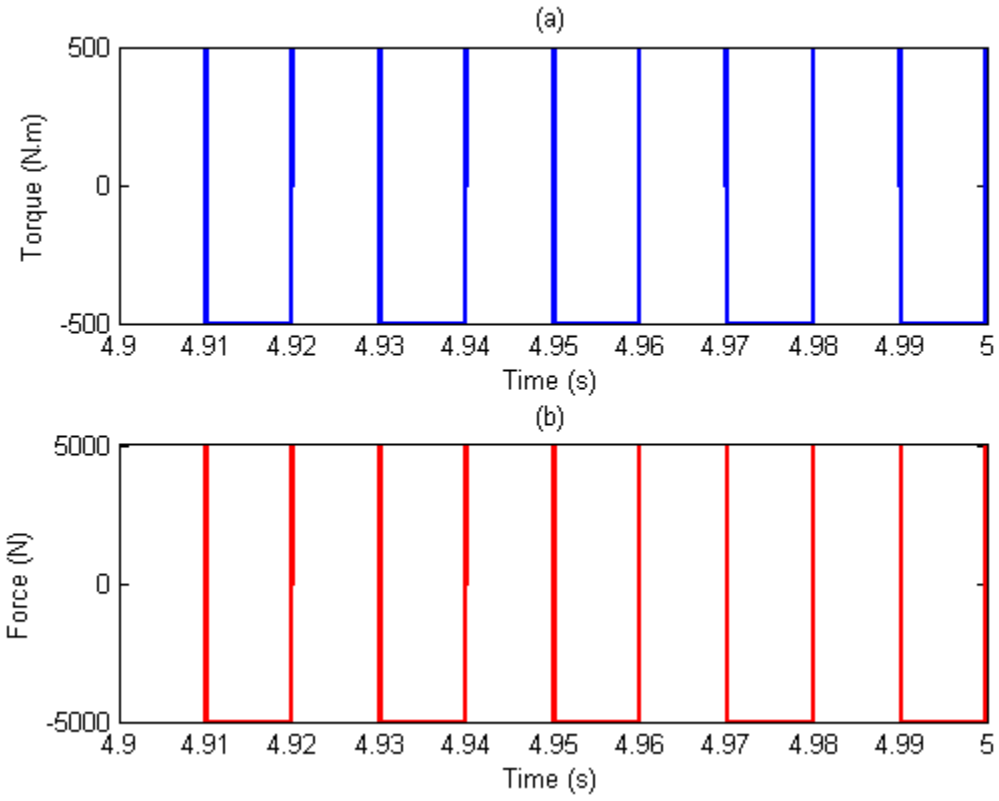

Published with MATLAB® R2014a

APPENDIX G. FLOATING FREQUENCY, HIGH AMPLITUDE IMPULSE INPUT FORCE SCENARIO

1. Simulink Input Force

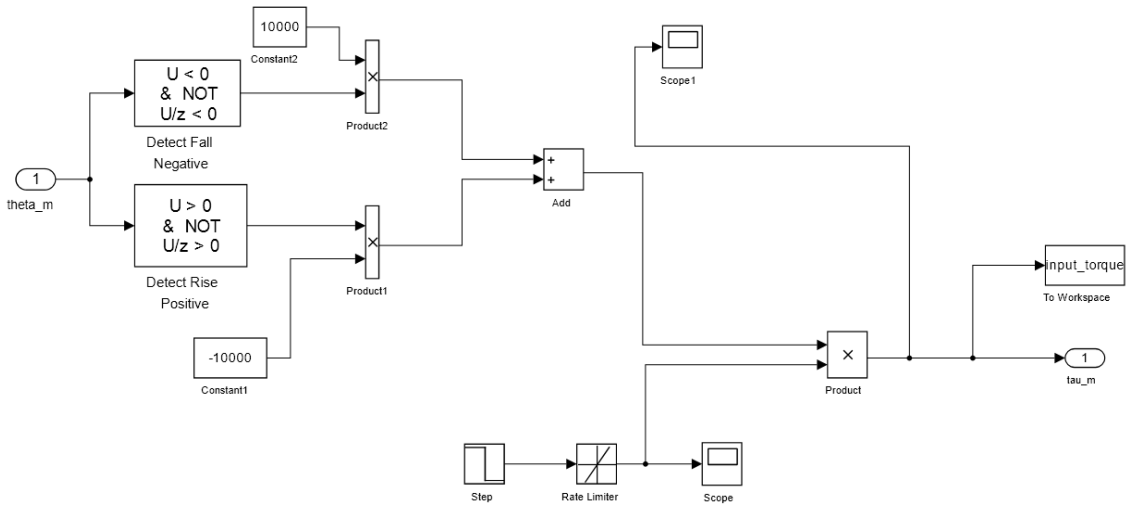

2. Defining Variables

```
format compact
close all;
clc
fig = 0;
ias=iabcs(:,1);
ibs=iabcs(:,2);
ics=iabcs(:,3);

vas=vabcs(:,1);
vbs=vabcs(:,2);
vcs=vabcs(:,3);

power = vdc.*idc;

energy_sum = (sum(abs(input_torque.*omega_mech))-sum(power)...
    -sum(Bm*omega_mech))/length(timev)

energy_out = sum(power(length(timev)-50000:length(timev)))/50000
energy_in = sum(abs(input_torque(length(timev)-50000:length(timev))...
    .*omega_mech(length(timev)-50000:length(timev))))/50000

efficiency = (energy_out / energy_in) * 100
```

```
funtime = linspace(0,2,1000);
fund = sin(2*pi*funtime);
harm3 = K3.*sin(2*pi*funtime*3);
harm5 = K5.*sin(2*pi*funtime*5);
harm7 = K7.*sin(2*pi*funtime*7);

zNormal = theta_mech ./ (2*pi); % normalized stator position

z = zNormal .* 2*pi * radius; % translator position (m)

v = omega_mech .* radius; % (m/s)
tau_frict = omega_mech*.0026;

frictionForce = tau_frict / radius;
inputForce = input_torque / radius; % (N)
springForce = tau_spring / radius; % (N)
electricForce = Te / radius; % (N)
```

```
energy_sum =
   68.7719
energy_out =
  147.6281
energy_in =
  207.2879
efficiency =
   71.2189
```

3. Lambdas

```
fig = fig +1;

figure(fig);
plot(timev,lambda_abc(:,1),timev,lambda_abc(:,2),timev,lambda_abc(:,3),...
    'LineWidth',1)
xlabel('Time (s)'); ylabel('Magnetic Flux (Wb)')
legend('\lambda_a_s','\lambda_b_s','\lambda_c_s','Location','Southwest')
% xlim([1,1.5])
xlim([4.9 5])
```

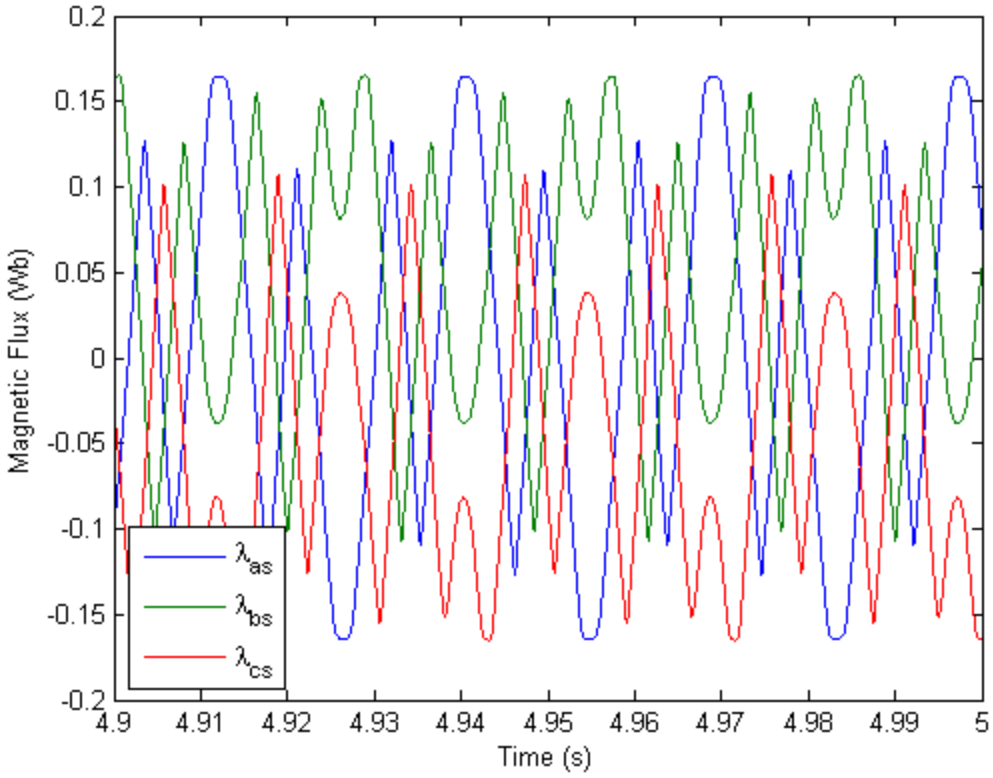

4. Forces at play

```
fig = fig+1;
figure(fig)
plot(timev,-inputForce/10000,timev,-(inputForce+springForce)/10000,...
    timev,z,timev,v/100,'LineWidth',2)
legend('F_i_n/10             (kN)','F_i_n+F_{spring}/10 (kN)',...
    'Position          (m)','Velocity/100  (m/s)','Location','Southwest')
xlim([max(timev)-.1 max(timev)])
xlabel('Time (s)'); ylabel('Amplitude')
```

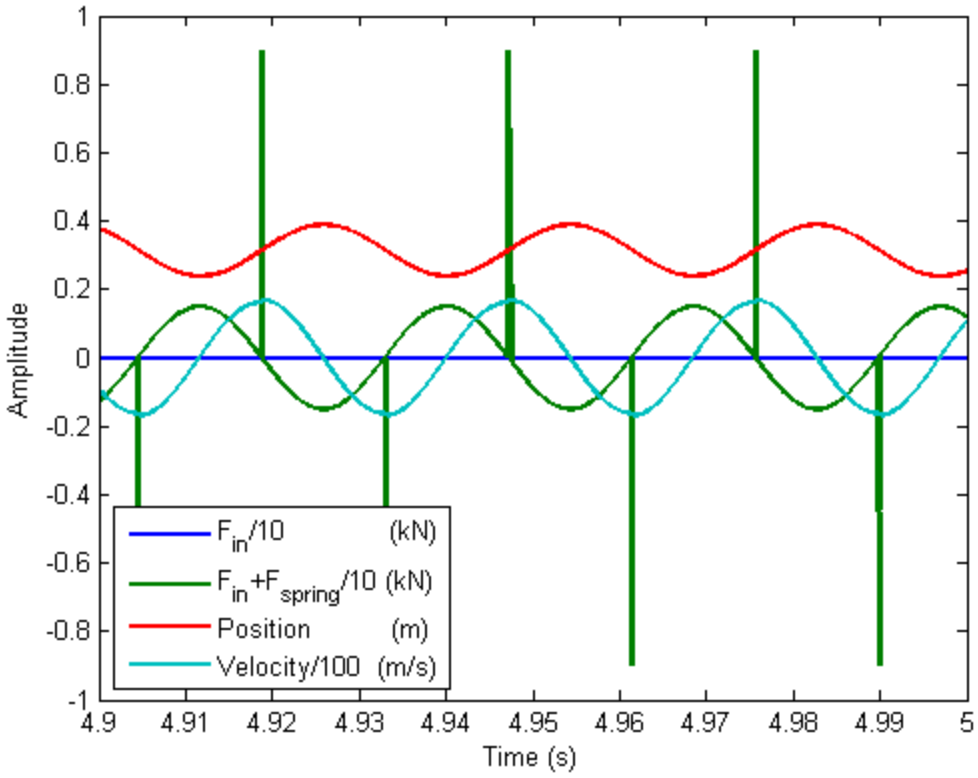

5. ABC Variables

```
fig = fig+1;
figure(fig)
subplot(2,1,1)
plot(timev,vas,timev,vbs,timev,vcs); title('(a)')
legend('v_a_s','v_b_s','v_c_s','Location','Southwest')
ylabel('Voltage (V)'); xlabel('Time (s)')

subplot(2,1,2)
plot(timev,ias,timev,ibs,timev,ics); title('(b)')
legend('i_a_s','i_b_s','i_c_s','Location','Southwest')
ylabel('Current (A)'); xlabel('Time (s)')
```

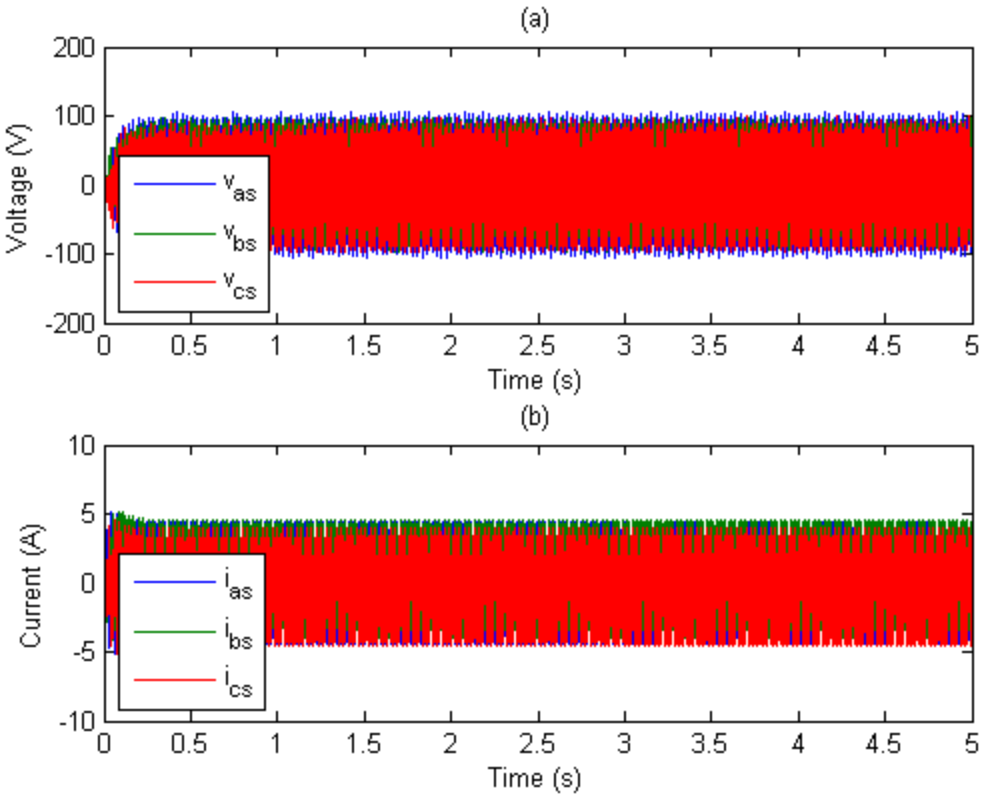

6. ABC Variables short timeframe

```
fig = fig+1;
figure(fig)
subplot(2,1,1)
plot(timev,vas,timev,vbs,timev,vcs,'LineWidth',2); title('(a)')
legend('v_a_s','v_b_s','v_c_s','Location','Southwest')
ylabel('Voltage (V)'); xlabel('Time (s)')
xlim([max(timev)-.1 max(timev)])

subplot(2,1,2)
plot(timev,ias,timev,ibs,timev,ics,'LineWidth',2); title('(b)')
legend('i_a_s','i_b_s','i_c_s','Location','Southwest')
ylabel('Current (A)'); xlabel('Time (s)')
xlim([max(timev)-.1 max(timev)])
```

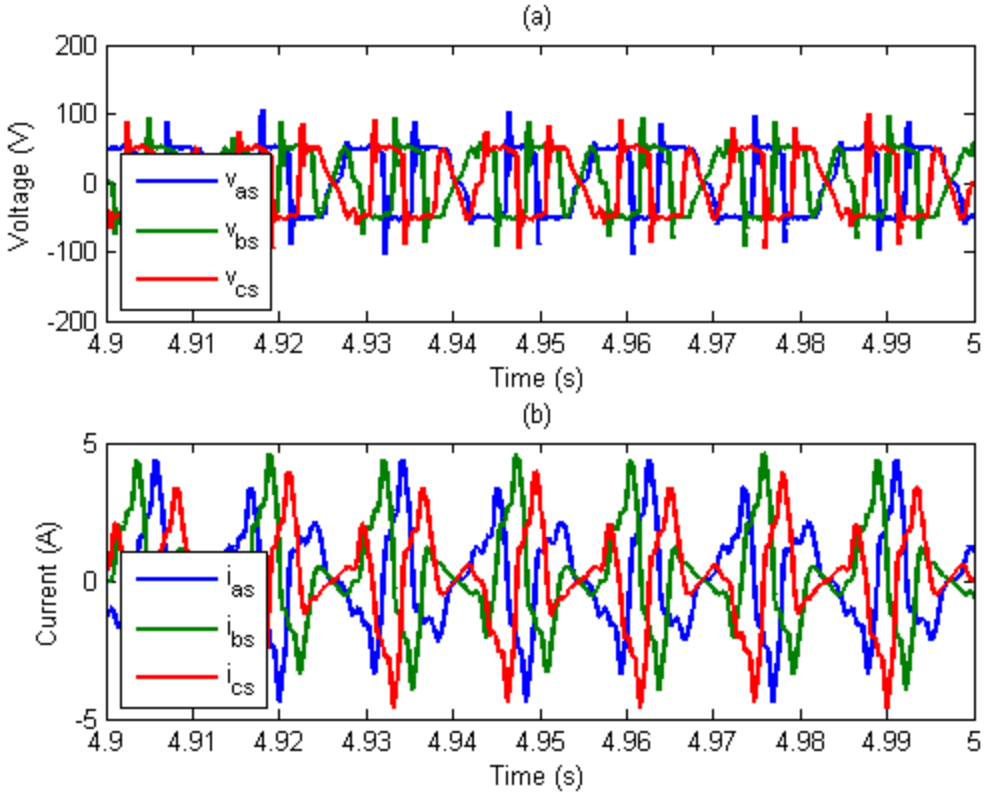

7. qd0 Variables

```
fig = fig+1;

figure(fig)
subplot(3,1,1)
plot(timev,i_qdos(:,1))
xlim([4.9 5])
legend('i_q')
subplot(3,1,2)
plot(timev,i_qdos(:,2))
xlim([4.9 5])
legend('i_d')
subplot(3,1,3)
plot(timev,i_qdos(:,3))
xlim([4.9 5])
legend('i_0')

iqs=i_qdos(:,1);
ids=i_qdos(:,2);
i0s=i_qdos(:,3);
theta_r=i_qdos(:,4);
iqd_angle=angle(iqs-1i*ids)*180/pi;
```

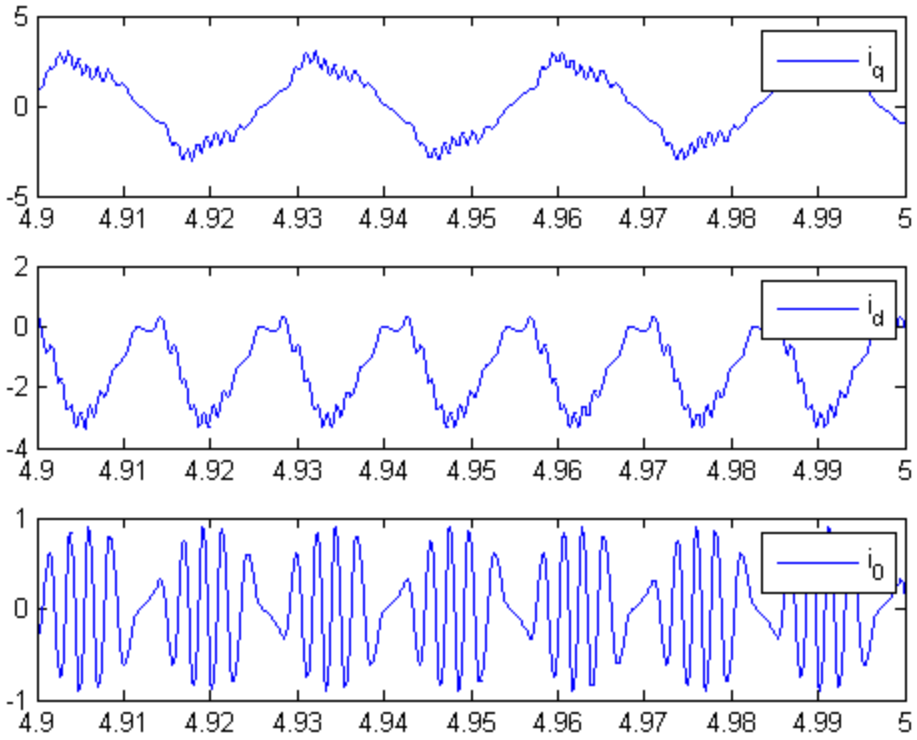

8. Velocity and Position (Electrical)

```
fig = fig+1;

figure(fig)
subplot(2,1,1)
plot(timev,wre_data,'LineWidth',2)
title('(a)')
xlabel('Time (s)'); ylabel('Angular Velocity (rad/s)')
xlim([4.9 5]); %ylim([-125 125])
%legend('\omega_r_e')

subplot(2,1,2)
plot(timev,theta_elec,'r','LineWidth',2)
title('(b)')
xlabel('Time (s)'); ylabel('Electrical Position (rad)')
xlim([4.9 5])
%legend('\theta_r_e')
%ylim([0,2*pi])
```

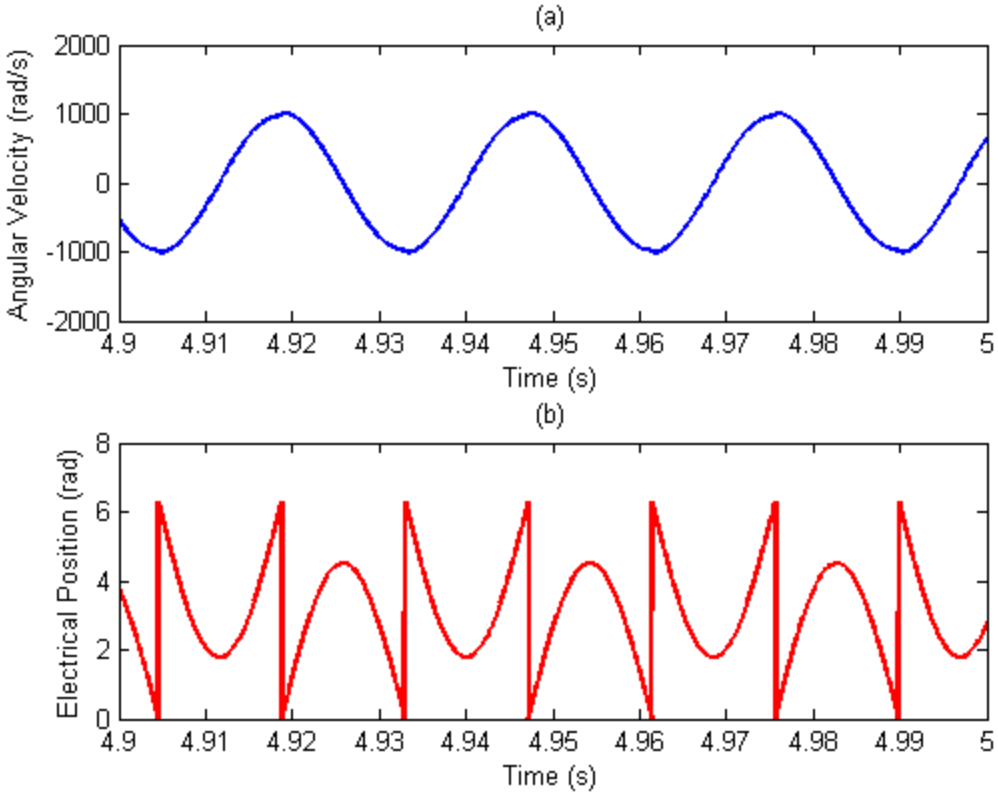

9. Velocity and Position (Mechanical)

```
fig = fig+1;

figure(fig)
subplot(2,1,1)
plot(timev,v,'LineWidth',2)
title('(a)')
xlabel('Time (s)'); ylabel('Velocity (m/s)')
xlim([4.9 5]);
%legend('Velocity')
xlabel('Time (s)')

subplot(2,1,2)
plot(timev,z,'r','LineWidth',2)
title('(b)')
xlim([4.9 5]); ylim([0 2*pi/10])
xlabel('Time (s)'); ylabel('Position (m)')
%legend('Position')
```

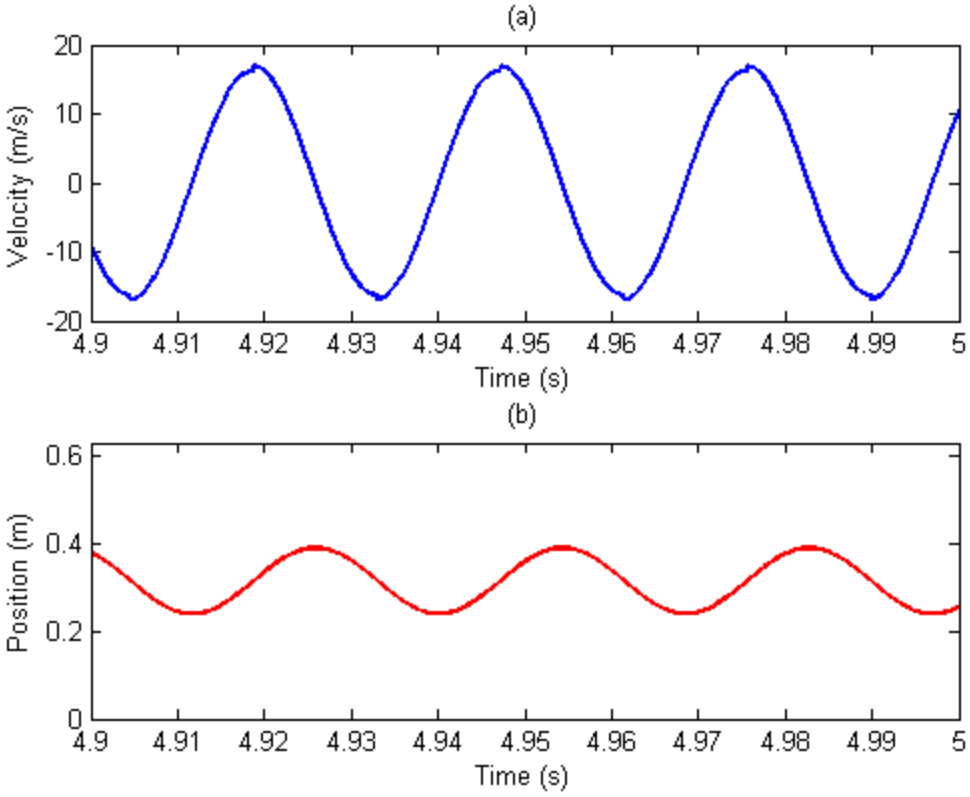

10. DC Variables

```
fig = fig+1;

figure(fig)
plot(timev,vdc,'LineWidth',2)
xlim([4.9 5]); %ylim([0 11])
xlabel('Time (s)'); ylabel('Voltage (V)')

fig = fig+1;

figure(fig)

plot(timev,vdc,'LineWidth',2); %title('(a)')
%xlim([0.5 0.6]); %%ylim([0 11])
xlabel('Time (s)'); ylabel('Voltage (V)')

fig=fig+1
figure(fig)
plot(timev,idcabc(:,1),timev,idcabc(:,2),timev,idcabc(:,3));
%title('(b)')
legend('i_a dc','i_b dc','i_c dc','Location','Best')
xlim([2.34 2.367]); %%ylim([-1 17])
xlabel('Time(s)'); ylabel('Current (A)')
```

```
% %% Lambda Harmonics
% fig = fig+1;
%
% figure(fig)
% plot(funtime,0.1549*(fund+harm3+harm5+harm7),'LineWidth',2)
% xlim([0 max(funtime)])
% %legend('\lambda_P_M')
% xlabel('Time (arbitrary)'); ylabel('Magnetic Flux (Wb)')
```

```
fig =
    10
```

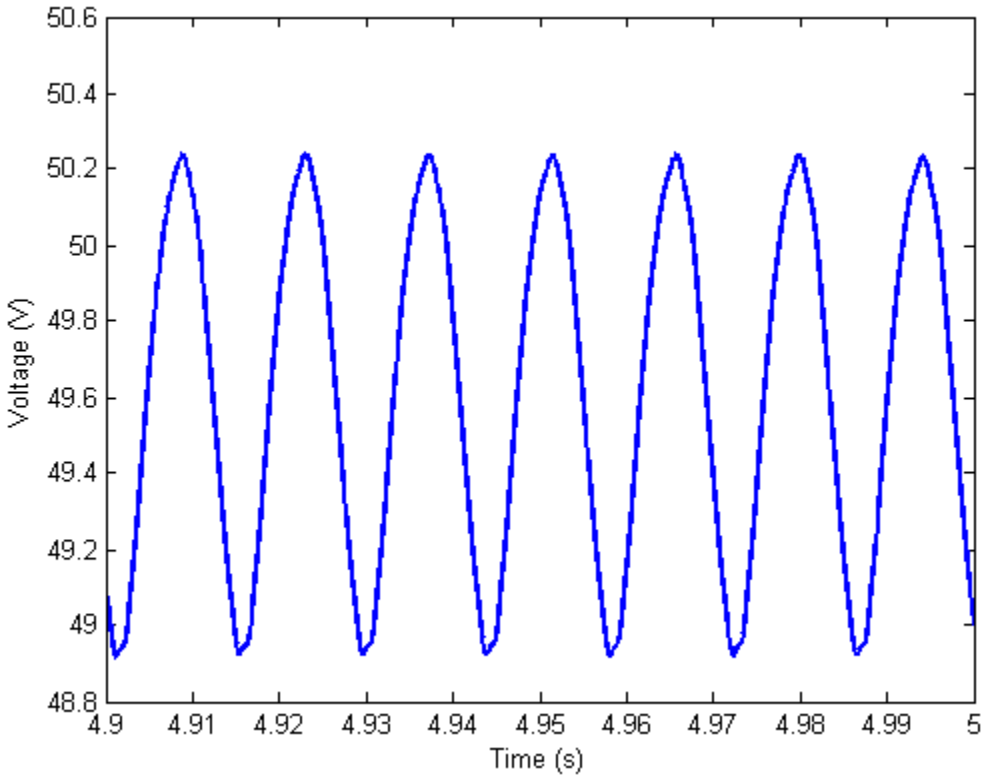

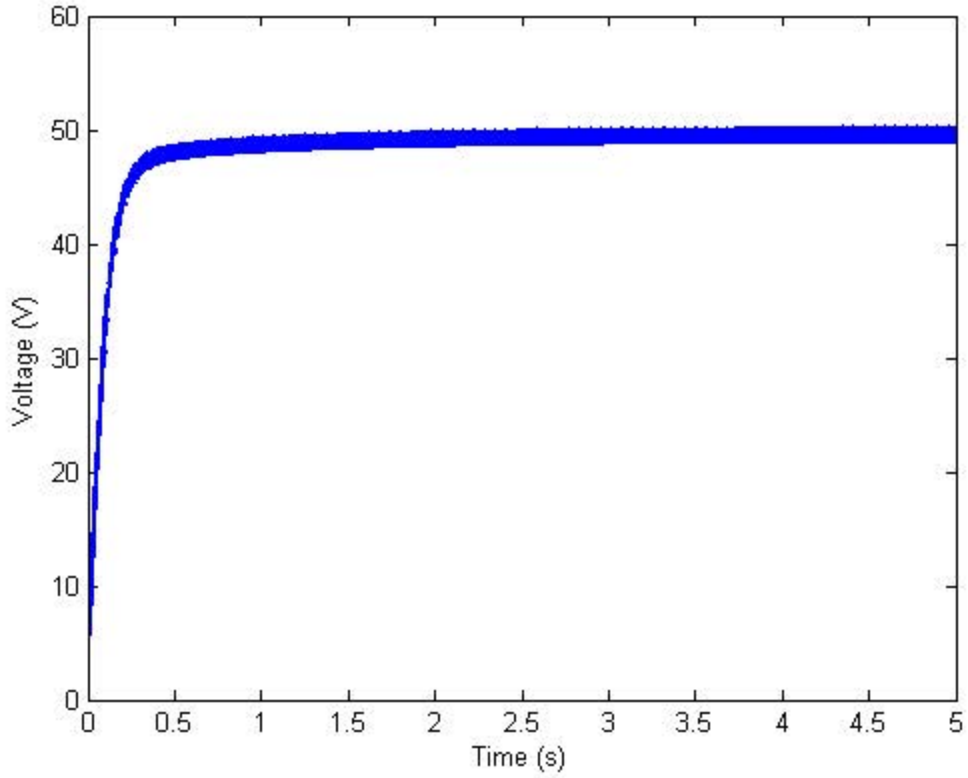
Voltage (V)
Time (s)
0
10
20
30
40
50
60
0
0.5
1
1.5
2
2.5
3
3.5
4
4.5
5

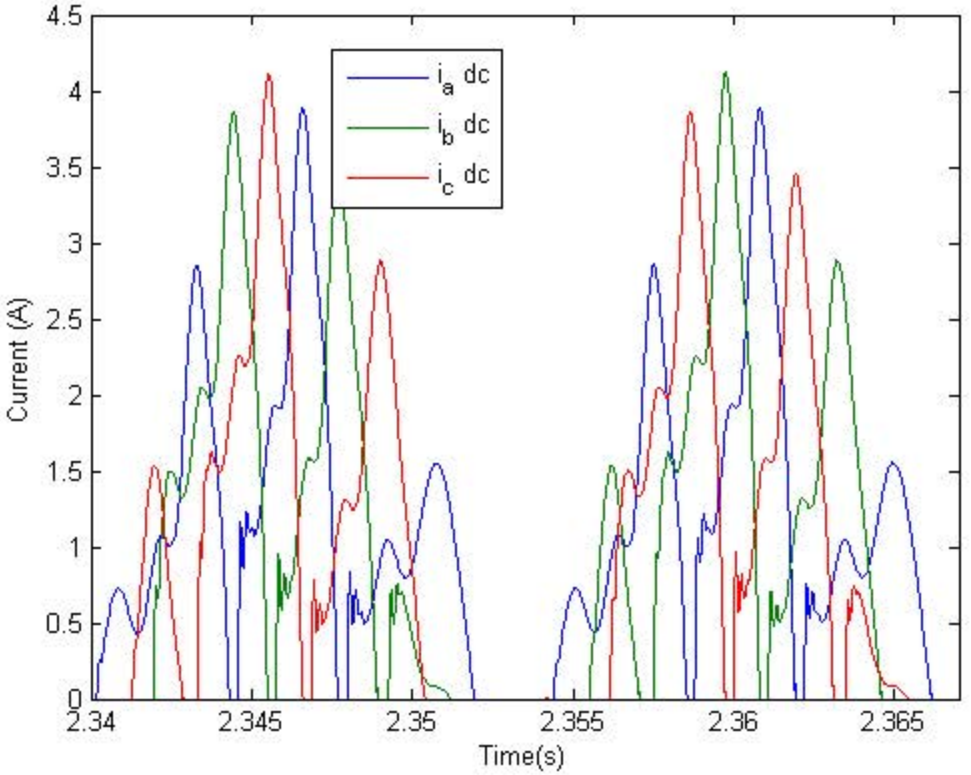
Current (A)
Time(s)
i_a dc
i_b dc
i_c dc
0
0.5
1
1.5
2
2.5
3
3.5
4
4.5
2.34
2.345
2.35
2.355
2.36
2.365

11. Input Torque and Force

```
fig = fig+1;

figure(fig)
subplot(2,1,1)
plot(timev,input_torque,'LineWidth',2)
title('(a)')
xlim([4.9 5]);
%legend('\tau_i_n','Location','Southeast')
ylabel('Torque (N\cdotm)')
xlabel('Time (s)')

subplot(2,1,2)
plot(timev,inputForce,'r','LineWidth',2)
title('(b)')
xlim([4.9 5])
%legend('F_i_n','Location','Southeast')
ylabel('Force (N)')
xlabel('Time (s)')
```

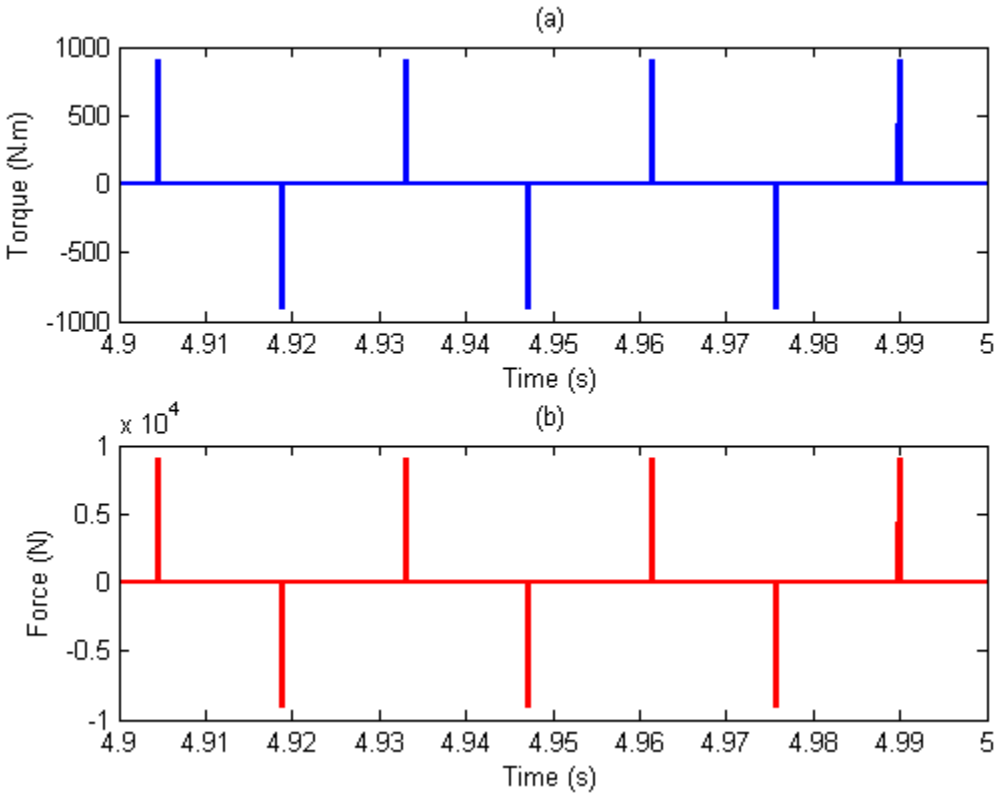

Published with MATLAB® R2014a

LIST OF REFERENCES

[1] T. Davenport, "Improvement in propelling machinery by magnetism and electro-magnetism." U.S. Patent 132, 1836, Feb. 25.

[2] M. Doppelbauer. (2014, Sep. 25) The invention of the electric motor 1800–1854: Elektrotechnisches Institut. [Online]. Available: http://www.eti.kit.edu/english

[3] T. Martin, *Faraday's Discovery of Electro-Magnetic Induction*, London: Edward Arnold & Co., 1949.

[4] A. Zehden, "Electric traction apparatus," U.S. Patent 782312, 1905, Feb. 14.

[5] Integrated Magnetics: FAQs. (n.d.). Ecreativeworks. [Online]. Available: http://www.intemag.com/faqs.html. Accessed Oct. 22, 2014.

[6] L. M. Bacon. (2011, Jul. 19). EMALS builder agrees to fixed-price deal. [Online]. Available: http://www.navytimes.com.

[7] K. B. Vlahos, (2012, Feb. 28). It's real! Navy test-fires first working prototype of railgun. [Online]. Available: http://www.foxnews.com

[8] Woods Hole Oceanographic Institution: REMUS. (Jan. 7, 2010). Woods Hole Oceanographic Institution, 7 January 2010. [Online]. Available: http://www.whoi.edu/main/remus

[9] K. Fulton-Bennet. (2012, May 11). MBARI power buoy. [Online]. Available: http://www.mbari.org/news/homepage/2012/powerbuoy/powerbuoy.html.

[10] N. Mohan, T. M. Undeland and W. P. Robbins, *Power Electronics: Converters, Applications and Design*, Hoboken, NJ: John Wiley & Sons, 2003.

[11] The Institute of Electrical and Electronics Engineers, Inc. (2000). *IEEE 100: The Authoritative Dictionary Of IEEE Standards Terms.* Seventh Edition. [Ebrary version]. [Online]. Available: http://libproxy.nps.edu/login?url=http://ieeexplore.ieee.org.libproxy.nps.edu/xpl/mostRecentIssue.jsp?punumber=4116785

[12] M. Elias, K. Nor and A. Arof, "Design of smart charger for series lithium-ion batteries," in *International Conference on Power Electronics and Drives Systems*, Kuala Lumpur, Malaysia, vol. 2, 2005.

[13] P. Zheng, C. Tong, J. Bai, B. Yu, Y. Sui and W. Shi, "Electromagnetic design and control strategy of an axially magnetized permanent-magnet linear alternator for free-piston Stirling engines," *IEEE Transactions on Industry Applications,* vol. 48, no. 6, pp. 2230–2239, 2012.

[14] G. Schmidt, R. Wiley and R. Furlong, "Radioisotope power systems for New Frontiers applications," presented at the NASA New Frontiers Program Pre-proposal Conference, Washington, DC, 2013.

[15] M. Li and J. Dong, "Modeling and simulation of solar dish-Stirling systems," in *Power and Energy Engineering Conference, Asia-Pacific*, Shanghai, China, 2012.

[16] F. Rinderknecht and H.-G. Herzog, "Calculation of a linear generator for a hybrid vehicle concept," in *XIX International Conference on Electrical Machines*, Rome, Italy, 2010.

[17] BMW USA: i3 specifications. (n.d.). BMW of North America. [Online]. Available: http://www.bmwusa.com. [Accessed Oct. 13, 2014].

[18] A. P. Cabiling, "Ultra low-voltage energy harvesting," M.S. thesis, Dept. of Electrical and Electronics Eng., Naval Postgraduate School, Monterey, CA, 2013.

[19] D. Shvets, "Analysis of ac low voltage energy harvesting," M.S. thesis, Dept of Electrical and Electronics Eng., Naval Postgraduate School, Monterey, CA, 2014.

[20] LORD MicroStrain Sensing Systems: Energy Harvesting Sensors. (n.d.). LORD MicroStrain. [Online]. Available: http://www.microstrain.com. [Accessed Oct. 20, 2014].

[21] R. B. Goldner and P. Zerigian, "Electromagnetic linear generator and shock absorber," U.S. Patent U.S. 6,952,060 B2, 2005, Oct. 4.

[22] H. Polinder, M. Mueller, M. Scuotto and M. Goden de Sousa Prado, "Linear generator systems for wave energy conversion," in *Proceedings of the 7th European Wave and Tidal Energy Conference*, Porto, Portugal, 2007.

[23] P. L. Chapman, S. D. Sudhoff and C. A. Whitcomb, "Multiple reference frame analysis of non-sinusoidal brushless dc drives," *IEEE Transactions on Energy Conversion,* vol. 14, no. 3, pp. 440–446, 1999.

[24] P. C. Krause, O. Wasynczuk and S. D. Sudhoff, *Analysis of Electric Machinery and Drive Systems*, 2nd ed., Piscataway, New Jersey: IEEE Press, 2002.

[25] P. Hammond, *Electromagnetism for Engineers: An Introductory Course*, Oxford, Massachussetes: Oxford University Press, 1997.

INITIAL DISTRIBUTION LIST

1. Defense Technical Information Center
   Ft. Belvoir, Virginia

2. Dudley Knox Library
   Naval Postgraduate School
   Monterey, California